T.C.
DOKUZ EYLÜL UNIVERSITY
IZMIR INTERNATIONAL
BIOMEDICINE AND GENOME
INSTITUTE

Investigation of miRNAs Regulating Therapy Response in Hepatocellular Carcinoma

EZGİ BAĞIRSAKÇI TEPE

MOLECULAR BIOLOGY AND GENETICS

PhD THESIS

IZMIR-2024

THESIS CODE: DEU.IBG.PhD-2017850004

T.C.
DOKUZ EYLÜL UNIVERSITY
IZMIR INTERNATIONAL
BIOMEDICINE AND GENOME
INSTITUTE

Investigation of miRNAs Regulating Therapy Response in Hepatocellular Carcinoma

MOLECULAR BIOLOGY AND GENETICS

PhD THESIS

EZGİ BAĞIRSAKÇI TEPE

Supervisor: Assoc. Prof. Muhammed Kasım DİRİL

Co-Supervisor: Prof. Dr. Safiye Neşe ATABEY

The first chapter of this research was supported by a project funded by TUBITAK with project number 118Z156.

THESIS CODE: DEU.IBG.PhD-2017850004

T.C.
DOKUZ EYLÜL ÜNİVERSİTESİ

İZMİR ULUSLARARASI BİYOTIP VE GENOM ENSTİTÜSÜ

Ph.D. THESIS DEFENSE EXAMINATION REPORT

Dokuz Eylül University Izmir International Biomedicine and Genome Institute Department of Genome Sciences and Molecular Biotechnology, Molecular Biology and Genetics graduate program Doctor of Philosophy student Ezgi Bağırsakçı Tepe with student ID 2017850004 has successfully completed her Doctor of Philosophy thesis titled "Investigation of miRNAs Regulating Therapy Response in Hepatocellular Carcinoma" on the date of 23/02/2024.

Assoc. Prof. Muhammed Kasım Diril
CHAIR

Prof. Dr. Şerif Şentürk
JURY MEMBER

Asst. Prof. Yavuz Oktay
JURY MEMBER

Asst. Prof. Ayşe Banu Demir
JURY MEMBER

Prof. Dr. Güneş Özhan
JURY MEMBER

Prof. Dr. Gökhan Karakülah
SUBSTITUTE MEMBER

Asst. Prof. Peyda Korhan
SUBSTITUTE MEMBER

T.C.
DOKUZ EYLÜL ÜNİVERSİTESİ
İZMİR ULUSLARARASI BİYOTIP VE GENOM ENSTİTÜSÜ

DOKTORA TEZ SAVUNMA SINAVI TUTANAĞI

Dokuz Eylül Üniversitesi İzmir Uluslararası Biyotıp ve Genom Enstitüsü Genom Bilimleri ve Moleküler Biyoteknoloji Anabilim Dalı Moleküler Biyoloji ve Genetik Doktora Programı 2017850004 numaralı öğrencisi Ezgi Bağırsakçı Tepe, "Hepatoselüler Karsinoma'da Tedavi Yanıtını Düzenleyen mikroRNA'ların Araştırılması" konulu Doktora tezini 23/02/2024 tarihinde yapılan savunma sınavı sonucunda başarılı olarak tamamlamıştır.

Doç Dr. Muhammed Kasım Diril
BAŞKAN

Prof. Dr. Şerif Şentürk
JÜRİ ÜYESİ

Dr. Öğr. Üyesi Yavuz Oktay
JÜRİ ÜYESİ

Dr. Öğr. Üyesi Ayşe Banu Demir
JÜRİ ÜYESİ

Prof. Dr. Güneş Özhan
JÜRİ ÜYESİ

Prof. Dr. Gökhan Karakülah
YEDEK ÜYE

Dr. Öğr. Üyesi Peyda Korhan
YEDEK ÜYE

INDEX

TABLE INDEX

FIGURE INDEX

ABBREVIATIONS

HCC: Hepatocellular carcinoma

HGF: Hepatocyte growth factor

Cav-1: Caveolin-1

FDA: Food and Drug Administration

VEGF: Vascular endothelial growth factor

PDGF: Platelet-derived growth factor

SF: Scattering factor

EMT: Epithelial-mesenchymal transition

FAK: Focal adhesion kinase

ECM: Extracellular matrix

MMP: Matrix metalloproteinase

EGFR: Epithelial growth factor receptor

FGFR: Fibroblast growth factor receptor

IR: Insulin receptor

miRNA: micro RNA

lncRNA: long non coding RNA

TME: tumor microenvironment

Nt: nucleotides

3' UTR: 3' untranslated region

RISC complex: RNA-induced silencing complex

DOX: Doxorubicin

RBP: RNA binding protein

HOTAIR: HOX transcript antisense intergenic RNA

Hybrid E/M phenotype: hybrid epithelial mesenchymal phenotype

CDS: Coding DNA sequence

FFPE: Formalin-fixed paraffin-embedded tissue

SOR: Sorafenib

ACKNOWLEDGEMENT

First, I would like to convey my heartfelt thanks to my supervisor and mentor Prof. Dr. Neşe Atabey who witnessed all my scientific adventures since my master's and always supported me to achieve every step. She inspired me with different ideas and encouraged me with her guidance.

I am grateful to my other supervisor Assoc. Prof. Muhammed Kasım Diril for his valuable efforts in my Ph.D. journey and for always supporting me.

I would like to thank my thesis committee; they were really helpful when I asked for anything about my thesis and eager to solve the problems or overcome any obstacles, and they led me positively about my thesis with their ideas.

Working in a fun and peaceful environment must be the best thing that can happen to someone. I felt lucky every day that we could provide this. I would like to express my sincere gratitude to Peyda Korhan, Yasemin Öztemur Islakoğlu, Yeliz Yılmaz, Hande Topel Batarlar, Dehan Çömez, Gülsün Bağcı and Ayşim Güneş. I worked in a warm, helpful, and reliable laboratory environment with them and felt gratitude for their friendship.

I would also like to thank my family for their unconditional love and support throughout my entire life and dedicate this thesis, especially to my beloved mother Sibel Bağırsakçı, my father Sami Bağırsakçı and my grandmother Gönül Bağırsakçı.

Lastly, I deeply thank TUBITAK; ARDEB 1001 program for supporting the first chapter of this thesis, the BIDEB 2211-C program for supporting me, and the YOK 100/2000 program for supporting me during my Ph.D.

Investigation of miRNAs Regulating Therapy Response in Hepatocellular Carcinoma

Ezgi Bağırsakçı Tepe, Izmir International Biomedicine and Genome Institute, Dokuz Eylül University Health Campus Balçova 35340 İzmir/Türkiye

ABSTRACT

Hepatocellular carcinoma (HCC) has one of the highest death rates among all cancers, and the reasons behind this are metastasis, recurrence, and therapy resistance. Sorafenib is the first multi-kinase inhibitor that has been used for HCC treatment and is still the most preferred and accepted drug. However, the long duration of therapy generates resistance to Sorafenib. The mechanism behind this is yet to be elucidated, but non-coding RNA-based mechanisms are counted as one of the reasons for therapy resistance. Recent studies have highlighted the influence of miRNAs in the development, progression, metabolic reprogramming, and therapy responses in HCC. Our previous studies showed that decreased expression of miR-181a-5p causes more aggressive phenotype in HCC. Cav-1 overexpression causes more aggressive phenotype, as well. HOTAIR overexpression promotes hybrid E/M (epithelial/mesenchymal) phenotype, which causes more aggressive phenotype and drug resistance. In this study, we aimed to enlighten the mechanism of Sorafenib-resistance, and investigate Cav-1/miR-181a-5p/HOTAIR axis in Sorafenib-resistance.

Our results showed that Cav-1 was overexpressed in Sorafenib-resistant HCC cell lines that we generated, and when Cav-1 expression was increased, Sorafenib IC50 values were increased, as well. In Sorafenib-resistant cell lines, caveolar structures were increased, stress fiber formations were increased, adhesion was decreased, hybrid E/M markers were increased, and miR-181a-5p expression was decreased. When we increased miR-181a-5p expression by mimic transfection, Sorafenib-resistant cells became more sensitized to Sorafenib, their motility and colony formation capability were decreased, and when we inhibited miR-181a-5p

expression, we obtained opposite results. When we analyzed HOTAIR expression in HCC cells, HOTAIR and miR-181a-5p expressions showed negative correlation.

Since Cav-1, miR-181a-5p and HOTAIR contribute to aggressive phenotype individually, they may contribute to Sorafenib resistance together by providing a hybrid E/M phenotype in HCC cells.

Keywords: Hepatocellular Carcinoma, Sorafenib Resistance, Cav-1, miR-181a-5p, HOTAIR, hybrid E/M phenotype

Hepatoselüler Karsinomada Tedavi Yanıtını Düzenleyen mikroRNA'ların Araştırılması

Ezgi Bağırsakçı Tepe, İzmir Uluslararası Biyotıp ve Genom Enstitüsü, Dokuz Eylül Üniversitesi Sağlık Yerleşkesi Balçova 35340 İzmir/Türkiye

ÖZET

Hepatoselüler karsinoma (HCC), kanser tipleri arasında en yüksek ölüm oranlarından birine sahiptir ve bunun arkasındaki nedenler metastaz, nüks ve tedavi direncidir. Sorafenib, HCC tedavisinde kullanılan ve hala en çok tercih edilen ve kabul gören ilk multikinaz inhibitörüdür. Ancak, uzun süreli tedavi sorafenibe direnç gelişmesine neden olmaktadır. Direnç mekanizması henüz aydınlatılmamıştır; fakat kodlanmayan RNA tabanlı mekanizmalar terapi direncinin nedenlerinden biri olarak sayılmaktadır. Yapılan son çalışmalar, HCC'de miRNA'ların gelişim, progresyon, metabolik yeniden programlama ve tedavi yanıtları üzerindeki etkisini vurgulamıştır. Önceki çalışmalarımız, miR-181a-5p'nin azalmış ifadesinin HCC'de daha agresif bir fenotipe yol açtığını göstermiştir. Cav-1 aşırı ekspresyonu da HCC'de daha agresif bir fenotipe neden olmaktadır. HOTAIR aşırı ekspresyonu, HCC hücrelerinde hibrit E/M fenotipini destekleyip, hücrelere daha agresif bir fenotip kazandırmakta ve ilaç direncine yol açmaktadır. Bu çalışmamızda, Sorafenibe direnç mekanizmasını aydınlatmayı amaçladık ve Sorafenib direncinde Cav-1, miR-181a-5p, HOTAIR ekseni üzerine odaklandık.

Elde ettiğimiz sonuçlarda, elde ettiğimiz Sorafenib dirençli HCC hücre hatlarında Cav-1 ekspresyonu artmış ve Cav-1 ifadesi artırıldığında, Sorafenib IC50 değerleri de artmıştır. Sorafenib dirençli hücre hatlarında, kaveolar yapılar ve stres fiberleri oluşumu artmış, adezyon azalmış, hibrit E/M (epitelyal/mezenkimal) fenotip belirteçleri yükselmiş, ve miR-181a-5p ekspresyonu azalmıştır. Sorafenib dirençli hücrelerde miR-181a-5p ifadesini mimik transfeksiyonuyla artırdığımızda, hücreler Sorafenibe daha duyarlı hale gelmiş, motilite ve koloni oluşumu yetenekleri azalmış ve miR-181a-5p ifadesini inhibe ettiğimizde, tam tersi sonuçlar elde edilmiştir.

Hücrelerde HOTAIR ifadesi incelendiğinde, HOTAIR ve miR-181a-5p ifadelerinin negatif korele olduğu görülmüştür.

Bireysel olarak Cav-1, miR-181a-5p ve HOTAIR'ın agresif fenotipe katkıları göz önüne alındığında, HCC hücrelerinde hibrit E/M fenotipi sağlayarak birlikte Sorafenib direncine katkıda bulundukları düşünülmektedir.

Anahtar Kelimeler: Hepatoselüler Karsinoma, Sorafenib Direnci, Cav-1, miR-181a-5p, HOTAIR, hibrit E/M fenotip

1. INTRODUCTION AND OBJECTIVES

Hepatocellular carcinoma (HCC) is the sixth most common cancer type and is the third when it comes to cancer-related deaths around the world (1). Although HCC diagnosis and therapy alternatives are well-studied and improving gradually, the prognosis is poor due to metastasis, recurrence, and resistance to therapy. Liver transplantation is the primary therapy option for HCC in the early stages; chemotherapy and radiotherapy are the following. In early HCC, resection is the commonly used approach, but in advanced HCC, Sorafenib treatment is the first-line therapy with the help of radiotherapy (2).

Sorafenib is the first multi-kinase inhibitor that was approved by the FDA for HCC therapy in 2007. Sorafenib targets Raf-1, B-Raf, and Ras/Raf/MEK/ERK signaling pathways by inhibiting these pathways and their kinase activity and suppressing tumor cell proliferation as a result. Moreover, Sorafenib has other targets, such as platelet-derived growth factor receptor (PDGFR), vascular endothelial growth factor receptor (VEGFR), and hepatocyte factor receptor (c-KIT) in order to inhibit tumor angiogenesis (3). Although many trials have been done as non-inferiority to Sorafenib and second-line treatments for HCC in recent years, Sorafenib treatment is still the most accepted and preferred therapy for HCC patients. Drug resistance is one of the biggest obstacles in Sorafenib therapy. Elucidating the resistance mechanism to Sorafenib is crucial for combatting HCC. Many factors can be defined as the cause of Sorafenib resistance, including non-coding RNA-based mechanisms, tumor microenvironmental factors, and receptor tyrosine kinase and growth factors activation by feedback mechanisms (2).

Caveolae, which are small invaginations of the plasma membrane, have roles in endocytosis, transcytosis, cholesterol transport as well as in signal transduction. Caveolin-1 (Cav-1) is the main protein component of caveolae structures and is a scaffolding protein. Caveolin-1 activation induces aggressive phenotype in HCC by increasing their motility and invasion and changing cellular morphology (4). We also reported that c-Met and Cav-1 are co-expressed in HCC cells and contribute to the initiation and progression of HCC by boosting downstream signaling (5).

It is known that noncoding RNAs have crucial roles in cancer development and progression (6). Dysregulation of miRNAs in either tumor tissue or its microenvironment, especially, has become a hallmark of cancer (7). They can behave as tumor-suppressive or oncogenic, as well as miRNAs can be altered in drug therapy and contribute to response to the therapy (8). LncRNAs play important roles in many biological processes by interacting with RNA-binding proteins and miRNAs as sponges. By this way of action, they have important roles in mediating drug resistance by interacting with miRNAs. However, no study has yet addressed the potential role of Cav-1 expression and its regulations by noncoding RNAs in Sorafenib resistance.

In this study, we aimed to enlighten the role of Caveolin-1 in the Sorafenib resistance in HCC with the underlying mechanisms. We hypothesized that noncoding RNAs mediated increase in Cav-1 expression and alterations in caveolar structures is involved in Sorafenib resistance. The specific objectives of the thesis are:

(i) generating new Sorafenib-resistant clones of HuH-7, MV, and SNU-449 cell lines,
(ii) determining Cav-1 transcript and protein expression levels in Sorafenib-resistant clones,
(iii) testing the relationship between Cav-1 expression levels and SOR IC50 values;
(iv) analyzing the alterations in the caveolar structures of Sorafenib-resistant cells,
(v) comparing adhesion, proliferation, EMT phenotype, motility, and invasion capabilities of Sorafenib-resistant clones with WT cells,
(vi) testing *in vivo* characteristics of Sorafenib-resistant cells in Zebrafish embryos,
(vii) understanding the influence of mir-34b-5p and miR-181a-5p and lncRNA HOTAIR in Sorafenib resistance and Cav-1 expression level,
(viii) testing contribution of HOTAIR-miR-181a-5p-Cav-1 axis in Sorafenib resistance.

2. LITERATURE SUMMARY/SCOPE OF THE STUDY

2.1. Hepatocellular carcinoma and therapy options

Hepatocellular Carcinoma is the most common type, accounting for 90% of primary liver cancer (9). It is the sixth most commonly diagnosed and the third most mortal cancer type in the world according to absolute numbers of GLOBOCAN 2022 data (1). In the early and intermediate stages of HCC, liver resection, ablation, and transplantation could be options for treatment; however, it is challenging to diagnose HCC in these stages. Often, it is diagnosed in the advanced stage that therapy options turn to systemic therapy, including chemotherapy, radiotherapy, transarterial chemoembolization (TACE), immunotherapy, and combinational therapy (10). Sorafenib was the first approved drug as a first-line targeted therapy for standard treatment of advanced HCC patients by the U.S. Food and Drug Administration (FDA) in 2007 as a result of the SHARP trial. Sorafenib (Nexavar) is a multikinase inhibitor designed to primarily inhibit the Ras/Raf/Mek/Erk and Vascular endothelial growth factor (VEGF) and Platelet-derived growth factor (PDGF) signaling pathways (11). Sorafenib was the only FDA-approved drug for HCC until 2017. Then, Regorafenib was approved as a second-line treatment for advanced HCC patients who received Sorafenib in first place in 2017. Over the past years, a few first-line treatment drugs and many second-line treatment drugs have been approved by the FDA for advanced HCC patients (12). The timeline below represents the FDA-approved drugs for HCC treatment (Figure 1). Regorafenib and Cabozantinib, multikinase inhibitors, and Ramucirumab, a VEGFR2 inhibitor, were approved by the FDA as a second-line treatment. Immune Checkpoint Inhibitors (ICIs) opened a new aspect as a treatment, and Nivolumab, Pembrolizumab and the combination of Nivolumab/ipilimumab were approved by the FDA as a second-line treatment. Additionally, Atezolizumab/bevacizumab combination was approved as a first-line treatment and increased the first-line treatment options (12, 13). Lenvatinib, another multikinase inhibitor, was approved by the FDA as a first-line treatment. Unlike Sorafenib, Lenvatinib targets the fibroblast growth factor (FGF) signaling pathway and is not inferior compared to Sorafenib. However, high levels of hepatocyte growth factor (HGF) decrease Lenvatinib activity in HCC through downstream of FGF signaling and eventually cause Lenvatinib resistance (13).

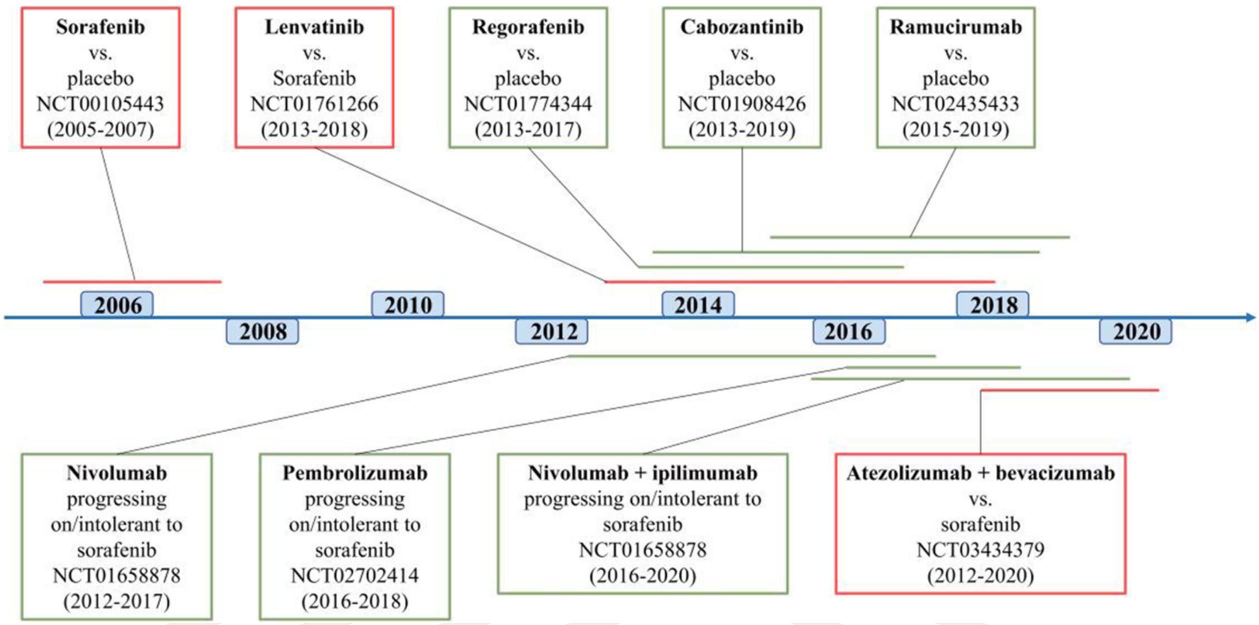

Figure 1. The timeline of FDA-approved drugs for HCC treatment (12)

Although there are new therapy options, Sorafenib remains the most used and accepted drug in the treatment of HCC (2). However, due to resistant development, Sorafenib only benefits about 30% of patients. In 6 months, patients start to show poor progression against the Sorafenib treatment, which is associated with acquired resistance. On the other hand, poor tumor response to Sorafenib as first-line therapy is associated with intrinsic resistance (3). Drug resistance is one of the biggest challenges in treating tumors, and most patients develop insensitivity to drugs, which causes tumor relapse and treatment failure (14). Since Sorafenib is still the most used therapy agent, it is crucial to understand the mechanism underlying the development of resistance.

2.2. Mechanism of Sorafenib resistance in HCC

The exact molecular mechanism underlying Sorafenib resistance is still unclear, but there are numerous factors responsible for resistance development as signaling pathways activation, hypoxia, autophagy, epithelial-mesenchymal transition (EMT), long non-coding RNAs (lncRNAs), microRNAs (miRNAs), stemness, tumor microenvironment (TME), tumor metabolism, etc. (15)(16). Figure 2 represents the mechanism of Sorafenib resistance in HCC.

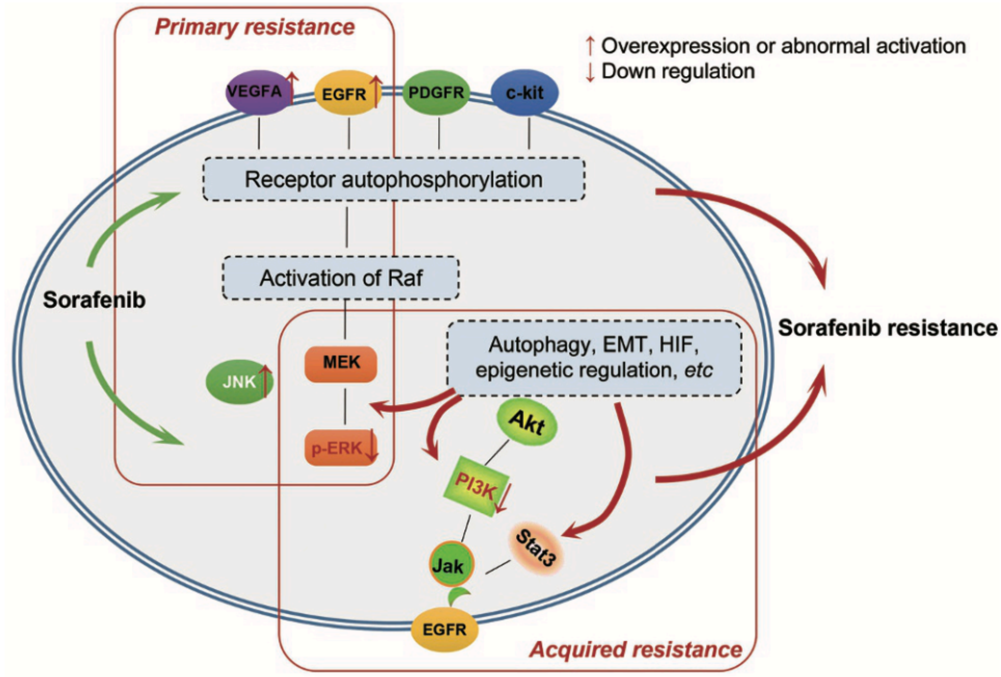

Figure 2. Mechanism of Sorafenib resistance in HCC (17)

Resistance mostly depends on the activation of growth factors and tyrosine kinases that are not targets of Sorafenib as a feedback mechanism (18).

<u>2.2.1. Sorafenib Resistance and c-Met</u>

Hepatocyte Growth Factor/Scattering Factor (HGF/SF) receptor c-Met is involved in the proliferation, survival, migration, and differentiation of epithelial cells. Met tyrosine kinase acquires its heterodimer structure by proteolytic cleavage of a single-chain precursor molecule and subsequent binding with a disulfide bond. A beta chain that passes through the membrane and an alpha chain that remains in the extracellular domain form the heterodimer structure of c-Met (Figure 3) (19).

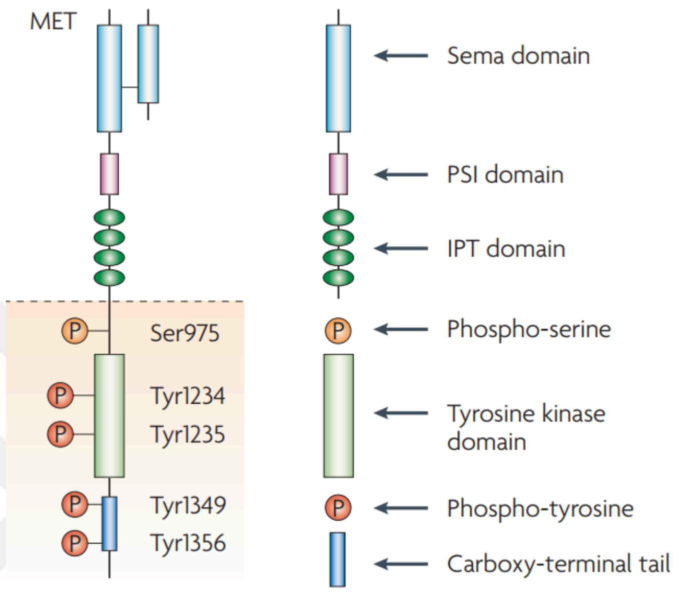

Figure 3. Protein structure of c-Met (20).

The HGF/c-Met signaling pathway is not active in healthy state cells but when liver damage occurs, it is activated. During hepatocarcinogenesis, c-Met becomes constitutively active, leading to the development of a more aggressive phenotype in cells (21). Our research group has been studying the molecular mechanism of c-Met tyrosine kinase activation in the development and progression of HCC, its downstream target molecules, other signal transduction pathways it interacts with, and the biological responses it elicits. Our previous studies showed that Sorafenib-resistant HCC cells have elevated c-Met activation and HGF expression (22). Our further studies showed that in addition to ligand-dependent activation, c-Met is activated in a ligand-independent manner through receptor crosstalk by external factors, including high glucose, hypoxia, heparin, and ROS (5)(23)(24)(25).

2.3. Caveolin-1 and its role in HCC

Known as one of the lipid raft types, caveolae are dynamic, small invaginations in the plasma membrane that are rich in cholesterol and sphingolipids, which have roles in endocytosis, cholesterol transport, and transcytosis. Cholesterol and sphingolipids in the structure give the membrane a more durable feature. The structure components are proteins such as Caveolin-1, Caveolin-2, Caveolin-3, Cavin-1, Cavin-2, Cavin-3, Cavin-4, EHD2, PACSIN2, Dynamin-2.

Caveolin-1 (Cav-1), a 21-24 kDa protein, is the core component of caveolae structure. The formation and dynamic regulation of caveolae structure is a multi-step process. The process begins with the oligomerization of the Cav-1 protein, which is synthesized as an integral membrane protein in the cytoplasm. Golgi carries Cav-1 to the membrane surface, where its conformation changes and binds to sphingolipids and cholesterol (26). Cavin proteins are responsible for the morphology of caveolae structure and bind to Cav-1, and together, they are critical for maintaining the caveolae dynamics. EHD2 is an ATPase, which is localized in the neck of caveolae and ensures the confinement of the structure to the membrane. PACSIN2 protein supports the structure with the BAR and SH3 domains (27) (28). Dynamin-2 is located in the neck part of the caveolae structure, and it is a GTPase that has a role in membrane fission and fusion processes (Figure 4) (29)(30). Caveolae present several different dynamics due to their function, such as stable caveolae, lateral moving caveolae on the membrane, “kiss and run” movement of caveolae with membrane, internalized caveolae, etc.

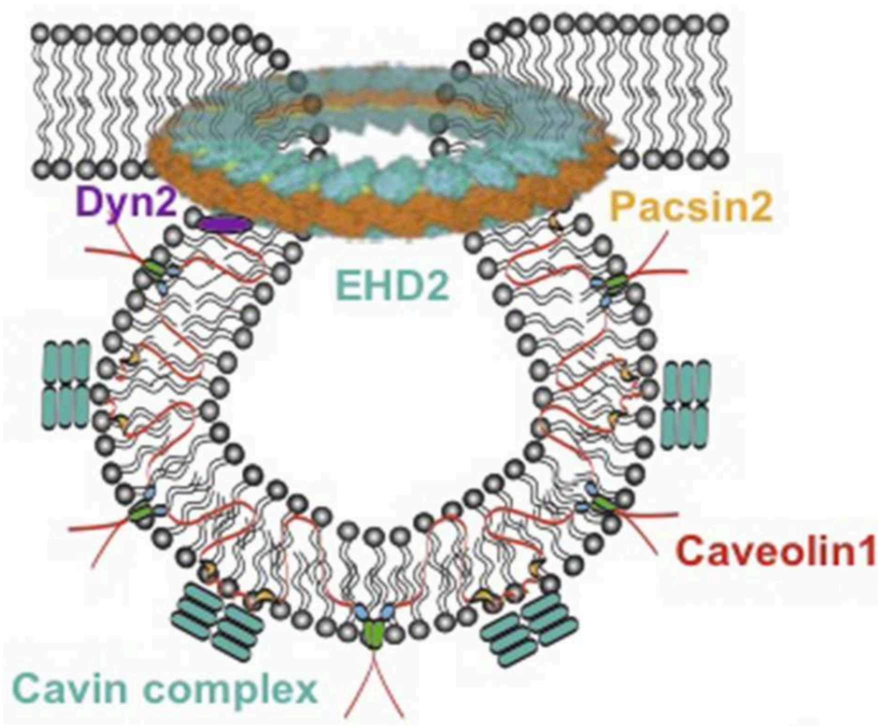

Figure 4. Caveolae structure and elements (31).

Caveolae structure is involved in signal transduction as well via activation of Cav-1 on its 14th tyrosine kinase in the presence of intracellular and/or extracellular stimuli (32). In this condition, Cav-1 undergoes a conformational change and exposes the domains to the receptors with which Cav-1 physically interacts (33). This activation creates a membrane region specialized for signal transduction, where receptors physically interact with intracellular and extracellular adaptor proteins. Activated Cav-1 signaling regulates biological processes such as cell-cell, cell-matrix mediated adhesion, cytoskeletal dynamics, cell survival, motility and anchorage-independent growth. In normal cells, when adhesion molecules that Cav-1 interacts with are eliminated, caveolae structure is internalized, and cells are driven to anoikis. However, when Cav-1 is overexpressed in cancer cells, they gain anchorage-independent growth ability (34). Cav-1 interacts with focal adhesion kinase (FAK) and actin filaments, activating stress fiber formation in mesenchymal cells (35). In hepatocarcinogenesis, Cav-1 is activated, and further activates PI3K/Akt, Erk1/2/MAPK, and IGF-1 signaling pathways and matrix metalloproteinases. Thus, cancer cells gain more metastatic potential and anchorage-independent growth capability (36)(37). Previous studies that were held in our group showed that overexpression of Cav-1 brings HCC cells more mesenchymal-like phenotype and anchorage-independent growth capability, which increases cell motility and invasion as a result (5). While performing these activities, Cav-1 is reciprocally activated via crosstalking with c-Met. Both c-Met and Cav-1 are activated and gain HCC cells more aggressive phenotype in motility, invasion, and branched morphogenic structure aspects (Figure 5).

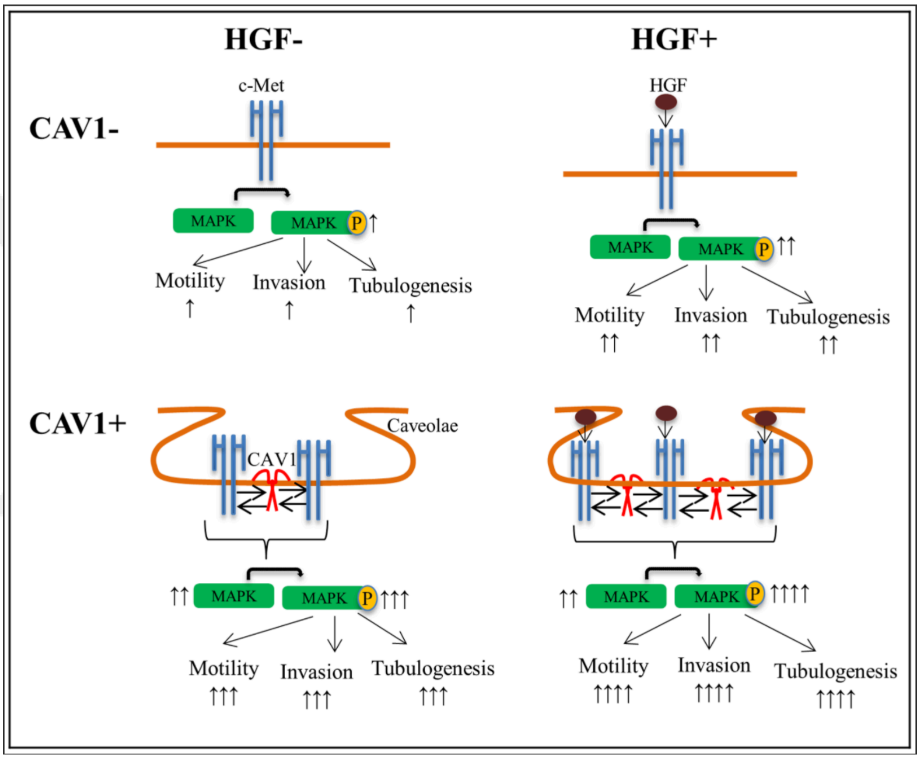

Figure 5. Biological responses of Cav-1 c-Met interaction (5)

2.4. Cav-1 and its effects on drug resistance

Cav-1 overexpression is associated with drug resistance in various cancer types. For instance, Cav-1 overexpression has a role in 5-FU-resistance in colon cancer cells (38), cisplatin-resistance in ovarian cancer cells (39), paclitaxel-resistance in lung cancer and breast cancer cells (40), etc. In gastric cancer cells, Cav-1 has a role in Wnt/β-Catenin activation, and together, they develop resistance to cisplatin (41). Cav-1 overexpression is observed mostly in multi-drug resistant (MDR) cells and their relationship is linked to the role of Cav-1 in cholesterol transport which is crucial for drug delivery (42). All these studies made us think that Cav-1 might have a role in Sorafenib resistance in HCC cells. We know that c-Met has an effect on Sorafenib resistance and aggressive phenotype in HCC cells and Cav-1 has an effect on aggressive phenotype together with c-Met. Since previous studies of ours and others supported the potential impact of Cav-1 on Sorafenib resistance in HCC, in this thesis, we aimed to elucidate the mechanism of Sorafenib resistance in HCC.

2.5. miRNAs and their roles in Sorafenib resistance

miRNAs are endogenous, single-stranded, short non-coding RNA molecules and mostly they have 19-24 nucleotides (nt) length. miRNAs bind to the 3′ untranslated region (3′ UTR) of their target mRNA transcripts and regulate their gene expression in this way. miRNAs are recognized to be significant in biological processes, cancer and the regulation of gene expression (6). Defects in miRNA regulation in tumor tissues and microenvironment are counted as a hallmark of cancer (7). miRNAs have both tumor suppressor and oncogenic features. By regulating their targets' expression levels, miRNAs have the potential to bring cancer cells more aggressive phenotype. miRNAs can be altered during drug treatment and these alterations affect the therapy response (8). miRNA biogenesis consists of several steps until generation of a mature miRNA. RNA polymerase II transcribes pri-miRNA which is around 1-4 kb primary transcript. Then, a nuclease called Drosha/DGCR8 crops the single-stranded sequences near the double-stranded stem-loop structure of pri-miRNA which turns precursor of pre-miRNA has around 70-nt length by this action. With the help of Exportin-5, pre-miRNA is transported from the nucleus to the cytoplasm and another nuclease Dicer in the cytoplasm cleaves the loop of the stem-loop structure and generates a miRNA-duplex. One of the strands, which is a guide strand, is loaded into the cytoplasmic RNA-induced silencing complex (RISC) and the other one is degraded. Depending on the complementary level between the miRNA and its target where they interact in the 3′ untranslated region (3′ UTR) of the target mRNA, translation repression happens or the target mRNA is cleaved. In perfect complementarity, mRNA cleavage happens and it is degraded at the end, whereas in imperfect complementarity, translation is repressed (Figure 6) (43).

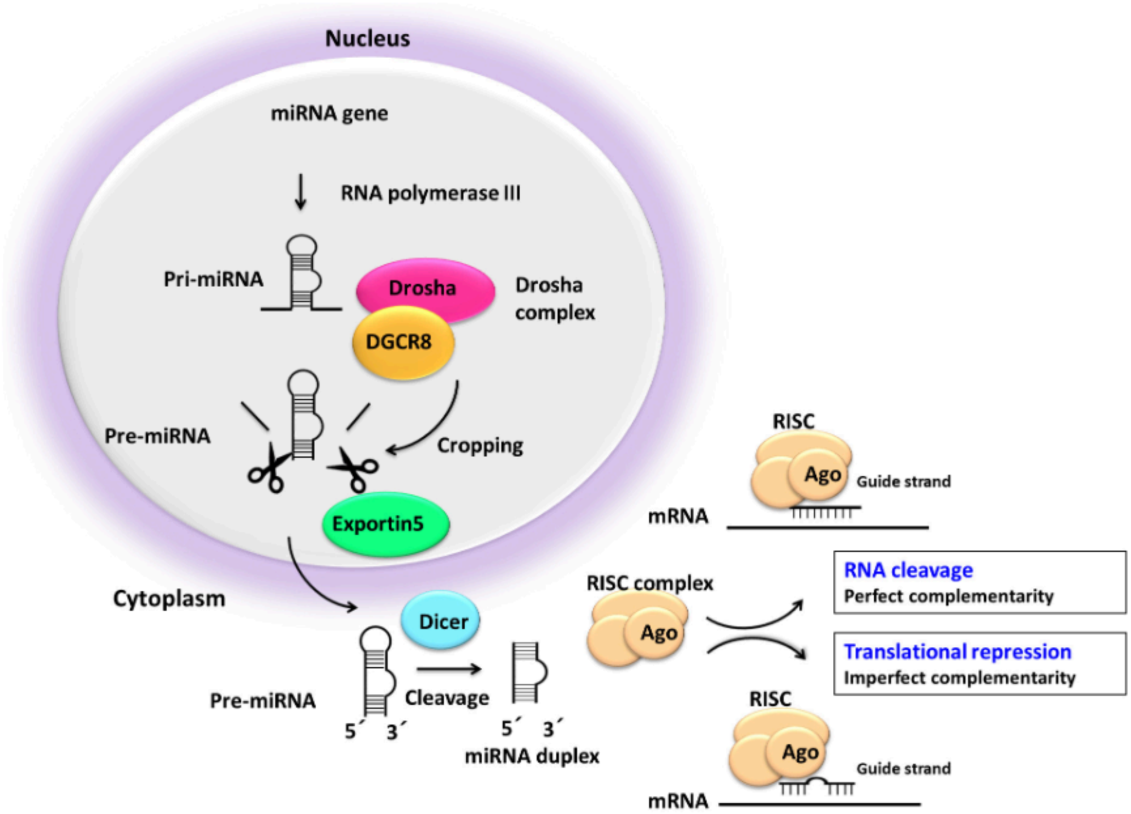

Figure 6. miRNA biogenesis (44)

With their highly conserved character and their essential functions in the regulation of various pathways, miRNAs are counted as potential biomarkers in HCC (45). Although miRNAs are only 1-3% of all human genome, they regulate 33% of human protein-coding genes (46). The effect is massive, and they are essential molecules in various biological functions. miRNAs have leading roles in proliferation, invasion, apoptosis, differentiation, metastasis, angiogenesis, metabolic reprogramming and drug resistance in HCC (47). In previous studies held in our group, we demonstrated miR-181a-5p targets c-Met and this leads to suppression of motility, invasion and branching morphogenesis in HCC, but generally, it is downregulated in HCC (48). Alterations in the miRNA levels in cancer may dramatically impact the susceptibility of the drug, as well (14). For instance, in Doxorubicin (Dox) resistance, there is a lack of capacity of Dox to accumulate in the nucleus that reduces DNA damage and this leads to prevent signal transduction of DNA damage into apoptosis. Additionally, in Sorafenib resistance, numerous complex genetic and epigenetic alterations happen and miRNAs are thought to regulate resistance by participating in some canonical drug resistance pathways. Genetic heterogeneity of HCC is thought to be the leading cause of primary resistance but the exact mechanism is not elucidated yet (49). As mentioned above, miRNAs are counted as one of the factors responsible for the development of Sorafenib resistance in HCC. Many oncogenic miRNAs can promote Sorafenib resistance, whereas with several tumor suppressor miRNAs, Sorafenib resistance can be overcome (50). A summary of some miRNAs and their role in Sorafenib resistance is given below (Table 1).

Table 1. List of miRNAs and their role in Sorafenib resistance (51).

miRNAs	Expression	Effects on sorafenib resistance	Target	Mechanism
miR-423-5p	up-regulated	Inhibiting	GADD45B	autophagy
miR-142-3p	down-regulated	Promoting	HMGB1, ATG5, ATG16L1	autophagy
miR-221	up-regulated	Promoting	Caspase-3	apoptosis
miR-541	down-regulated	Inhibiting	ATG2A/RAB1B	autophagy
miR-30e-3p	down-regulated	Promoting	TP53/MDM2, EpCAM, PTEN, p27	CSCs
miR-486-3p	down-regulated	Inhibiting	FGFR4, EGFR	AKT activation
miR-122	down-regulated	Inhibiting	SERPINB3	HIF-2α/CSCs
miR-30a-5p	down-regulated	Inhibiting	CLCF1	AKT activation
miR-1226-3p	down-regulated	Inhibiting	DUSP4	JNK-Bcl-2 axis
miR-552	up-regulated	Promoting	PTEN	AKT activation
miR-124	down-regulated	Inhibiting	CAV1	CSCs
miR-181a	up-regulated	Promoting	RASSF1	MAPK
miR - 222	up-regulated	Promoting	PI3K/AKT	AKT activation
miR-378a-3p	down-regulated	Inhibiting	IGF-1R	EMT
miR-744	down-regulated	Inhibiting	PAX2	EMT
miR-374b	down-regulated	Inhibiting	hnRNPA1/PKM2	glycolysis
miR-21	up-regulated	Inhibiting	PTEN	AKT activation
miR-375	down-regulated	Inhibiting	AEG-1	AKT activation
miR-223	down-regulated	Promoting	FBW7	apoptosis
miR-145-5p	down-regulated	Inhibiting	HDAC11	metabolism
miR-96	up-regulated	Promoting	TP53INP1	apoptosis
miR-494	up-regulated	Promoting	p27, puma, PTEN, mTOR	AKT, CSCs
miR-21-5p	down-regulated	Inhibiting	EZH2	NOTCH1
miR-26a-1-5p	down-regulated	Inhibiting	EZH2	NOTCH1
miR-3609	down-regulated	Inhibiting	EPAS-1	metabolism
miR-101/122/125b/139	up-regulated	Promoting	IGF1R	apoptosis
miR-193b	down-regulated	Inhibiting	Mcl-1	apoptosis
miR-1	down-regulated	Inhibiting	PD-L1	apoptosis
miR-137	down-regulated	Inhibiting	ANT2	CSCs
miR-216a/217	up-regulated	Promoting	PTEN, SMAD7	EMT

2.6. LncRNAs and their roles in Sorafenib resistance

LncRNAs are long RNAs in the class of non-coding RNAs with a length of more than 200-nt and they have no protein-coding capability. They appear in five types: sense, antisense, bidirectional, intronic and intergenic. Although they are called non-protein coding and seen as "by-products" or "dark matter", they have crucial roles in regulating the expressions of target genes by interacting with DNA, RNA and proteins and forming complexes. They can act in two ways: first, by interacting with RNA-binding proteins (RBPs) and second, by being a sponge for miRNAs and in these ways, they can be included in several biological processes such as proliferation, invasion, apoptosis, differentiation, metastasis, EMT transition and drug resistance, etc (50)(51). HOX transcript antisense intergenic RNA (HOTAIR) is a lncRNA and it has 2148-nt and is polyadenylated. HOTAIR regulates HOXD and it is located between HOXC11 and HOXC12. HOTAIR is known to be overexpressed in numerous cancer types such as breast cancer, cervical cancer, gastric cancer, colorectal cancer and HCC related to poor prognosis, invasiveness and aggressive behaviors of cancer (52). In our group, we showed that HOTAIR has a role in the downregulation of c-Met and stimulates the hybrid epithelial/mesenchymal (hybrid E/M) phenotype in HCC (53). In the hybrid E/M phenotype, tumor cells express mesenchymal and epithelial markers at the same time, and this phenotype gives tumor cells survival advantages, which are anchorage-independent growth ability, better metastatic ability, resistance to fluidic shear stress in circulation, collective migration ability and resistance to drugs, etc (54). Numerous studies have shown that lncRNAs and miRNAs interact to mediate drug resistance (50). Thus, lncRNAs join the potential mechanism of the drug resistance game in this way. A summary of some lncRNAs and their role in Sorafenib resistance is given below (Table 2).

Table 2. List of lncRNAs and their role in Sorafenib resistance (51).

lncRNAs	Expression	Effects on sorafenib resistance	Interact with	Target	Mechanism
SNHG1	up-regulated	Promoting	miR-21	SLC3A2	transfer
HANR	up-regulated	Promoting	miR-29b	ATG9A	autophagy
FAM225A	up-regulated	Promoting	miR-130a-5p	CCNG1	apoptosis
NEAT1	up-regulated	Promoting	miR-149-5p	AKT1	Akt activation
HEIH	up-regulated	Promoting	miR-98-5p	PI3K/AKT	Akt activation
SNHG16	up-regulated	Promoting	miR-140-5p	FEN1	EMT
KCNQ1OT1	up-regulated	Promoting	miR - 506	PD - L1	apoptosis
MALAT1	up-regulated	Promoting	miR-140-5p	Aurora-A	EMT
H19	up-regulated	Promoting	miR-675	miR - 675	EMT
FOXD2-AS1	down-regulated	Inhibiting	miR-150-5p	TMEM9	transfer
TTN-AS1	up-regulated	Promoting	miR-16-5p	cyclin E1	Akt activation
NEAT1	up-regulated	Promoting	miR-204 miR-335 miR-149-5p	ATG3 c-Met-AKT	autophagy apoptosis AKT activasion
POIR	up-regulated	Promoting	miR-182-5p	FOXF2	EMT
TUC338	up-regulated	Promoting	/	RASAL1	gluconeogenesis
VLDLR	up-regulated	Promoting	/	ABCG2	transfer

As we know, HOTAIR has a role in promoting hybrid E/M in HCC and hybrid E/M provides survival advantages to HCC cells; thus, one of the advantages of hybrid E/M might be promoting Sorafenib resistance in HCC. Moreover, miRNAs could be joined to this process by interacting with HOTAIR, thus contributing to Sorafenib resistance.

3. MATERIALS AND METHODS

3.1. Type of the research

This thesis is an experimental research.

3.2. Location and the time frame of the research

The research was carried out in the laboratories of Izmir Biomedicine and Genome Center (iBG) between September 2017 and February 2024.

3.3. Research population, sampling and experimental groups

No human studies were conducted in this research.

3.4. Research materials

In this research, HCC cells were kindly provided by Prof. Dr. Mehmet Öztürk, and they have been using for years in our group, which are HuH-7, Mahlavu, SNU-449, SNU-475, SNU-423, SNU-182, SNU-398, SNU-387, HEPG2, FOCUS, SK-HEP-1 and HEP3B. Additionally, Cav-1 overexpressing HuH-7-pCAV1 and its MOCK-transfected clones were obtained in our previous studies were used in this study. In this thesis period, HuH-7, Mahlavu, SNU-449 and HuH-7-pCAV1 Sorafenib resistant clones were generated. HOTAIR overexpressing SNU-449-HOTAIR and its MOCK-transfected clones were generated, as well. Zebrafish studies were held in Izmir Biomedicine and Genome Center, Güneş Özhan's laboratory and wild-type zebrafish embryos were used in this study.

3.5. Research variables

HCC cell lines and clones that were generated are independent variables, the dependent variables are their protein and RNA expression levels. Biological responses that were obtained from independent variables are dependent variables. The

Sorafenib dose is independent, and the response to Sorafenib is a dependent variable.

3.6. Data collection tools

3.6.1 Materials and Equipment

Table 3. List of chemicals, reagents and kits used in research

Chemicals/Supplements	Brand	Catalog Number
Dulbecco's Modified Eagle Medium(DMEM)	Biological Industries	01-050-1A
Fetal Bovine Serum (FBS)	Gibco	10500-064
Penicillin/Streptomycin (P/S)	Biological Industries	03-031-1B
L-Glutamine	Biological Industries	03-020-1B
Non-Essential Amino Acid Solution (NEAA)	Biological Industries	01-340-1B
Trypsin-EDTA(0.25%)	Biological Industries	03-052-1B
Dimethyl sulfoxyde(DMSO)	AppliChem	A3672,0100
Phosphate Buffered Saline(PBS),10X	Gibco	70011044
Trypan Blue 0.5% Solution	Biological Industries	03-102-1B
Aquaguard-1	Biological Industries	01-867-1B
Aquaguard-2	Biological Industries	01-916-1A
cOmplete ULTRA Tablets, Mini, EASYpack, Protease Inhibitor Coctail Tablets	Roche	05892970001
PhosSTOP EASYpack, Phosphatase Inhibitor Tablets	Roche	04906837001
Pierce™ BCA Protein Assay Kit	ThermoFisher Scientific	23227
PageRuler™ Prestained Protein Ladder	ThermoFisher Scientific	26616

Thick Chromatography Blotting Paper	Ahlstrom	2228-2020
Immobilon®-FL Transfer Membrane	Merck Millipore	IPFL00010
Phospho-Caveolin-1 (Y14) Primary Antibody	Cell Signaling Technology	3251S
Caveolin-1 (N20) Primary Antibody	Santa Cruz Biotechnology	sc-894
Phospho-Met (Y1234/1235) Primary Antibody	Cell Signaling Technology	3129L
Met (C-28) Primary Antibody	Santa Cruz Biotechnology	sc-161
Calnexin (H-70) Primary Antibody	Santa Cruz Biotechnology	sc-11397
IRDye® 680RD Goat anti-Rabbit Secondary Antibody	LI-COR	926-68071
IRDye® 800CW Goat anti-Mouse Secondary Antibody	LI-COR	926-32210
E-Plate 16	ACEA Biosciences,Inc.	05469830001
Sorafenib, 20 mg	SelleckChem	S7397
Thiazolyl Blue Tetrazolium Bromide (MTT)	Sigma Aldrich, Merck	M5655
NucleoZOL RNA isolation reagent	Macherey-Nagel (MN)	740404.200
RevertAid First Strand cDNA Synthesis Kit	Thermo Scientific	K1622
Luminaris Color HiGreen qPCR Master Mix, high ROX	Thermo Scientific	K0364
FuGENE® HD Transfection Reagent	Promega	E2312

Table 4. List of equipment used in research

Equipment Name	Brand	Catalog number
Class 2 Biosafety Cabinet	Thermo Scientific	51026638
CO_2 Incubator Galaxy 170 S	New Brunswick, Eppendorf	223100148
Water Bath	Nüve	Z10.NB
Inverted Phase Fluorescent Microscopy	Carl Zeiss	Axio Vert.A1
Centrifuge, for falcon tubes	Eppendorf	Z606936
Hemocytometer, Neubauer chamber	Marienfield Superior	0630010
Thermal Cycler	Applied Biosystems	A24812
Vortex	Thermo Scientific	88880018
Power Supply PowerPac^{TM} Basic	Bio-Rad	1645050
Western Blotting Electrophoration and Transfer System	Bio-Rad	1658029
ChemiDoc Imaging Device	Bio-Rad	
Magnetic Stirrer with heater	Thermo Scientific	SP88857105
xCelligence RTCA DP	Roche, ACEA Biosciences,Inc.	00380601050
Microplate Spectrophotometry	Thermo Scientific	51119200
Transilluminator Gel Doc^{TM} XR+	Bio-Rad	170-8195
Benchtop Orbital shaker	Thermo Scientific	SHKE4000
NanoDrop	Thermo Scientific	ND2000
Precision Balance	Sartorious	8221S
Microfuge	Thermo Scientific	75004061
Microcentrifuge	Thermo Scientific	75002450
Upright Immunofluorescence Microscopy	Olympus	BX61
Real Time PCR system 7500 Fast	Applied Biosystems	4351106
Digital Heating Shaking Drybath	Thermo Scientific	88880028

3.6.2. Media and Solutions

3.6.2.1. Cell culture

Complete medium	for 500 mL	Final concentration
DMEM	435 mL	1X
FBS	50 mL	10%
Penicillin/Streptomycine	5 mL	100U/ml / 0.1 mg/ml
L-Glutamine	5mL	2 mM
NEAA	5 mL	1%

Cell counting solution	Final volume
Trypan blue	2X
PBS	2X
Cell suspension	1X

Cell Freezing Medium	Final concentration
Complete medium	60%
FBS	30%
DMSO	10%

3.6.2.2. Protein isolation, protein electrophoresis and blotting

RIPA Lysis Buffer	Final concentration
Tris-Cl (pH=7.4)	50 mM
NaCl	150 mM
EDTA (pH=8.0)	1 mM
NP-40	%1
NaF	1 mM
Na_3VO_4	1 mM
Complete Mini Protease	1X

Inhibitor Coctail Tablet	
PhosSTOP Phosphatase Inhibitor Tablet	1X

10X PBS	for 1 L
NaCl	80 g
KCl	2 g
$NaHPO_4.2H_2O$	18.1 g
KH_2PO_4	2.4 g
dH_2O*	up to 1 L

* dH_2O was added until the total volume reached 1L and pH was adjusted to 7.4, diluted to 1X concentration by dH_2O if needed.

10X TBS	for 1 L
NaCl	80 g
KCl	2 g
Tris base	30 g
dH_2O*	up to 1 L

* dH_2O was added until the total volume reeached 1L and pH was adjusted to 7.4, diluted to 1X concentration by dH_2O if needed.

1.5 M Tris Solution

18.165 g Tris base was dissolved in dH_2O and final 100 mL solution was prepared and pH adjusted to 8.8

1 M Tris Solution

12.11 g Tris base was dissolved in dH_2O and final 100 mL solution was prepared and pH adjusted to 6.8

30% Acrylamide-Bisacrylamide Solution (29:1)

29 g Acrylamide and 1 g Bisacrylamide was dissolved in dH_2O and final 100 mL solution was prepared. Solution was filtered by 0.2 μm filter and stored in dark at 4 ^oC.

8% Resolving polyacrylamide gel	for 10 mL
H_2O	4.6 mL
30% Acrylamide-Bisacrylamide Solution	2.7 mL
1.5 M Tris (pH=8.8)	2.5 mL
10% SDS	0.1 mL
10% Ammonium persulfate (APS)	0.1 mL
TEMED	0.006 mL

15% Resolving polyacrylamide gel	for 10 mL
H_2O	2.3 mL
30% Acrylamide-Bisacrylamide Solution	5 mL
1.5 M Tris (pH=8.8)	2.5 mL
10% SDS	0.1 mL
10% Ammonium persulfate	0.1 mL
TEMED	0.004 mL

5% Stacking polyacrylamide gel	for 10 mL
H_2O	6.8 mL
30% Acrylamide-Bisacrylamide Solution	1.7 mL
1 M Tris (pH=6.8)	1.25 mL
10% SDS	0.1 mL
10% Ammonium persulfate	0.1 mL
TEMED	0.01 mL

Run Buffer	for 1 L
Tris base	3.075 g
Glycine	14.4 g
10% SDS	10 mL
dH_2O	up to 1 L

Transfer Buffer	for 1 L
Tris base	3.075 g
Glycine	14.4 g
10% SDS	2 mL
dH_2O	800 mL
Methanol	200 mL

Blocking Solution	for 10 mL	Final concentration
Bovine Serum Albumin (BSA) or skimmed milk powder (MP)	0.5 g	5%
TBS (1X)	10 mL	

Primary Antibody Solution	for 10 mL	Final concentration
Bovine Serum Albumin (BSA) or skimmed milk powder (MP)	0.3 g	3%
Tween-20	20 µl	0.2%
Primary Antibody	10 µl	1:1000 as optimized
TBS (1X)	10 mL	

Washing Solution	for 500 mL	Final concentration
Tween-20	500 µl	0.1%
TBS (1X)	500 mL	

Secondary Antibody Solution	for 50 mL	Final concentration
Bovine Serum Albumin (BSA) or skimmed milk powder (MP)	1.5 g	3%
Tween-20	100 µl	0.2%
SDS (10%)	50 µl	0.01%
Secondary Antibody	2.5 µl	1:20000
TBS (1X)	50 mL	

3.6.2.3. Proliferation assays

MTT Solution	for 10 mL	Final concentration
MTT	50 mg	5 mg/mL
PBS (1X)*	up to 10 mL	

* Solution was dissolved in dark and filtered by 0.2 µm filter and stored in dark at -20 ^{o}C.

3.6.3. Methods

3.6.3.1. Cell culture and passaging

HCC cell lines that were used in this study were kindly provided by Prof. Dr. Mehmet Öztürk and they have been used in our laboratory for a long time. These HCC cell lines were HuH-7, SNU-449 and Mahlavu (MV) cell lines. Cav-1 overexpressing HuH-7 cells (HuH-7-pCav1) and HOTAIR overexpressing SNU-449 cells (SNU-449-HOTAIR) were cloned in previous studies in our lab (5)(53). HuH-7 Sorafenib-resistant (HuH-7 SORRES), MV Sorafenib-resistant (MV SORRES) and SNU-449 Sorafenib-resistant cell (SNU-449 SORRES) clones were established in this study. All these HCC cells were cultured in DMEM media supplemented with 10% FBS, 1% Penicillin/Streptomycin, 1% L-Glutamine and 1% Non-essential amino acid solutions. All operations related to the cells were carried out in the laminar cabinet. Cells were incubated at 37 °C incubator supplemented with 5% CO_2. Passaging was performed when the cells reached 70% confluency. First, the cells were washed with sterile 1X PBS, and then Trypsin/EDTA 0.25% solution was used to detach the cells from the surface and from each other. Cells to which trypsin/EDTA was added were incubated at 37 °C, where enzyme activity is optimum until the cells detach from the surface. Trypsin activity was stopped by adding FBS at least three times the amount of Trypsin/EDTA added to detach cells. Cells were passaged into new plates in an appropriate density. When HuH-7-pCav1 and SNU-449-HOTAIR clones and their MOCK-transfected clones were thawed after freezing, first they were treated with 400 µg/ml Geneticin and 12 µg/ml Puromycin respectively for 4 days, and after selection, experiments were carried out by passage of resistant cells.

3.6.3.2. Establishment of Sorafenib resistant cell clones

To obtain sorafenib-resistant cells, their Sorafenib GI50 (Growth Inhibition 50) values should be increased. To do this, HuH-7, MV and SNU-449 cells were treated with Sorafenib continuously every 2 days and with increasing doses to mimic acquired resistance by continuous selection (55). They all became resistant up to 8 µM Sorafenib concentration. When cells were thawed after freezing, they were treated with Sorafenib again continuously and treatment was stopped one passage before the experiment.

3.6.3.3. Cell counting

After washing the cells with 1X PBS and resuspending the cells with Trypsin/EDTA, 100 µl of cell suspension was transferred to a tube that already contained 200 µl of Trypan blue and 200 µl of 1X PBS. From this mixture, 10 µl was added to each of the two regions of the Neubauer slide and 10 areas were counted hemocytometrically.

Total cell number in 1 mL = $\frac{cells\ counted\ X\ dilution\ factor}{areas\ counted\ in\ Neubauer\ slide}$X 10^4

Once the cells were calculated, the desired number of cells was seeded into plates.

3.6.3.4 Cell thawing and freezing

1. The cells, which were stored in cryovials in liquid nitrogen tanks, were taken out and thawed rapidly in a water bath at 37 °C.
2. The thawed cell suspension was transferred to a 15 ml falcon containing 5 ml of complete DMEM medium and centrifuged at 1500 rpm for 5 minutes.
3. After the supernatant was removed, the cell pellet was resuspended with 5ml of complete DMEM media, and cells were seeded in an appropriate flask according to the cell pellet size.
4. The flask was placed into an incubator and checked after 24 hours. When cells reached 70% confluency, cell passaging was performed.

Cell freezing was performed when there were remaining cells from the experiment or stocking was necessary for those cells.

1. Cells were washed with 1X PBS and detached with Trypsin/EDTA. Resuspended cell suspension with complete DMEM was transferred to a 15 ml falcon and centrifuged at 1500 rpm for 5 minutes.
2. After the supernatant was removed, the cell pellet was resuspended with the freezing media, which contains 60% complete DMEM, 30% FBS and 10% DMSO and transferred to cryovials.
3. The cryovials were placed into Mr.Frosty freezing box, which has isopropanol inside and around and helps cooling process proceed slowly. Mr. Frosty with cells were incubated overnight at -80 °C then they were transferred into a liquid nitrogen tank.

3.*6.3.5 Total RNA isolation*

For total RNA isolation NucleoZol reagent (Macherey Nagel) has been used.

1. 600000 cells were seeded into 60 mm^2 dish.

2. When cells were reached 70% confluency, cells were washed with 1X PBS.
3. 1 mL Nucleozol reagent were added to the dish onto cells and were lysed with pipetting up and down.
4. Lysate was transferred to eppendorf tube.
5. 400 µl nuclease free water added to lysate and shake vigorously for 15 seconds.
6. Lysate was incubated for 10 minutes at room temperature.
7. Lysate was centrifuged at 12000 x g for 15 minutes at room temperature.
8. There would be two phases after centrifugation. The upper phase, which is called supernatant, was transferred into a new tube, and 1 mL isopropanol was added to the supernatant to precipitate RNA.
9. In this step, overnight incubation of the samples at -20 °C is recommended.
10. After overnight incubation, samples were centrifuged at 12000 x g for 10 minutes at room temperature.
11. The supernatant was discarded, and RNA pellet was washed with 1 mL 75% ethanol and then centrifuged at 8000 x g for 3 minutes.
12. The supernatant was discarded, and the washing step was repeated.
13. The RNA pellet was dried by waiting around 20 minutes upside down on tissue paper.
14. The RNA pellet was dissolved with around 20-50 µl nuclease-free water according to the size of the pellet.
15. The tubes were put into a heat block at 65 °C for 10 minutes for better dissolution.
16. RNA concentration and purity were measured by NanoDrop (Thermo).

3.*6.3.6 miRNA reverse transcriptase polymerase chain reaction (RT-PCR)*

Within the total RNA isolation, small RNAs were isolated as well, including miRNAs. RT-PCR method was used to make complementary DNA from the miRNAs that we isolated. TaqMan™ probe system (TaqMan™ microRNA assay, 4440887) (TaqMan™

microRNA reverse transcription kit, 4366596) was used to make cDNAs from just the desired miRNA because of the expressional issues in the whole RNA pool.

<u>Components per reaction</u>	<u>Volume per reaction</u>
dNTP	0.15 µl
Reverse transcriptase	1 µl
10X RT buffer	1.5 µl
RNase inhibitor	0.19 µl
Nuclease free H_2O	up to 15 µl
20X RT primer	0.75 µl
RNA	10 ng

Reaction mixture was prepared and placed into thermal cycler and started incubation protocol for 30 minutes at 16 °C, for 30 minutes at 42 °C, for 5 minutes at 85 °C. When the reaction finished, cDNA samples can be stored at -20 °C.

3.*6.3.7 Quantitative real time polymerase chain reaction for TaqMan™ miRNA assay (qPCR)*

In order to detect and quantitate miRNA, TaqMan miRNA assay was used. By using this assay, the problem in miRNA quantitation was overcome which was the short length of mature miRNAs (~22 nucleotides) prevents the conventional design of a random-primed RT step followed by a specific real-time assay. Thus, TaqMan miRNA assays use a target-specific stem loop reverse transcription primer, which creates RT primer/mature miRNA couple that provides specificity for only the mature miRNA target (Figure 7).

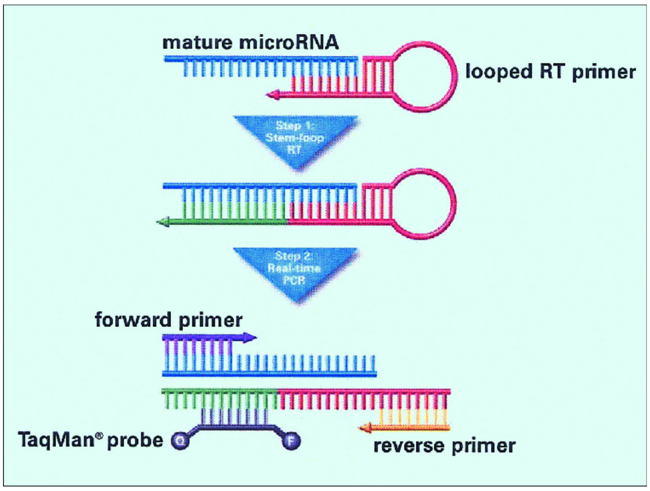

Figure 7. TaqMan probe system

Components per reaction	Volume per reaction
20X TaqMan miRNA assay	1.5 µl
2X PCR mastermix (no UNG) (Thermo 4440040)	15 µl
cDNA	3.99 µl
Nuclease free H_2O	9.51 µl for total 30 µl distribute 10 µl in each well

Reaction mixture was prepared for triplicate conditions in one tube and distributed 10 µl in each three well of the PCR plate. RNU6B was used as an endogenous control. Once all the conditions were added to PCR plate, it was sealed and spinned to ensure all the liquid at the bottom of the plate. Then the plate was placed into ABI 7500 Fast device and reaction was performed as described below.

Step	Temperature	Time	Cycles
Enzyme activation	95 °C	10 minutes	1
Denaturing	95 °C	15 seconds	40
Annealing/Extension	60 °C	60 seconds	

3.*6.3.8 Reverse transcriptase polymerase chain reaction (RT-PCR)*

RT-PCR was performed in order to make cDNA from total RNA that was isolated previously. RevertAid First Strand cDNA synthesis kit (Thermo K1622) was used.

Components per reaction	Volume per reaction
Oligo DT	1 µl
Random hexamer	1 µl
dNTP	2 µl
Reverse transcriptase	1 µl
5X reaction buffer	4 µl
RNase inhibitor	1 µl
RNA	1000 ng
Nuclease free H_2O	up to 20 µl

First, oligo Dt and random hexamer were added to the 1000 ng RNA and nuclease free H_2O mixture and incubated at 65 °C for 5 minutes. Then, the tubes were chilled on ice for 10 minutes. The rest of the reaction mixture was prepared and placed into a thermal cycler, and the incubation protocol started: for 5 minutes at 25 °C, for 60 minutes at 42 °C, and for 5 minutes at 70 °C. When the reaction finished cDNA samples can be stored at -20 °C.

3.*6.3.9 Quantitative real time polymerase chain reaction (RT-qPCR)*

RT-qPCR reaction was performed using the cDNAs and custom-synthesized primers specific to the genes we were interested in. Primers were designed for a gene-specific region of the coding DNA sequence (CDS) from NCBI-Gene bank, with a length of 20-25 bases, a binding temperature of 60-61 °C, and a GC base ratio of 50-55%. The primers used for the qPCR reaction are shown in the table below. RPL41 was used as the reference gene.

Table 5. List of primers used for the Quantitative Real-Time PCR reaction

Primer name	Forward Primer Sequence	Reverse Primer Sequence
CAV1	TGAGCGAGAAGCAAGTGTACG	CTGTGTGTCCCTTCTGGTTCT
MET	TGGGCACCGAAAGATAAACCT	TCTCGGACTTTGCTAGTGCC
RPL41	GAAACCTCTGCGCCATGA	TCTTTCTTCTTTTGCGCTTCA
HOTAIR	GGTAGAAAAAGCAACCACGAAGC	ACATAAACCTCTGTCTGTGAGGTCC
CDH1	TACACTGCCCAGGAGCCAGA	TGGCACCAGTGTCCGGATTA
CDH2	ATTGGACCATCACTCGGCTTA	CACACTGGCAAACCTTCACG
VIM	CCTTGACATTGAGATTGCCACCTA	TCATCGTGATGCTGAGAAGTTTCG
CTNNB1	GCTGGGACCTTGCATAACCT	TCCACTGGTGAACCAAGCAT
HPRT1	TGGCGTCGTGATTAGTGATG	GACGTTCAGTCCTGTCCATA

Reaction mixture was prepared by using Luminaris Color HiGreen qPCR master mix high ROX (Thermo K0364) and was performed by ABI 7500 Fast real-time thermal cycler. Melting curve analysis was added to the reaction protocol.

Components per reaction	Volume per reaction
2X master mix	5 µl
10 µM forward primer	0.3 µl
10 µM reverse primer	0.3 µl
cDNA	10 ng
Nuclease free H_2O	up to 10 µl

Step	Temperature	Time	Cycles
UDG pre-treatment	50 °C	2 minutes	1
Initial denaturation	95 °C	10 minutes	1

Denaturation	95 °C	15 seconds	40
Annealing/Extension	60 °C	60 seconds	

3.*6.3.10 Total protein isolation*

1. 1500000 cells were seeded into 100 mm^2 dish.
2. When they reached 70% density, they were taken from the incubator and placed on ice.
3. Cells were washed three times with ice-cold 1X PBS, which contains 0.1 mM NaF and 0.1 mM Na_3VO_4 protease inhibitors.
4. Cells were scraped with a cell scraper and transferred to 1.5 mL Eppendorf tubes.
5. Cells were centrifuged at 1500 rpm for 5 minutes at 4 °C.
6. Supernatant was removed, and RIPA buffer (RadioImmunoPrecipitation Assay Buffer, protocol written in 3.6.2.2) was added approximately 3 times the amount of the cell pellet to the tube. Tubes were incubated for 30 minutes on ice and vortexed every 3-4 minutes to be lysed well.
7. To remove cell debris, lysate was centrifuged at maximum speed at 4 °C for 20 minutes.
8. The supernatant was transferred to a new tube, and after quantification, lysate was stored at -80 °C.

3.*6.3.11 Protein quantification*

The amount of protein in the lysate was calculated by performing BCA (bicinchoninic acid) assay.

1. Different concentrations of bovine serum albumin (BSA) were used to create the standard graph.
2. BCA reagents A and B were mixed and added to the standard concentrations and the protein lysates that obtained and the reaction was started.
3. The reaction mixture was incubated at 55 °C for 15 minutes.

4. As a result of the reaction, the BCA/copper complex, which increased with the protein concentration, was measured spectrophotometrically at 562 nm.
5. The measurements obtained based on BSA concentrations were used to draw the standard graph. From the standard graph and its equation, the protein amount of the unknown samples was calculated.

3.*6.3.12 Protein electrophoresis on SDS-PAGE*

1. 8 ml of resolving gel (described in 3.6.2.2) was prepared according to the protein size of interest and added between the glasses in the casting. To avoid over-polymerization, the contact of the gel with air was blocked with isopropanol and waited until the gel was polymerized.
2. Meanwhile, 5% stacking gel (described in 3.6.2.2) was prepared, and after the lower gel was polymerized and isopropanol was removed, approximately 2 ml was added to the resolving gel, and a comb was placed and waited until it was polymerized.
3. From total protein lysate, 50-80 µg protein was transferred to a new tube and mixed with 4X loading buffer containing 20% beta-mercaptoethanol to denature the proteins. The volume of the samples should be equal before loading to gel and this could be done with lysis buffer.
4. The prepared protein samples were boiled at 95 °C for 10 minutes to complete denaturation.
5. The boiled protein samples were kept at room temperature until the loading process was started.
6. Run buffer was prepared (described in 3.6.2.2) and added into the electrophoresis tank, and after the gels were placed appropriately, the samples were loaded into the wells with long, thin pipette tips.
7. In order to visually follow protein migration, 4 µl of the prestained protein marker was loaded into an empty well.
8. First, 70 Volts (V) was applied to ensure that the stacking gel aligned the proteins.

9. After the samples passed the stacking gel, the proteins were run in the resolving gel with a voltage of 110 V until the bands on the marker were placed appropriately for the protein of interest.

3.*6.3.13 Transfer to the membrane, blocking, blotting and detection*

1. When the electrophoresis was finished, the gels were removed from the glass apparatus and soaked in the transfer buffer (protocol written in 3.6.2.2). Membrane and Whatmann papers were cut in the size of transfer cassettes size to fit properly.
2. The membrane was left in methanol for 1 minute to open its pores. It was then soaked in the transfer buffer to equilibrate.
3. A sandwich form was created by placing the sponge, Whatmann paper, gel, membrane, Whatmann paper and sponge on top of each other in the transfer buffer, keeping the black side of the cassette at the bottom.
4. The cassette was closed and placed into the transfer tank, which was filled with transfer buffer.
5. Transfer was performed for approximately 3 hours at 400 milliAmperes (mA). Since the current was very high and it would heat up immediately, we did not want the gel structure and, therefore, the protein structures to degrade. The ice box was placed in the transfer tank, and it was changed from time to time, avoiding of the buffer from overheated.
6. When the transfer process was completed, the membrane was incubated for one minute in TBS.
7. The membrane was placed in the falcon tube and incubated with rotation for 1 hour with the 5% blocking solution (described in 3.6.2.2) to prevent the antibody from recognizing non-specific regions and giving a false signal.
8. After blocking, membranes were incubated with the primary antibody solution (described in 3.6.2.2) overnight at 4 °C with rotation in a falcon tube so that the primary antibody could bind equally to all parts of the membrane.

9. The next day, the membrane was washed three times for five minutes each with 0.1% TBS-T solution (described in 3.6.2.2).
10. After washing, the secondary antibody that produces infrared radiation was selected to suit the animal for which the primary antibody was prepared (anti-mouse, anti-rabbit, etc.) and the secondary antibody solution was prepared (described in 3.6.2.2). The membrane was incubated with secondary antibody solution for two hours at room temperature with rotation in a falcon tube. Since a secondary antibody that produces infrared radiation was used, work in the dark from that point.
11. The membrane was washed five times for 5 minutes with 0.1% TBS-T solution.
12. The membrane was rinsed with TBS solution at the end before imaging.
13. Detection was done by the ChemiDoc imaging system from BioRad. Since this system has different fluorescent channels, it allows imaging of primary antibodies prepared for different channels simultaneously.

3.*6.3.14 Determination of cell viability by xCelligence*

By using the Roche xCelligence device, the proliferation rate of the cells and effect of Sorafenib on cell proliferation are examined. In this system, the surface where the cells adhere and proliferate is covered with a gold electrode. The adhesion of the cells and the area that the cells cover is measured by the resistance against an electric current called "Cell index". For this assay, E-plates were used which have the electrodes at the bottom surface.

1. E-plates were placed on the “assembly tool” and 30 µl medium was added to each well of the E-plate.
2. The plates were incubated for 30 minutes in the incubator for the equilibrium and after that E-plate was inserted into the device, and measured the background value.
3. 3.000 cells were seeded in each well, and at least one well was left with only medium for blank measurement.

4. The E-plates were inserted into the device again and set to measure the “cell index” every 15 minutes for 96 hours.
5. The next day, after the cells were attached the experiment was paused and Sorafenib was added to the wells according to the dose of the conditions, and then the experiment was resumed.
6. After 96 hours the experiment was finished and data was collected from the device to analyze.

3.*6.3.15 Determination of cell viability by MTT assay*

MTT assay is a colorimetric test that tests cell metabolic activity. NAD(P)-H dependent cellular oxidoreductase enzymes are expressed in living cells. These enzymes reduce the tetrazole dye MTT in living cells and transform it into an insoluble formazan dye. This formazan is soluble in DMSO and acquires a purple color. This colored solution is measured spectrophotometrically to test the viability and determine the Sorafenib IC50 of the cells.

1. 2000 cells were seeded into wells of 96-well plate with 200 µl medium.
2. After 24 hours, the drug of interest which is mostly Sorafenib to us were added to wells in increasing doses in each condition.
3. 24, 48 and 72 hours after the dose addition, experiment was stopped by adding 15 µl MTT solution (described in 3.6.2.3) to each well of 96-well plate.
4. Cells to which MTT solution was added were incubated in the incubator for 4 hours in the dark.
5. After 4 hours, the solution in the wells was removed and 100 µl DMSO was added to the wells, gently shaking for 15 minutes in the dark to ensure that the formazan was thoroughly dissolved and mixed.
6. The absorbance of the wells was measured spectrophotometrically at 570 nm, and the "background" value was measured at 720 nm.

3.6.3.16 Boyden chamber motility assay

Boyden chamber assay is an in vitro cell motility testing assay that includes inserts which can be inserted in each well of 24-well plate. Each insert has a PET membrane with pores that cells can move through the membrane that represents its motility.

1. 24-well plate was taken and 750 μl 10% FBS-containing medium was added to the wells of the plate.
2. Inserts which have pores in 8 μm diameter were placed into the wells carefully trying to avoid making bubbles between the membrane and the medium.
3. In each insert, 10000 cells (for SNU-449) were seeded with 500 μl 2% FBS-containing medium.
4. After 24 hours, the experiment was finished and cells in the inserts were fixed with a fixative containing methanol.
5. Then, eosin staining, which stains the cytoplasm the basic part of the cell, and hematoxylin staining, which stains the nucleus the acidic part, were performed. The inserts were passed through distilled water and the cells that did not pass through the insert membrane were cleaned with a Q-tip.
6. The remaining cells which passed through the membrane were counted under the microscope for each condition.

3.6.3.17 2D-Colony formation assay

1. 24-well plate was taken and 300 cells were seeded in each well and ensured that cells were single cells under the microscope.
2. Cells were cultured around 10 days and their medium was changed every three days.
3. After colonies get bigger and still distinct, experiment was finished.
4. First, the medium in the wells were removed and cells were washed with 1X PBS twice.
5. Then, cells were fixed with cold 1:1 Acetone : Methanol fixative solution and waited at -20 °C for 20 minutes with fixative.

6. Fixative was removed and cells were stained with 20% Giemsa staining solution at room temperature for 30 minutes.
7. Staining solution was removed and cells were washed with distilled water until the excess stain was removed.
8. The plate is left at room temperature for air drying.
9. Cells were imaged by BIO-RAD Gel Doc™ XR+Gel Documentation System and analyzed by ImageJ Colony Area plug-in.

3.*6.3.18 miRNA transfections*

SNU-449 and MV cells were transiently transfected with miRNA mimics and inhibitors for overexpressing and repressing miRNA levels in the cells, respectively.

1. 500000 cells were seeded into a 60 mm^2 culture dish.
2. The next day when cells were attached, 100 nM miR-181a-5p-mimics (Ambion, MC10421) or 100 nM miR-181a-5p-inhibitor (Ambion, MH10421) and their control mimics and inhibitor (Ambion, AM:17010) transfected to cells by Fugene HD transfection reagent (Promega, E2312).
3. After 24 hours of transfection, cells were used in biological assays or isolated in RNA or protein.

3.*6.3.19 Silencing experiments with Cav-1 targeting siRNA*

1. Cells were seeded into culture dishes and cultures until 80% of confluency was reached.
2. Before transfection medium was changed to 5% FBS-containing medium without antibiotics.
3. 5 nM scrambled siRNA (LSG-4390844) and 10 nM Cav-1 siRNA (LSG-4390826, s2448) were transfected to cells by Lipofectamine RNAimax transfection reagent (Thermo LSG-13778150).
4. After 48 hours of transfection, cells were used in biological assays or isolated in RNA or protein.

3.*6.3.20 Retroviral cloning and generating HOTAIR overexpressing stable cell lines*

SNU-449 cells were chosen to overexpress HOTAIR and viral particles containing retroviral vectors were introduced into SNU-449 cells.

1. Viral particles are generated through transfection of HEK-293T cells with VSV-G envelope protein expressing vector (5 µg), gag-pol expressing vector (5 µg) and retroviral target vectors (LZRS-HOTAIR and LZRS-IRESGFP) (5 µg) by Roche X-tremeGENE^{TM} HP DNA transfection reagent.
2. 24 hours after transfection medium was changed and again after 24 hours which is 48 hours after transfection the medium was collected and filtered for infection of the cells.
3. SNU-449 cells were infected with 1:1 collected retrovirus medium : fresh medium mix.
4. 48 hours after infection SNU-449 cells were selected with the selective antibody which is puromycine for these vectors. 13 µg/mL puromycine was added to SNU-449 cells and they were selected for at least 3 passages. They were called polyclone cells afterwards.
5. For monocloning, cells were seeded as a single cell into a plate to generate colonies from a single cell. Then these colonies were picked and cultured and at the end, they were called monoclonal stable cell lines (53).

3.*6.3.21 Immunofluorescence microscopy sample preparation*

1. Cells were seeded on coverslips in the 24-well plate as 10000 cells in each well.
2. The next day when cells were attached, they were washed with 1X PBS for 3 times on ice.

10. Cells were fixed with cold 1:1 Acetone : Methanol fixative solution at -20 °C for 20 minutes.

3. Fixative solution was removed and cells were washed with 1X PBS.
4. Cells were blocked with 1% BSA/0.05% TritonX/1X PBS solution at room temperature for an hour.

5. Cells were incubated with antibody binding solution containing 0.5% BSA/0.05% TritonX/1X PBS and the antibody of interest in its optimized concentration (Cav-1;1/200 c-Met;1:100) at room temperature for 2 hours.
6. Cells were washed with 0.1%TritonX/1X PBS solution 6 times for 5 minutes.
7. Cells were incubated with antibody binding solution which contains 0.5%BSA/0.05%TritonX/1X PBS and the secondary antibodies in the dilution of 1/2500 (goat anti-mouse Alexa 488 (A11001 Invitrogen) and/or goat anti-rabbit Alexa 594 (A11037 Invitrogen)) at room temperature for an hour.
8. Cells were washed with 0.1% TritonX/1X PBS solution 6 times for 5 minutes.
9. Cell nuclei were stained with DAPI solution for 5 minutes and washed with H_2O.
10. Coverslips were placed onto slides and mounted by Dako Fluorescence Mounting Medium (S3023).
11. Images were taken under the Olympus BX61 upright fluorescence microscope with 40X objective.
12. Some images were taken under confocal microscope (Zeiss LSM880) with 20X and 63X objectives.

3.*6.3.22 Phalloidin staining*

1. Cells were seeded on coverslips in the 24-well plate as 10000 cells in each well.
2. The next day when cells were attached, they were washed with 1X PBS for 2 times.
3. Cells were fixed with 4% paraformaldehyde (PFA) fixative solution at room temperature for 30 minutes.
4. Cells were permeabilized with 0.1%TritonX/1X PBS solution for 10 minutes at room temperature.
5. If cells were co-stained with another antibody, they were blocked with 1%BSA/0.05%TritonX/1X PBS solution at room temperature for 30 minutes.

6. Cells were incubated with antibody binding solution which contains 0.5%BSA/0.05%TritonX/1X PBS and with Phalloidin working solution (Abcam Phalloidin 555, #176756), and an antibody of interest if co-staining would be performed, for 90 minutes at room temperature.
7. Cells were washed with 0.1%TritonX/1X PBS solution 6 times for 5 minutes.
8. If co-staining were performed secondary antibody treatment was applied except for Phallodin since it is pre labelled.
9. Cell nuclei were stained with DAPI solution for 5 minutes and washed with H_2O.
10. Coverslips were placed onto slides and mounted by Dako Fluorescence Mounting Medium (S3023).
11. Images were taken under the Olympus BX61 upright fluorescence microscope with 40X objective.

3.*6.3.23 Fluorescent In-Situ Hybridization (FISH)*

1. Cells were seeded on coverslips in the 24-well plate as 10000 cells in each well.
2. The next day after seeding, cells were fixed with 3:1 methanol:acetic acid fixative solution for 10 minutes.
3. HOTAIR mRNA was hybridized using Stellaris FISH probes Human HOTAIR Quasar 570 Dye (LGS Technologies VSMF-2178-5) with 500 nM HOTAIR targeting probes at 37 °C for 4 hours.
4. Cell nuclei were stained with DAPI solution for 5 minutes and washed with H_2O.
5. Coverslips were placed onto slides and mounted by Dako Fluorescence Mounting Medium (S3023).
6. Images were taken under confocal microscope (Zeiss LSM880) with 20X and 63X objectives.

3.*6.3.24 Electron microscopy sample preparation*

1. 800000 cells were seeded in 100 mm^2 culture dish and cultured until 70% confluency was reached which represents 48 hours.
2. Cells were washed with Cacodylate buffer (0.1 M, pH=7.4) for 3 times.
3. Cells were fixed with freshly prepared fixative (500 µl 25% glutaraldehyde solution, 1 mL 25% PFA solution, 8.5 mL cacodylate buffer, 2.2 mg $CaCl_2$) for 72 hours at 4 °C.
4. Cells were scraped and transferred into a tube and centrifuged at 2500rpm for 5 minutes.
5. Pellet in fixative solution was sent for sectioning and imaging to Medipol University REMER center. In there, cell pellets were embedded in Epon 812 and then sectioned in 60 nm and analyzed and imaged by Zeiss Gemini 500 microscope and STEM detector.

3.*6.3.25 Zebrafish xenograft assay*

1. 800000 cells were seeded in a 100 mm^2 culture dish.
2. The following day cells were transfected with Cav-1 siRNA and scrambled siRNA for 48 hours.
3. After 48 hours cells were trypsinized and washed with 1X PBS.
4. Cells were stained with 2mg/mL DiL dye (Thermo V22885) for 20 minutes at 37 °C in dark.
5. Cells were first washed with FBS and then 1X PBS twice.
6. Cell pellet was diluted as 40000 cells/µl in 10% FBS in 1X PBS.
7. Approximately 100 cells were injected into the yolks of the 48-hour post-fertilization (hpf) of each wild-type zebrafish embryo.
8. After 4 hours, embryos were selected by successfully injected.
9. After 5 days, zebrafish were analyzed as with metastasis or no metastasis under the fluorescent stereomicroscope (Olympus SZX16).

3.7. Research plan and time-line

WP no	WP name		Years					
			2018	2019	2020	2021	2022	2023
1	The relationship between Sorafenib Resistance and Caveolin-1 expression	generating new Sorafenib-resistant clones of HuH-7, MV, and SNU-449 cell lines	X	X		X		
		determining Cav-1 transcript and protein expression levels in Sorafenib-resistant clones	X	X		X		
		testing the relationship between Cav-1 expression levels and SOR IC50 values	X	X		X	X	
		analyzing the alterations in the caveolar structures of Sorafenib-resistant cells			X	X	X	
		comparing adhesion, proliferation, EMT phenotype, motility, and invasion capabilities of Sorafenib-resistant clones with WT cells	X	X			X	X
		testing in vivo characteristics of Sorafenib-resistant cells in zebrafish embryos		X	X	X		
2	The relationship between Sorafenib Resistance and miR-181a-5p	understanding the influence of mir-34b-5p in Sorafenib resistance			X	X		
		understanding the influence of miR-181a-5p in Sorafenib resistance and Cav-1 expression level					X	X
		understanding the influence of miR-181a-5p in Sorafenib resistance via altering the expression levels of miR-181a-5p						X
3	The significance of HOTAIR in Cav-1/miR-181a-5p relationship	Understanding the role of HOTAIR in hybrid E/M phenotype in HCC cells	X	X			X	X
		Understanding the influence of HOTAIR in Sorafenib resistance, miR-181a-5p and Cav-1 expression levels						X
		testing contribution of HOTAIR-miR-181a-5p-Cav-1 axis in Sorafenib resistance.						X

3.8. Data analysis

GraphPad Prism 8 software was used for statistical analysis. Student's t-test was used when comparing two conditions, Analysis of Variance (ANOVA) was used when comparing more than two conditions and nonlinear regression was used when obtaining Sorafenib IC50 values. $p<0.05$ were considered as statistically significant.

3.9. Limitations of the research

1- Since Sorafenib treatment is applied to advanced stage and inoperable HCC patients, it is not possible to find primary tumor or liver tissues after treatment. Therefore, we could not confirm our data in patient samples and this is a limitation.
2- There is only one microarray dataset available for evaluating the response to Sorafenib treatment. The absence of another dataset to examine and validate the mechanisms involved in treatment response is another significant limitation.
3- Due to time and budget constraints, direct evidence for the interactions of Cav-1, miR-181a-5p, and HOTAIR could not be provided, which is another limitation.
4- Due to time and budget constraints, studies could not conducted with other small inhibitors which may increase Cav-1 expression and Cav-1 might have a role in resistance to this small inhibitor/s. Also, Cav-1 might have a role in therapy resistance in other cancer types besides HCC and we could not conduct a study for them which is another limitation.

However, the development of acquired Sorafenib resistance in 3 wild-type and one Cav-1 overexpressing cell lines, and performing experiments with Cav-1 silenced, Cav-1 overexpressing, and HOTAIR overexpressing cells, contribute to our data. Therefore, our data contains strong evidence regarding the relationship between Sorafenib treatment and Cav-1, as well as the regulation of this process by non-coding RNAs. In order to increase the impact of the study, advanced studies are planned to determine the physical interaction of Cav-1-miR-181a-5p-HOTAIR.

3.10. Ethical committee approval

This thesis study was unanimously decided as ethically appropriate to perform by IBG-HADYEK on 11/11/2020 with the protocol number 2020-038. The ethical committee approval form was attached.

4. RESULTS

4.1. The relationship between Sorafenib Resistance and Caveolin-1 expression

Sorafenib-resistant cells were generated by continuous treatment of Sorafenib in ascending doses. To determine their resistance level to Sorafenib, we performed the MTT assay in a dose and time-dependent manner. We generated new Sorafenib-resistant clones of HuH-7, MV, and SNU-449 cell lines. After performing the MTT assay, absorbance values were obtained and analyzed to determine Sorafenib IC50 values of the cells via *GraphPad Prism* (Figure 8). We observed that Sorafenib IC50 values were increased in all three resistant cell lines compared to their wild-type counterparts.

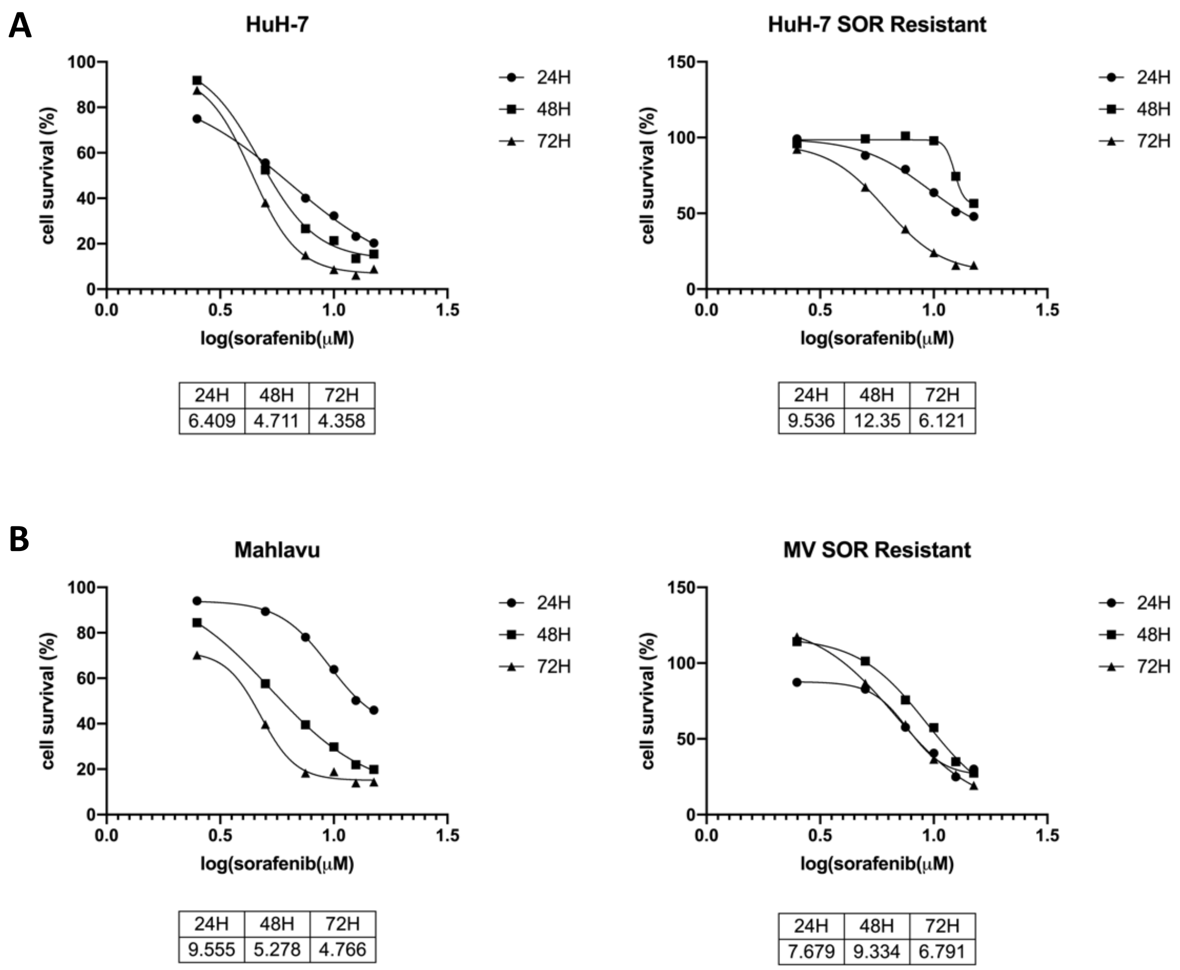

C

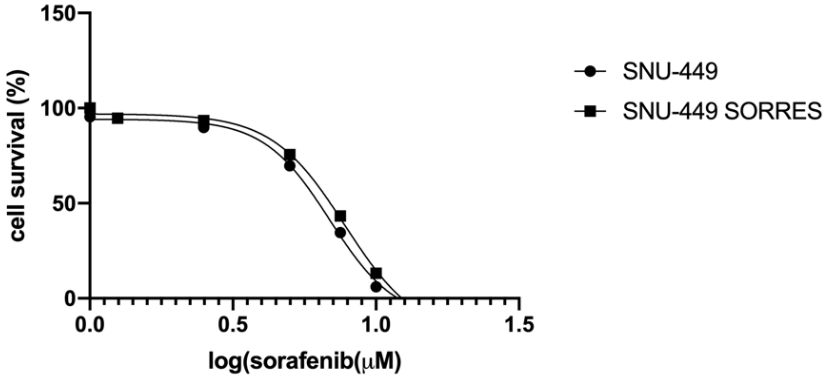

48H	SNU-449	SNU-449 SORRES
IC50	6.898	7.797

Figure 8. Effect of sorafenib treatment on cell viability in HuH-7 SORRES (A), MV SORRES (B), SNU-449 SORRES (C) and their wild-type counterparts. Sorafenib was administered at regularly increasing doses of 0, 0.625, 1.25, 2.5, 5, 7.5, 10, and 12.5 μM, and viability values were determined by measuring absorbance values via the MTT assay as a result of 24, 48, and 72 hours of incubation. The analysis was performed using the "Dose-response-Inhibition variable slope" tool in the GraphPad Prism program. IC50 values are higher in Sorafenib-resistant cells at all time points than in their wild-type counterparts.

In our previous studies, it was demonstrated that Sorafenib resistant cell clones have elevated c-Met expression levels. Additionally, it is known that c-Met and Cav-1 are activated by reciprocal crosstalk and HCC cells gain more aggressive phenotype. By this information, Cav-1 transcription and protein expression levels were determined via RT-qPCR and Western Blotting (WB), in three sorafenib resistant cell lines we developed (Figure 9).

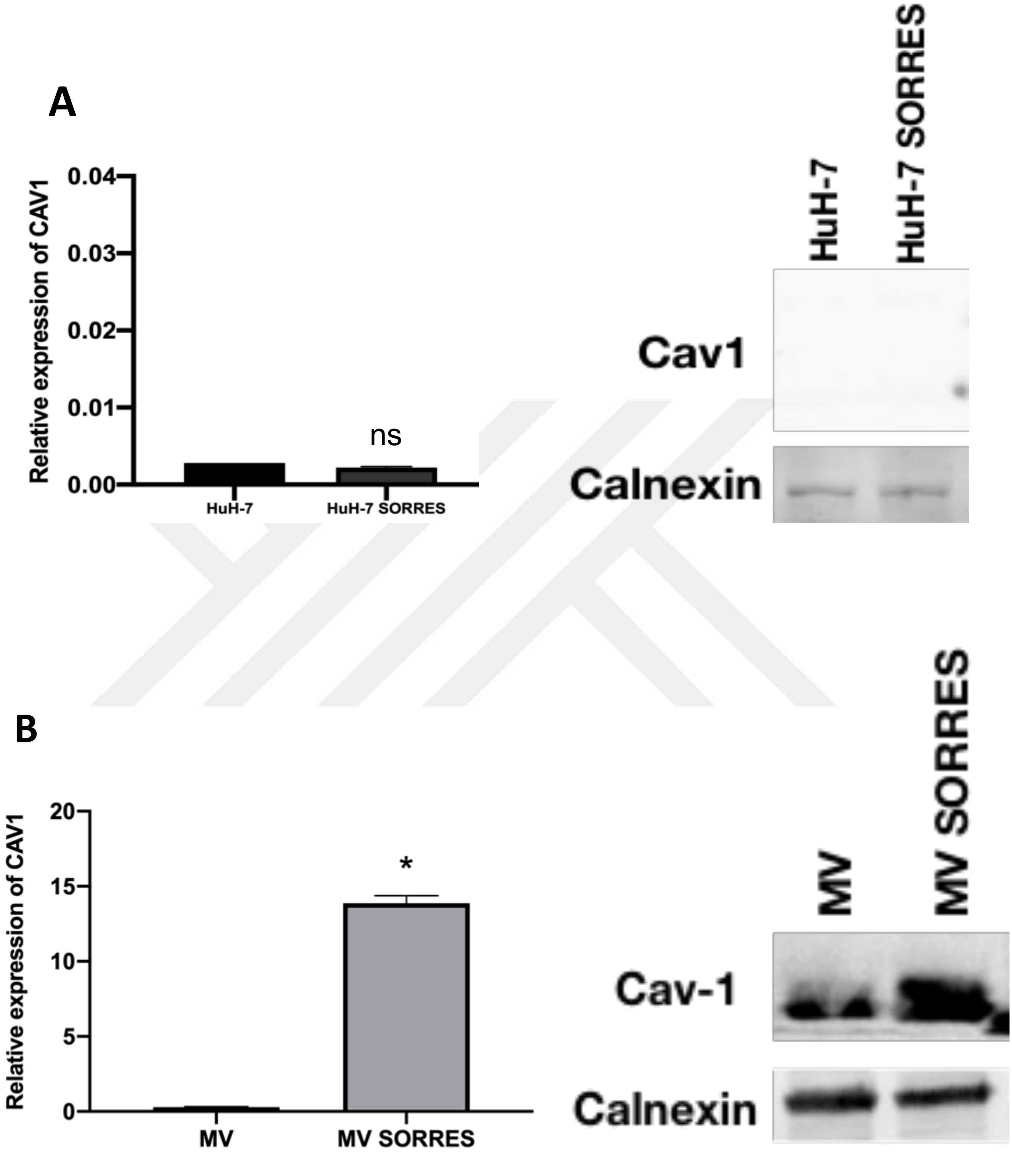
A
Relative expression of CAV1
0.04
0.03
0.02
0.01
0.00
ns
HuH-7
HuH-7 SORRES
HuH-7
HuH-7 SORRES
Cav1
Calnexin
B
Relative expression of CAV1
20
15
10
5
0
*
MV
MV SORRES
MV
MV SORRES
Cav-1
Calnexin

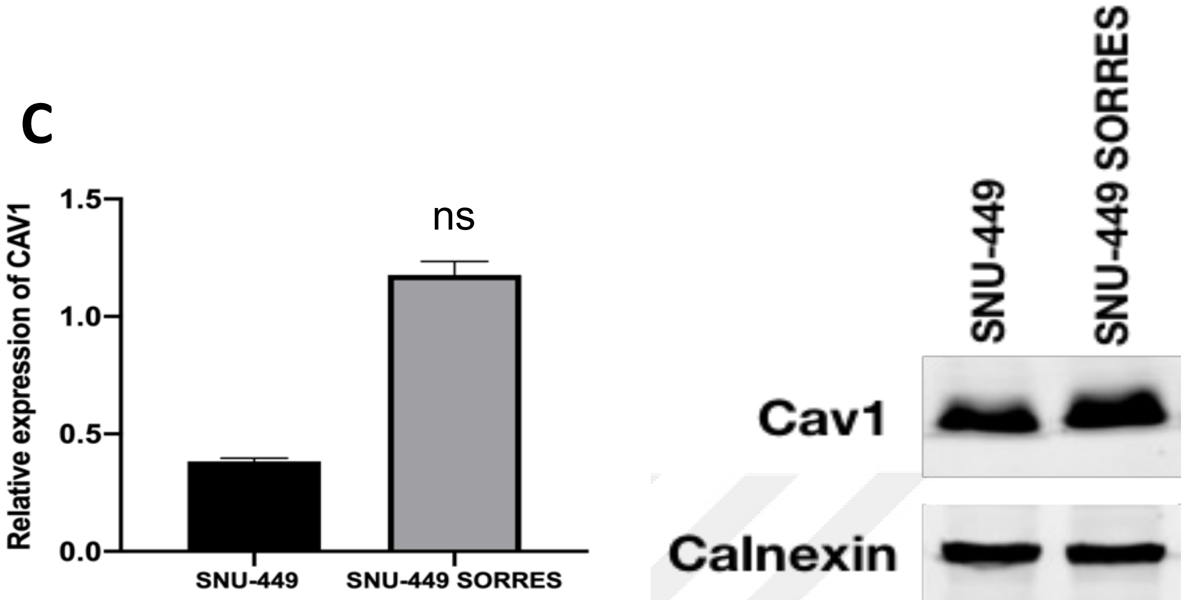

Figure 9. Cav-1 expressions of Sorafenib resistant clones (A: HuH-7, B: MV, C:SNU-449).; transcriptional expression levels were determined via RT-qPCR (left side), protein expression levels were determined via WB (right side). Statistical analysis was done by Graphpad Prism using Mann-Whitney test. (ns: $p>0.05$, *: $p<0.05$)

When we examined the expression levels in MV (Figure 9B) and SNU-449(Figure 9C) cell lines Cav-1 expression was increased in both mRNA and protein level whereas in HuH-7 there was no change in the expression of Cav-1 neither in mRNA or protein levels (Figure 9A). The reason why there was no change in the Cav-1 expression could be in HuH-7 wild-type cells, there was nearly no expression of Cav-1 in mRNA level and no expression in protein level.

Additionally, protein expression of Cav-1 was demonstrated via immunofluorescence staining (IF) of Cav-1 protein in MV and SNU-449 SORRES cells and their wild-type counterparts (Figure 10) (Figure 11). Double staining of Cav-1 and c-Met were performed simultaneously in MV and MV SORRES cells (Figure 10).

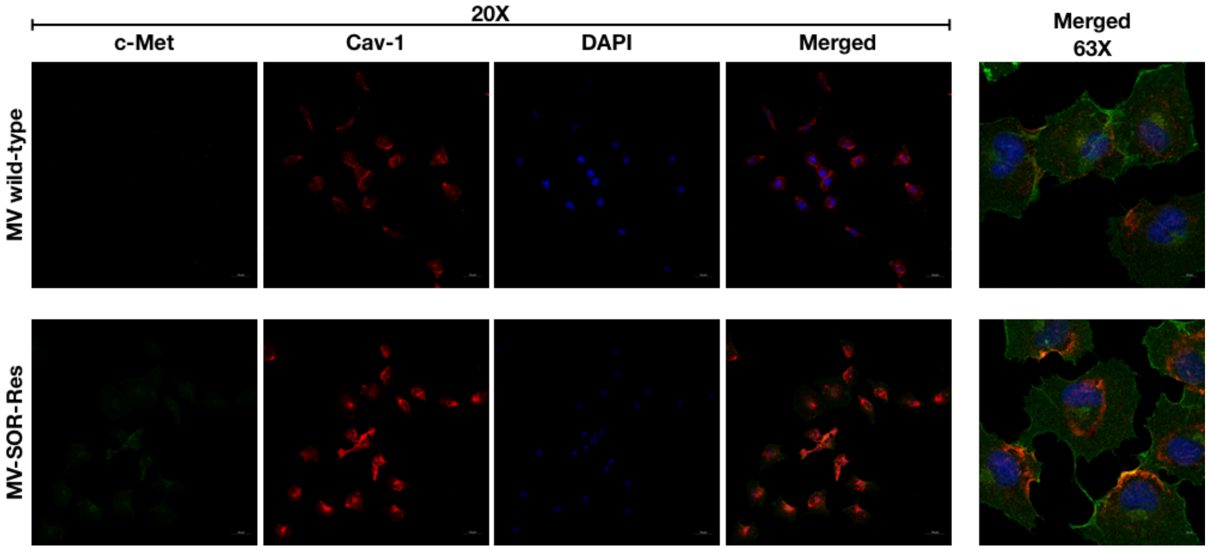

Figure 10. Immunofluorescence double staining of c-Met and Cav-1 in MV and MV SORRES cells. For c-Met determination, Alexa 488 (green) secondary antibody and for Cav-1 determination, Alexa 594 (red) secondary antibody were used. DAPI staining was performed to stain the nuclei of the cells. 20X images were taken under Olympus BX61 upright fluorescence microscopy, 63X images were taken under Zeiss confocal microscopy (LSM880).

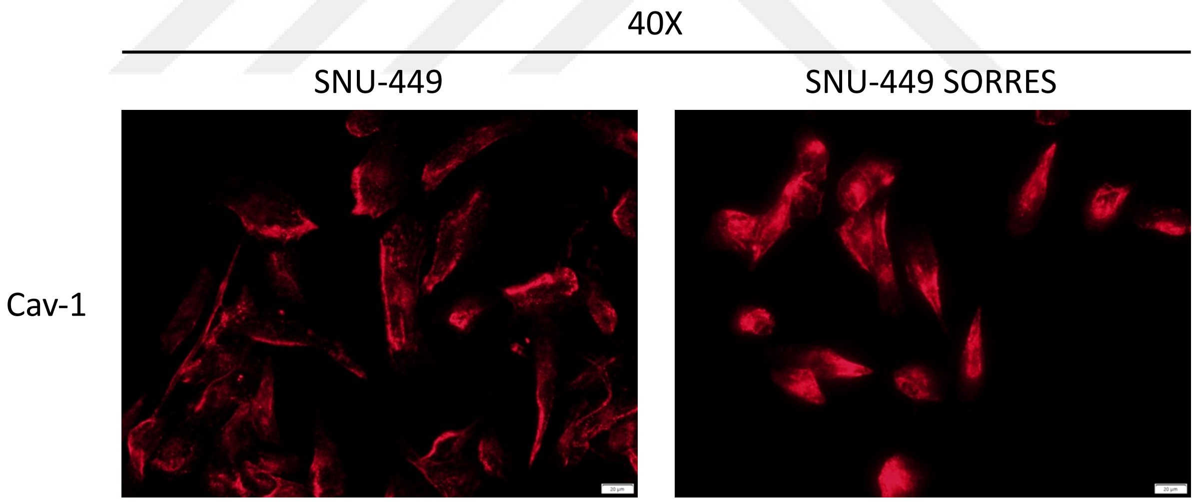

Figure 11. Immunofluorescence staining of Cav-1 in SNU-449 and SNU-449 SORRES cells. For Cav-1 determination, Alexa 594 (red) secondary antibody were used. 40X images were taken under Olympus BX61 upright fluorescence microscopy.

By WB and RT-qPCR, the increase in the Cav-1 expression determined in MV and SNU-449 SORRES cells. The increase in the Cav-1 expression determined in both cells by IF staining.

From the expressional changes of Cav-1 in Sorafenib resistant cell clones, we can assume that there is a relationship between sorafenib resistance and Cav-1 expression. Depending on the Cav-1 expression level in the cells (Figure 12), the resistance to Sorafenib can be predicted. For instance, for 3 HCC cells all of them have different Sorafenib IC50 values according to their expression levels of Cav-1 (Table 6).

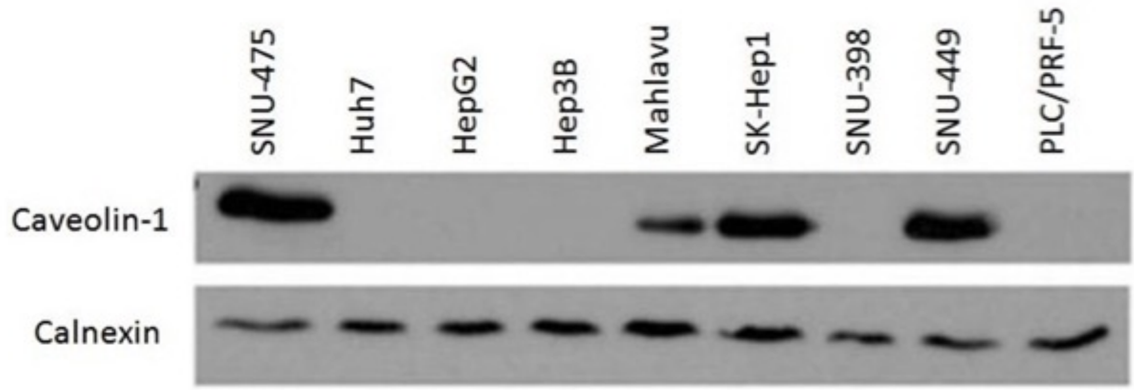

Figure 12. Cav-1 expression values in HCC cells (4).

Table 6. Relationship between Cav-1 expression levels and SOR IC50 values

Cell line	Cav-1 level	SOR IC50 (µM)
HuH-7	-	4.7
MV	+	5.3
SNU-449	++	6.9

According to Cav-1 protein expression levels and SOR IC50 values shown in Figure 12 and Table 6, we inferred that Cav-1 and resistance to Sorafenib are linked. In HuH-7 there is no Cav-1 expression and in SNU-449 the expression is the highest among them. Thus, SNU-449 is the most resistant to Sorafenib among these 3 cell lines.

Since Cav-1 expression is important for Sorafenib resistance, HuH-7 Cav-1 overexpressing clones (HuH-7 pCAV1) were used which were obtained in our previous studies. SOR IC50 levels of HuH-7 pCAV1 cells were tested via MTT assay and showed that when Cav-1 expression was increased, SOR IC50 values were increased (Figure 13).

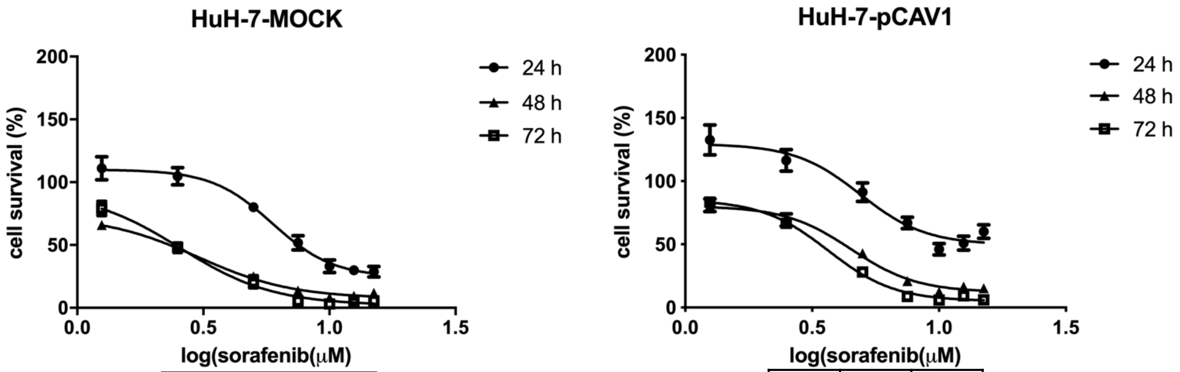

24h	48h	72h
7.5	3	2.6

24h	48h	72h
10	4.5	3.7

Figure 13. SOR IC50 values of Cav-1 overexpressing HuH-7 and MOCK-transfected cells. The analysis was performed using the "Dose-response-Inhibition variable slope" tool in the GraphPad Prism program. IC50 values are higher in Cav-1 overexpressing cells at all time points than in their MOCK-transfected cells.

From HuH-7 pCAV1 cells, we generated Sorafenib resistant cell clones by the same technique that we used for the others and determined its Cav-1 expression and saw that in HuH-7 pCav1 Sorafenib resistant cell clone (HuH-7 pCAV1 SORRES) Cav-1 expression was increased compared to HuH-7 pCav1 cells (Figure 14).

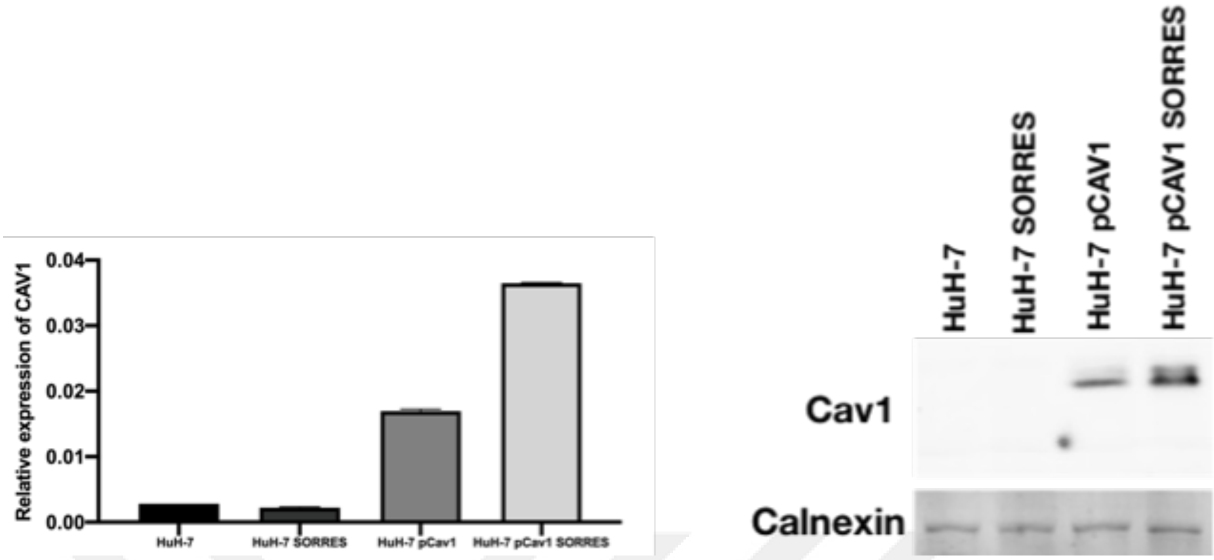

Figure 14. Cav-1 expression of HuH-7 Sorafenib resistant and Cav-1 overexpressing cells in mRNA (left) and protein level (right).

According to the results, we can assert that Cav-1 is important for Sorafenib resistance. It is known that Cav-1 can exist in lipid rafts independently and in caveolar structures. Therefore, we investigated caveolar structures of Sorafenib-resistant cells and their wild-type counterparts by performing electron microscopy technique (Figure 15).

A. HuH-7

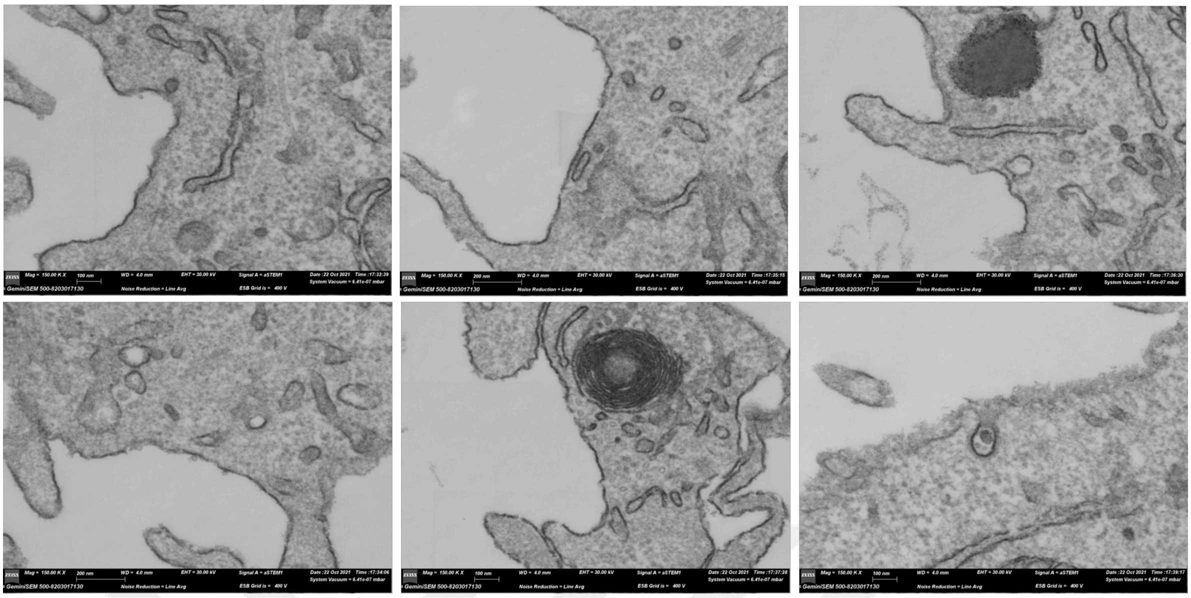

B. HuH-7-SOR-Res

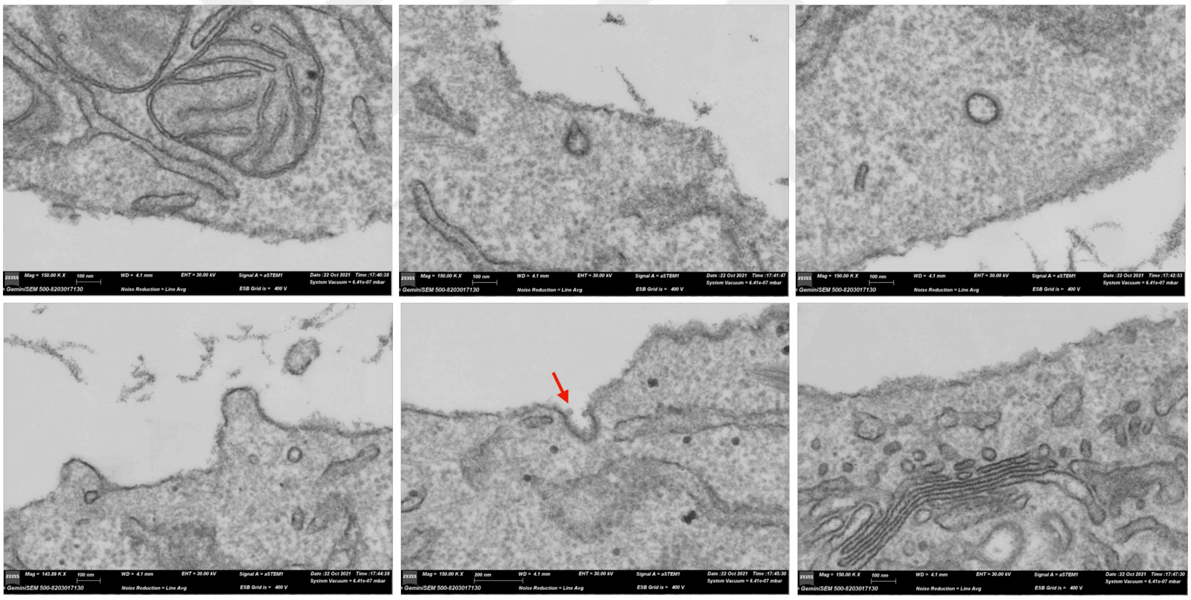

C. MV

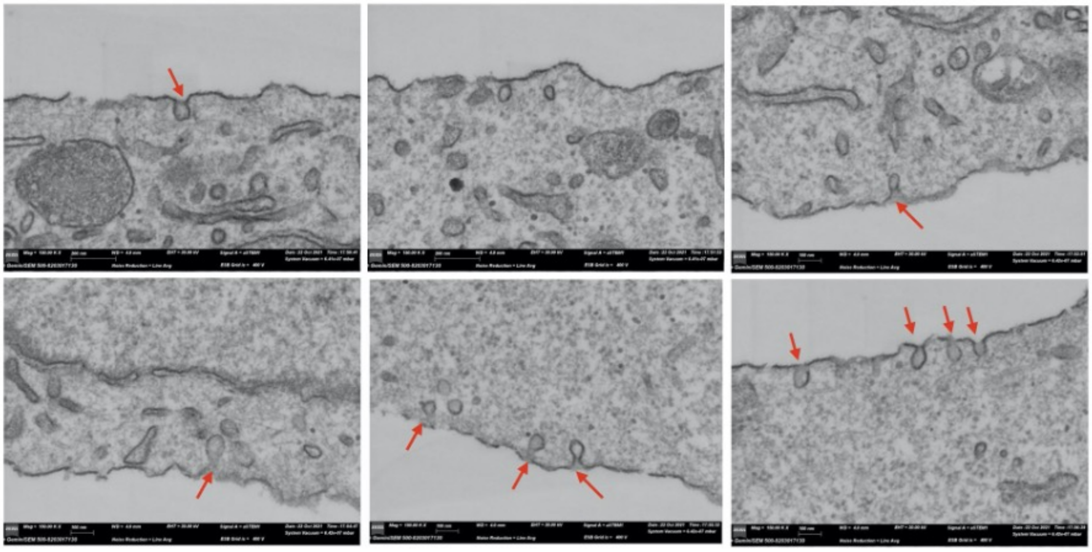

D. MV-SOR-Res

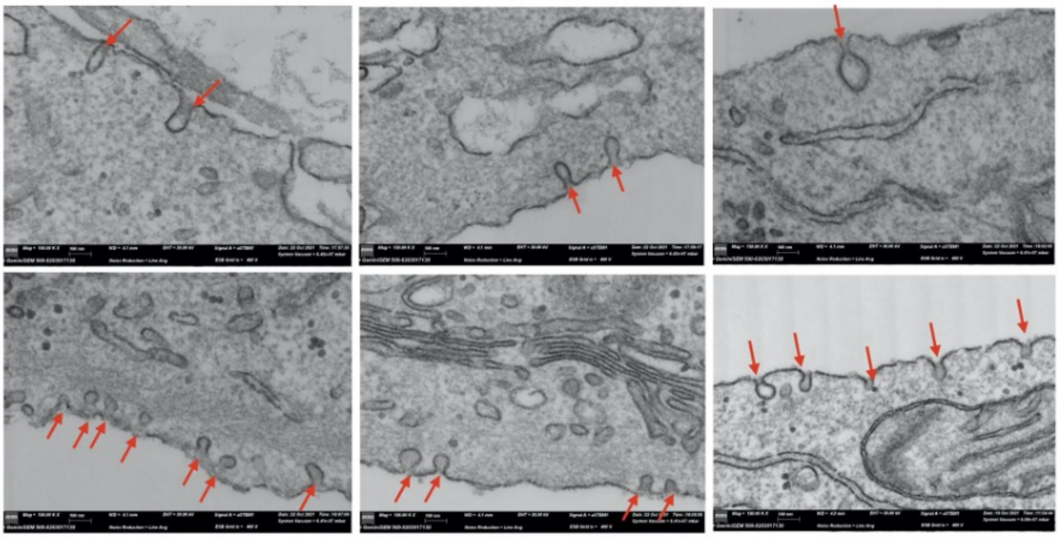

G. SNU-449

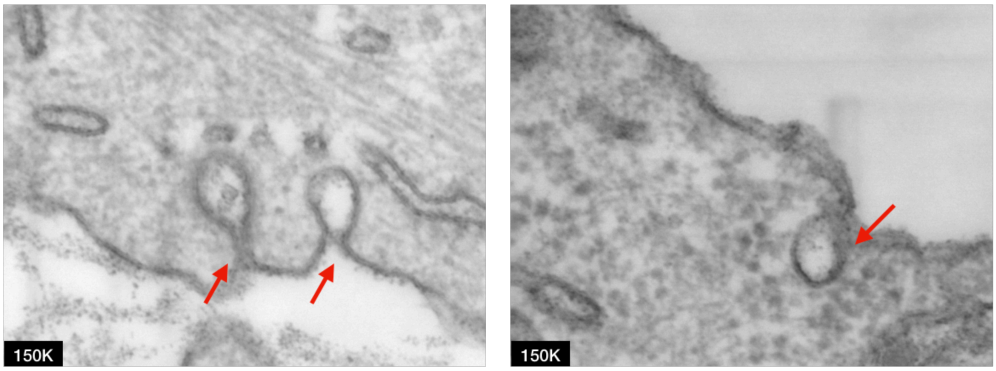

H. SNU-449-SOR-Res

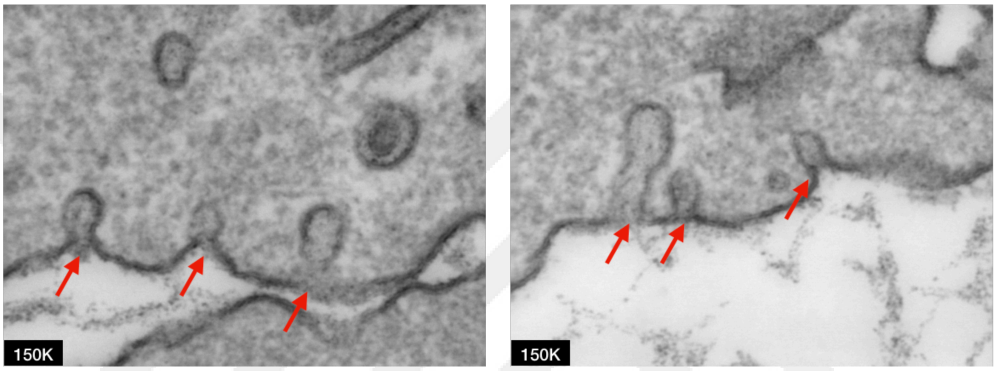

E. HuH-pCAV1

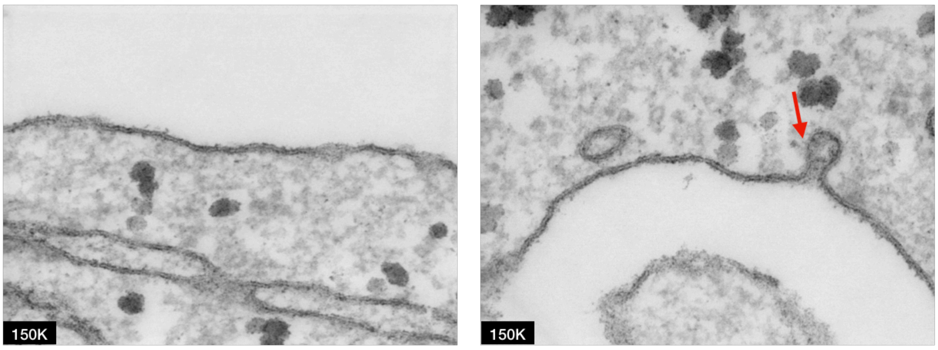

F. HuH-pCAV1-SOR-Res

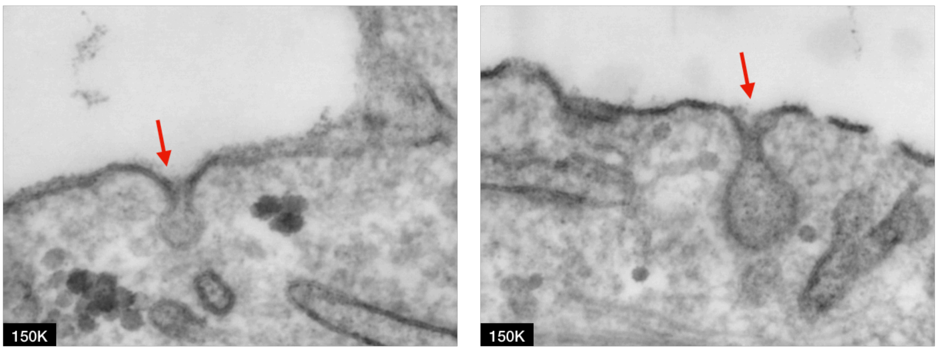

Figure 15. Electron microscopy images of cells and their number of caveolar structures vary in cell line and its Cav-1 expression. Images were taken in 150K X magnification and caveolar structures were indicated in red arrows.

Number of caveolar structures is correlated with Cav-1 expression levels of the cells. In Sorafenib-resistant cells the number of caveolar structure was increased according to the Cav-1 expression of the cell. Caveolar structures were increased in all Sorafenib-resistant cells compared to their wild-type counterparts especially in MV and SNU-449 SORRES cells but the increase was not significant. (Figure 16).

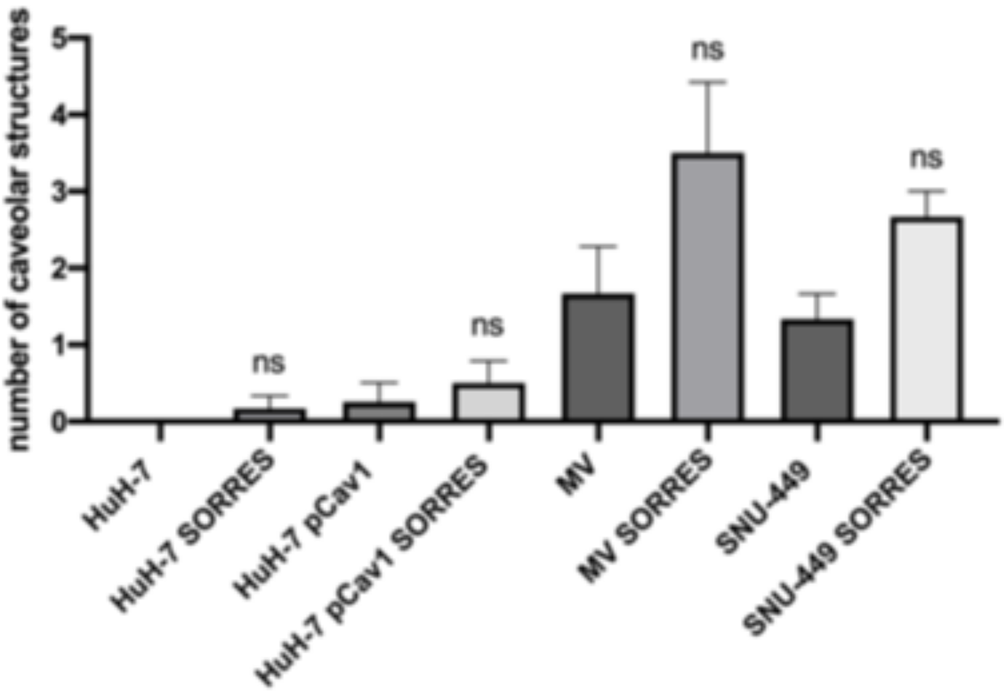

Figure 16. The quantification of caveolar structures from electron microscopy images. (ns: $p>0.05$)

Actin filaments are generally related with Cav-1 expression in the cell (35). They are presented as stress fibers in mesenchymal cells. We observed stress fibers in Sorafenib resistant cells by Phalloidin staining, stress fiber formation increased in Sorafenib resistant cells (Figure 17).

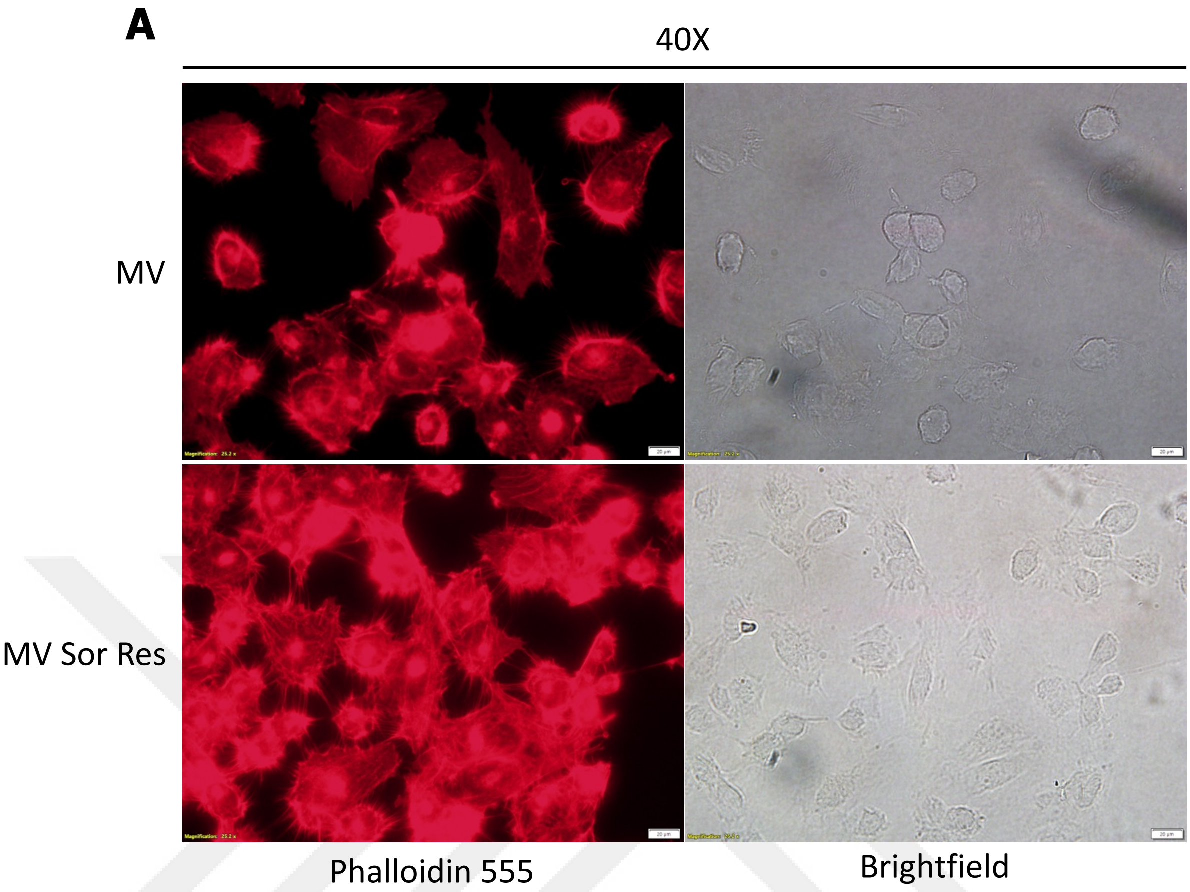
A
40X
MV
MV Sor Res
Phalloidin 555
Brightfield

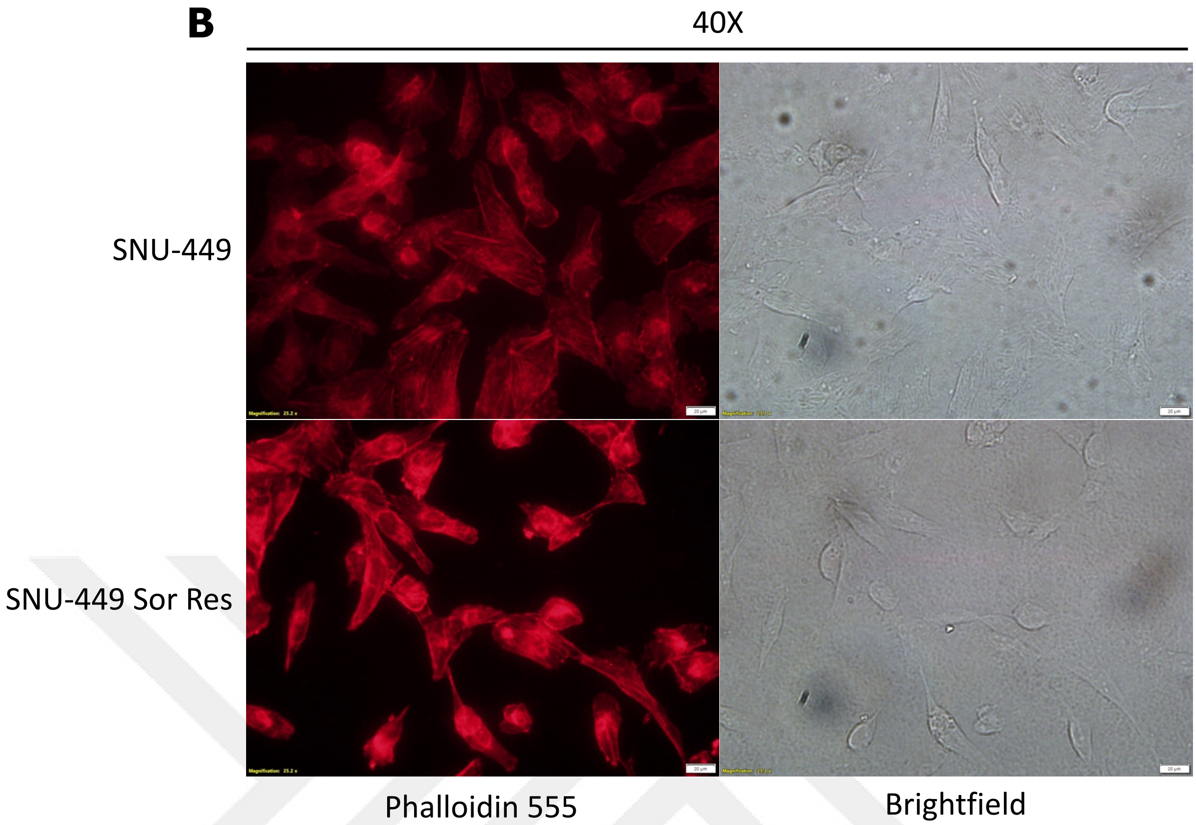

Figure 17. Determination of stress fiber formation by Phalloidin staining (A: MV, B: SNU-449). Alexa 555 tagged Phalloidin was used. 40X images were taken under Olympus BX61 upright fluorescence microscopy.

EMT markers E-cadherin and Vimentin levels were determined in the Sorafenib-resistant cells and their wild-type counterparts by IF and/or Western blotting (Figure 18). In HuH-7 SORRES cells, E-cadherin was decreased, and Vimentin was increased Figure 18A, 18B). In MV SORRES cells, Vimentin was increased according to IF, and there was no change in E-cadherin, possibly due to the no expression of E-cadherin in the wild-type MV cells (Figure 18A, 18B).

A

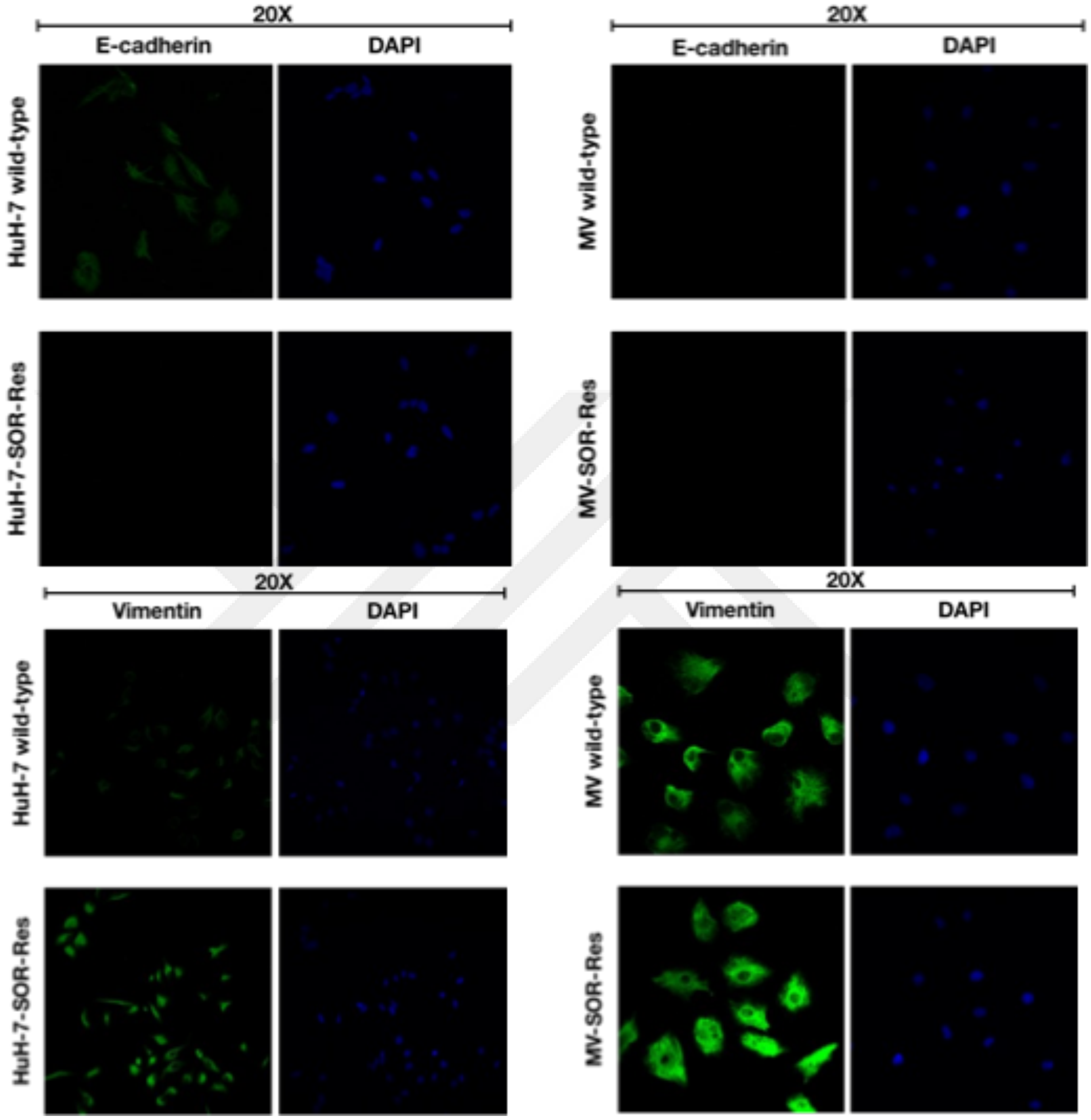
20X
E-cadherin
DAPI
HuH-7 wild-type
HuH-7-SOR-Res
20X
E-cadherin
DAPI
MV wild-type
MV-SOR-Res
20X
Vimentin
DAPI
HuH-7 wild-type
HuH-7-SOR-Res
20X
Vimentin
DAPI
MV wild-type
MV-SOR-Res

B

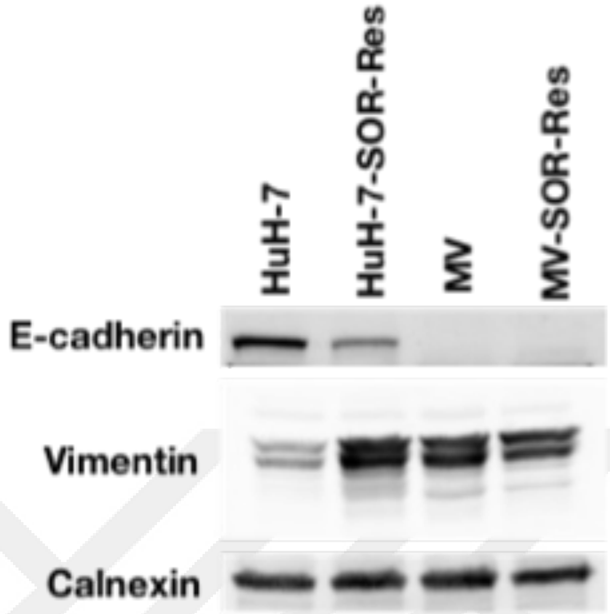

Figure 18. EMT markers E-cadherin and Vimentin expressions of Sorafenib resistant cells and their wild-type counterparts. The IF staining was performed by using Alexa 488 (green) as a secondary antibody for both E-cadherin and Vimentin. 20X images were taken under Olympus BX61 upright fluorescence microscopy (A). WB was performed as well and obtained the same expressional pattern that we determined by IF (B).

We then performed proliferation, motility, and invasion assays. Our results showed that HuH-7 pCAV1 cells are more proliferative compared to its MOCK-transfected cells (Figure 19).

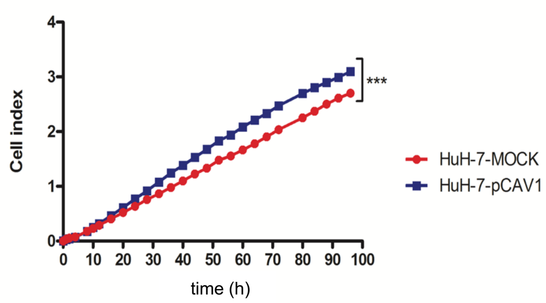

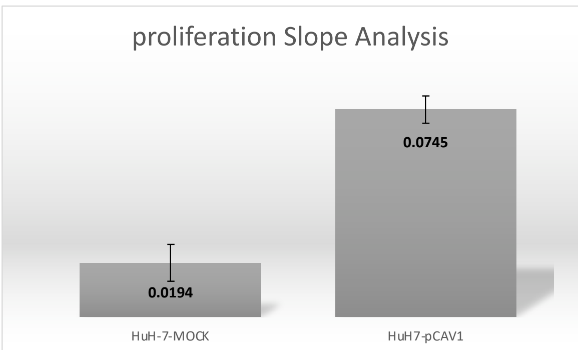

Figure 19. The proliferation of HuH-7 pCAV1 and MOCK-transfected cells was determined via xCelligence for 96 hours. Cell index values were collected and analyzed (left; (56). (***:p ≤0.001)

We also observed that HuH-7 pCAV1 cells are more resistant to Sorafenib treatment than MOCK-transfected cells at the IC10-IC50 concentrations (Figure 20).

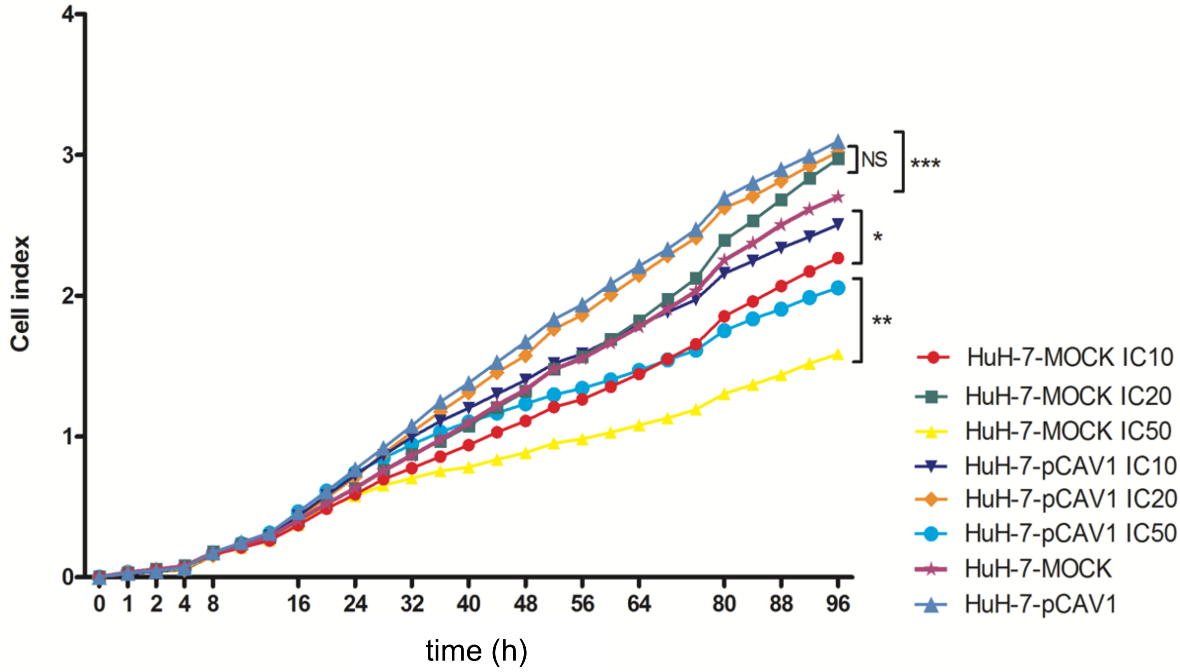

Figure 20. Proliferation of HuH-7 pCAV1 and MOCK-transfected cells when Sorafenib treatment is performed up to its IC50 value. Experiment performed via xCelligence for 96 hours. Cell index values were collected and analyzed (56). (ns: p>0.05, *:p≤ 0.05, **:p ≤0.01, ***:p ≤0.001)

When adhesion rate of MV and SNU-449 SORRES cells were tested, Sorafenib resistant clones were found to be less adhesive than WT cells (Figure 21). This may be related to anchorage-independent growth ability induced by elevated Cav-1 expression.

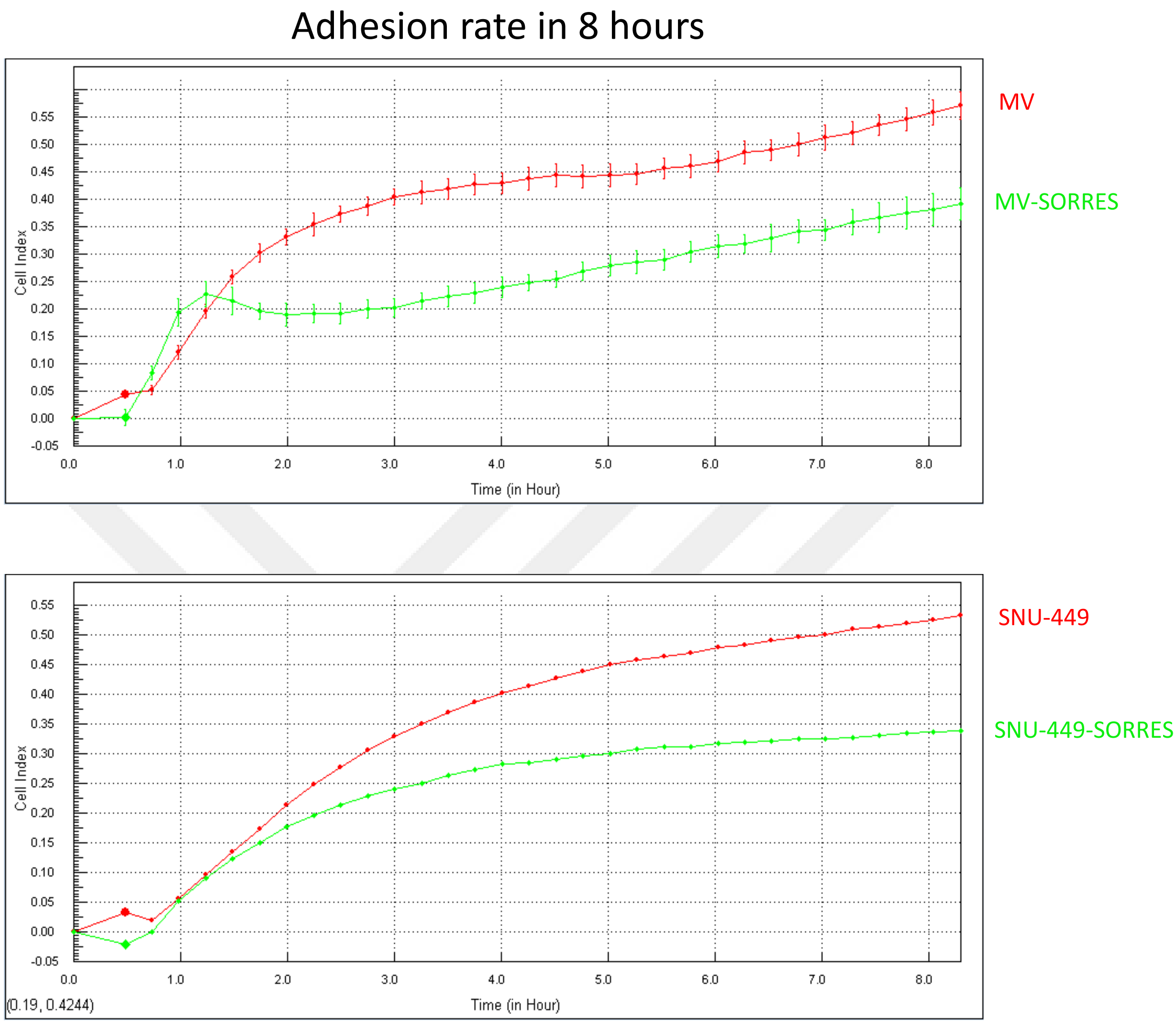

Figure 21. Adhesion rate of MV and SNU-449 SORRES cells and their wild-type counterparts. Cell index values were collected for 8 hours which represent the adhesion capability of cells by xCelligence.

To determine the effect of Cav1 expression of motility and invasion of Sorafenib-resistant cells, Boyden chamber motility and invasion assays were performed with Cav-1 silenced Sorafenib-resistant cells by Cav-1 siRNA. In Cav-1 silenced conditions both motility and invasion were decreased in Sorafenib resistant cell lines (Figure 22).

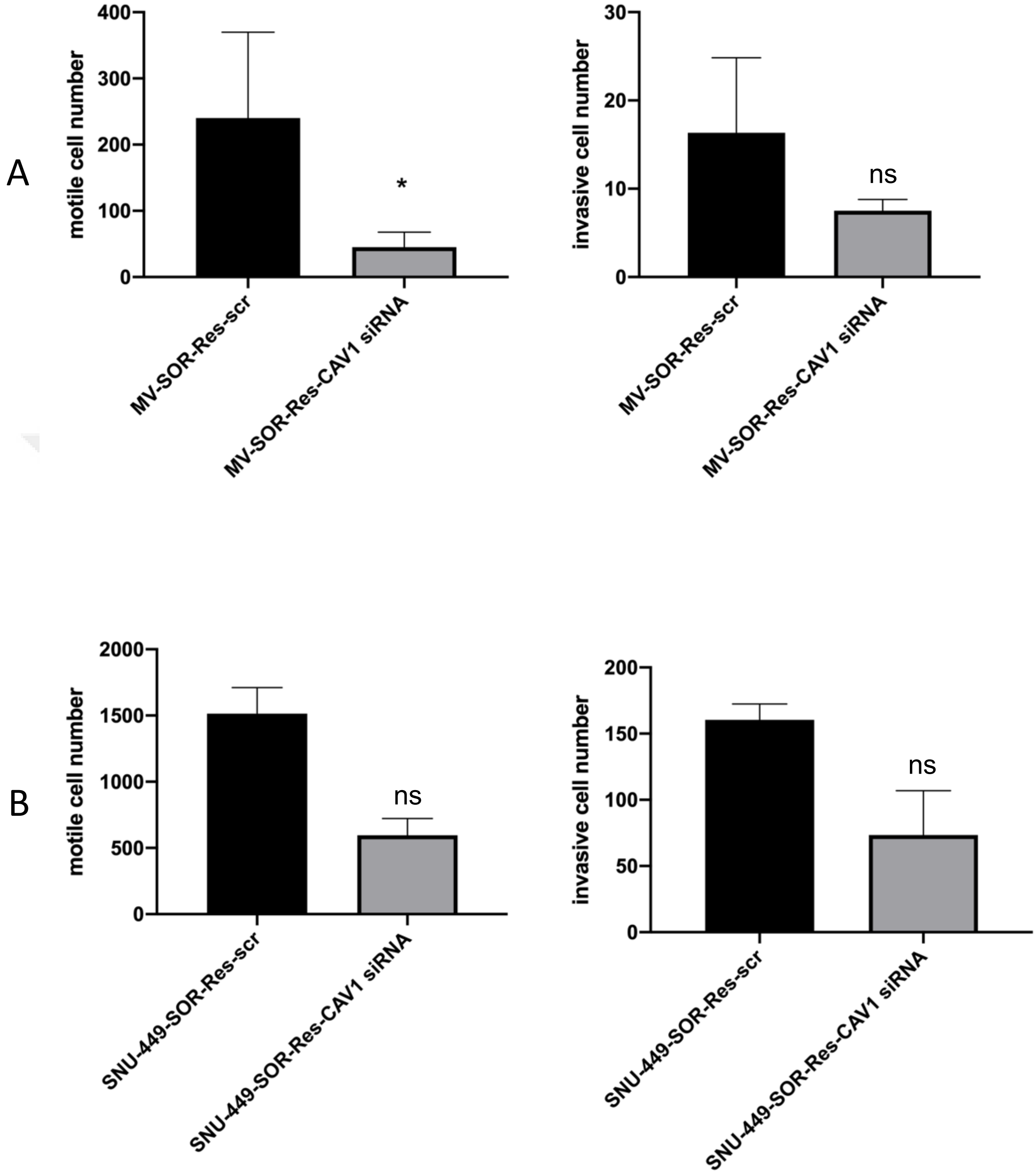

Figure 22. Motility and invasion of Sorafenib resistant and Cav-1 silenced Sorafenib resistant MV (A) and SNU-449 (B) cells. Boyden chambers were used to determine motility and invasion. (ns: $p>0.05$, *:$p\leq 0.05$)

To test in vivo characteristics of Sorafenib-resistant cells, Zebrafish xenograft experiment was performed in collaboration with Ozhan Lab at IBG. First, dose of Sorafenib and cell-number-injected optimizations were done (Figure 23) (Figure 24).

For dose optimization, different doses of Sorafenib were given to E3 medium where zebrafish embryos live at their 72 hpf (hours post fertilization) state and observed for 96 hours. At the end of 96 hours, they were imaged and checked in terms of their viability and morphology (Figure 23).

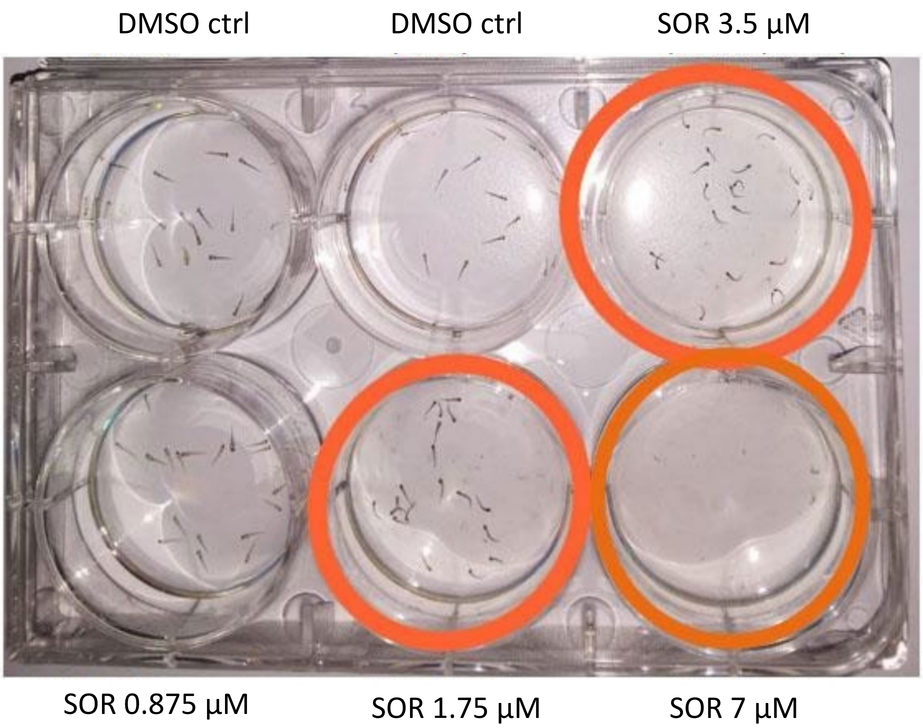

Figure 23. Zebrafish Sorafenib dose optimization results. Orange circles represent the doses where all zebrafish have died. They were imaged at the end of 96 hours.

For the xenograft experiment, MV cells were used thus an optimum number of cells injected into zebrafish yolks should be determined. For this, different number of cells were injected to zebrafish yolks and observed and imaged. 200 cells per injection was the optimized number of cells for MV cells (Figure 24).

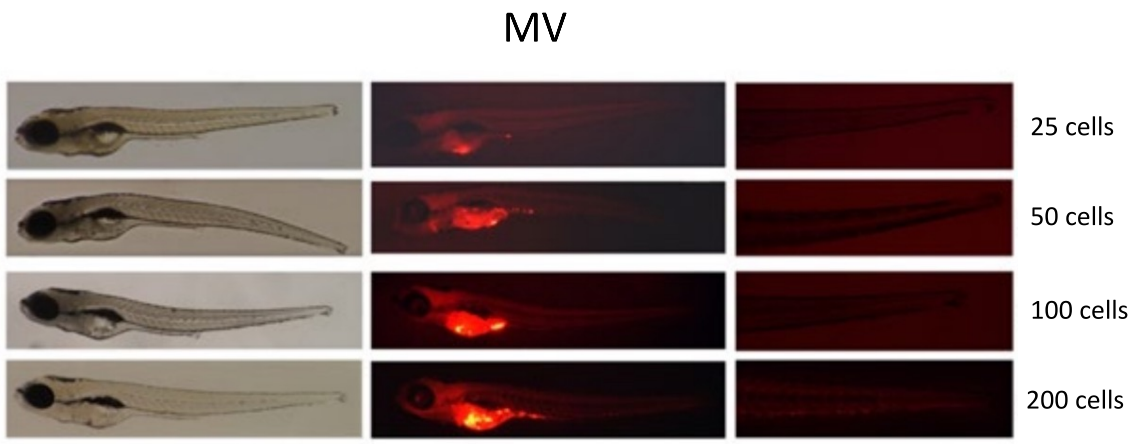

Figure 24. MV cell number optimization results in zebrafish

After optimizations, xenograft experiments were performed. For this experiment, again Cav-1 silenced MV SORRES cells were used. Cells were treated with sorafenib in their IC20 doses for 48 hours. After, cells were stained with DiL dye and injected into the yolk of zebrafish embryos and observed for 5 days. After 5 days, zebrafish were observed and checked if metastasis happened under fluorescence stereomicroscope. In vivo metastasis capacity of MV SORRES cells in zebrafish embryos was decreased in Cav-1 silenced conditions compared to scrambled control (Figure 25).

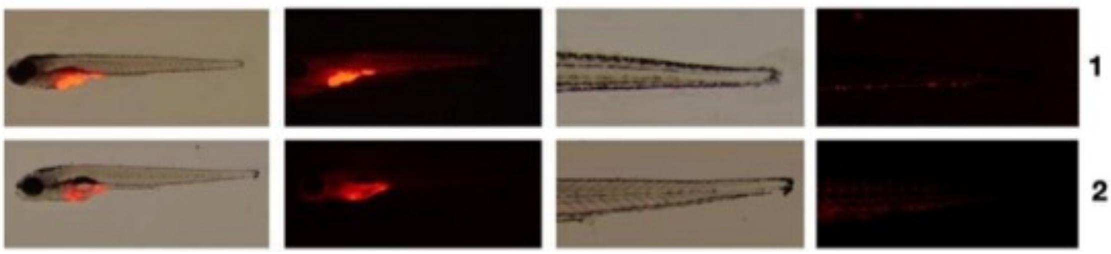

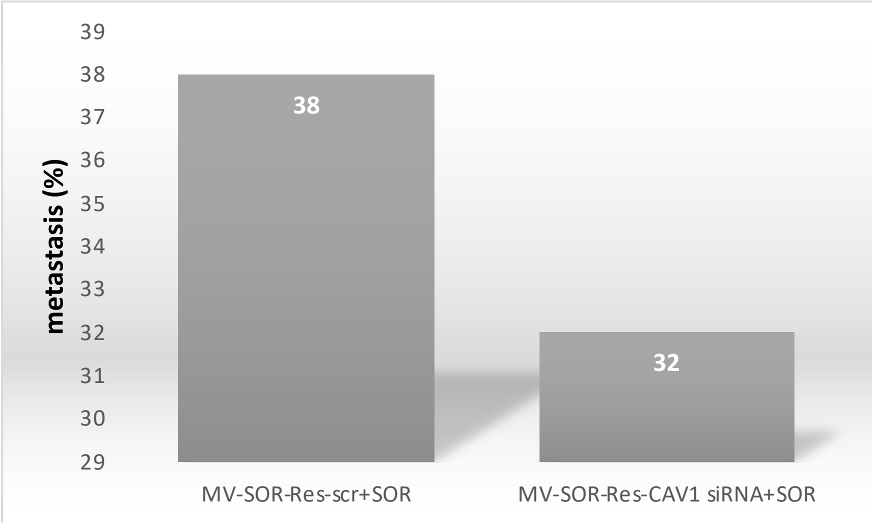

Figure 25. Zebrafish xenograft experiment results. After 5 days, zebrafish were checked under the fluorescent stereomicroscope (Olympus SZX16) to determine whether metastasis was observed or not.

As a result of the first chapter, we observed that Cav-1 is crucial for Sorafenib resistance and promotes Sorafenib resistance and aggressive phenotype.

4.2. The relationship between Sorafenib Resistance and miR-181a-5p

As we mentioned in the first chapter, Cav-1 is important for Sorafenib resistance, and it is known that c-Met has a role in Sorafenib resistance (22). The mechanism behind this needs to be elucidated. Furthermore, it is known that miRNAs have crucial roles in regulating gene expression and biological processes, and they can be altered during therapy (8). Therefore, we hypothesized that miRNAs may influence response to Sorafenib treatment and may contribute to the resistance mechanism by simultaneously targeting Cav-1 and c-Met.

To test this hypothesis, we first performed bioinformatics analysis. Two miRNA target prediction tools were used to find a miRNA that targets both Cav-1 and c-Met. DianaTools-MicroT-CDS (https://dianalab.e-ce.uth.gr/) (Figure 26) and miRDB-miRNA target prediction database (https://mirdb.org/) (Figure 27) were used since they were the most preferred and used miRNA targeting tools and they follow different algorithms to determine targets. Thus these two tools were used to find miRNA targets Cav-1 and c-Met. From the list, the most possible one was selected and that was hsa-miR-34b-5p.

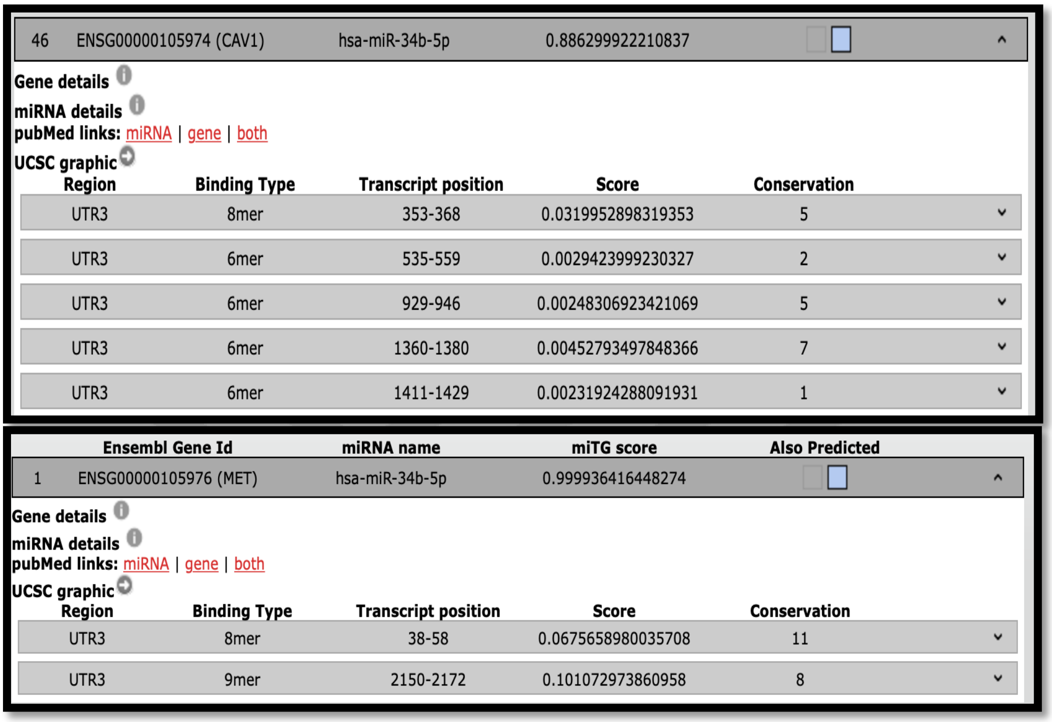

46	ENSG00000105974 (CAV1)	hsa-miR-34b-5p	0.886299922210837	

Gene details
miRNA details
pubMed links: miRNA | gene | both
UCSC graphic

Region	Binding Type	Transcript position	Score	Conservation
UTR3	8mer	353-368	0.0319952898319353	5
UTR3	6mer	535-559	0.0029423999230327	2
UTR3	6mer	929-946	0.00248306923421069	5
UTR3	6mer	1360-1380	0.00452793497848366	7
UTR3	6mer	1411-1429	0.00231924288091931	1

	Ensembl Gene Id	miRNA name	miTG score	Also Predicted
1	ENSG00000105976 (MET)	hsa-miR-34b-5p	0.999936416448274	

Gene details
miRNA details
pubMed links: miRNA | gene | both
UCSC graphic

Region	Binding Type	Transcript position	Score	Conservation
UTR3	8mer	38-58	0.0675658980035708	11
UTR3	9mer	2150-2172	0.101072973860958	8

Figure 26. Using DianaTools-MicroT-CDS tool to find a miRNA targeting c-Met and Cav-1.

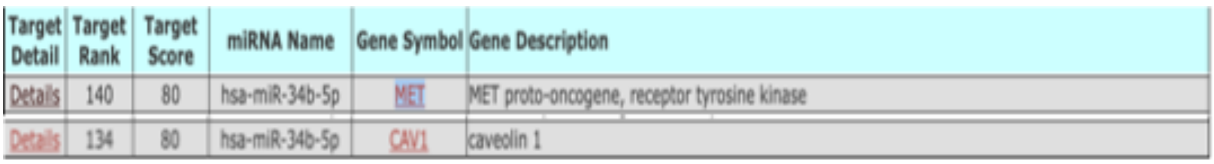

Target Detail	Target Rank	Target Score	miRNA Name	Gene Symbol	Gene Description
Details	140	80	hsa-miR-34b-5p	MET	MET proto-oncogene, receptor tyrosine kinase
Details	134	80	hsa-miR-34b-5p	CAV1	caveolin 1

Figure 27. Using miRDB-miRNA target prediction database to find a miRNA targeting c-Met and Cav-1.

We then reanalyzed an HCC patient dataset (GSE109211). We grouped the HCC patients as sorafenib responders and sorafenib non-responders and checked the genes that significantly changed between these two groups. In this analysis, we found that CAV1 and MET are two genes that are significantly increased in the non-responder group whereas MIR34B precursor gene is significantly decreased (Figure 28).

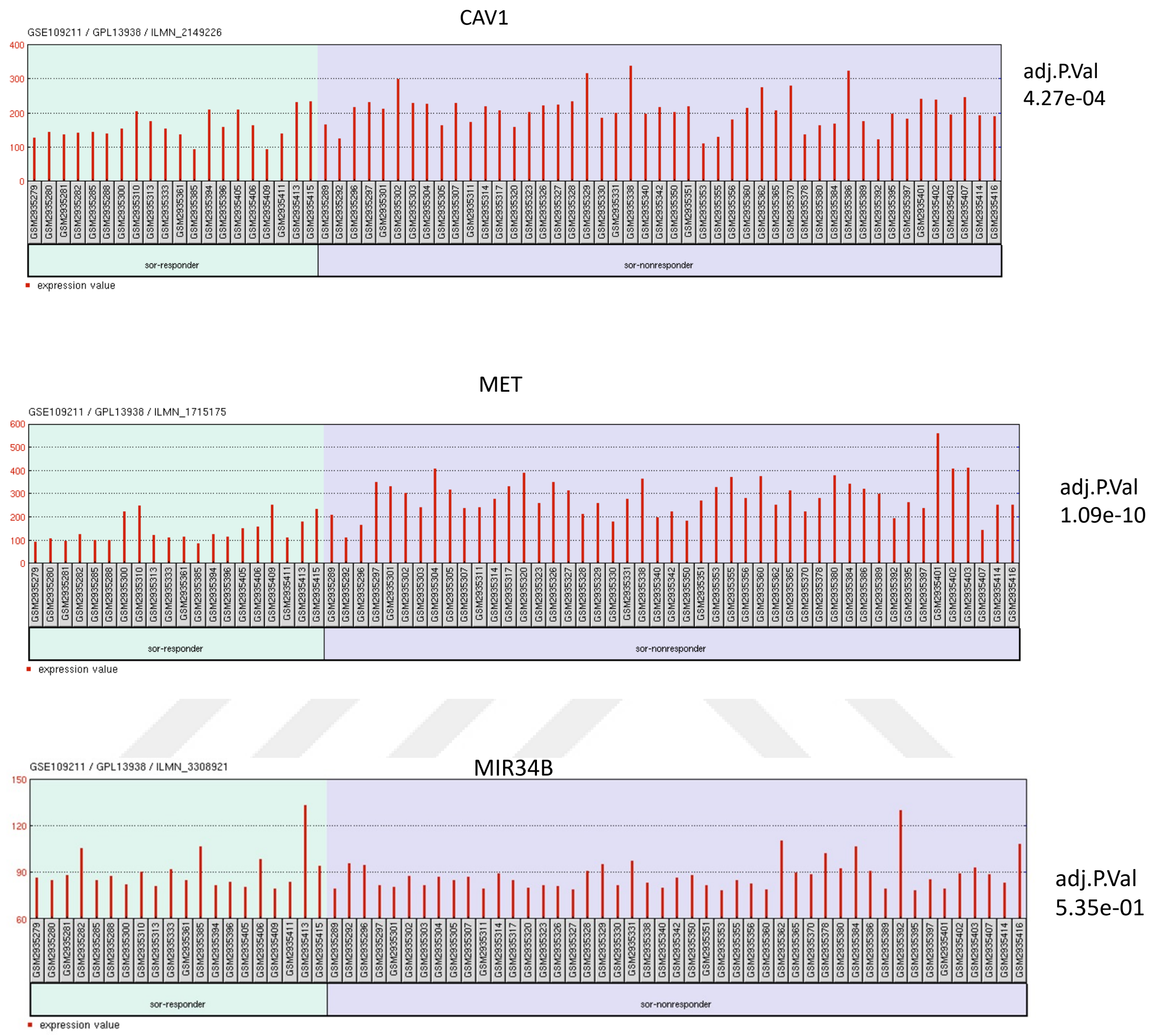

Figure 28. HCC patient dataset (GSE109211) was analyzed, CAV1 and MET were significantly increased, MIR34B was decreased almost significantly in the Sorafenib non-responder group.

The mRNA level of miR-34b-5p was examined in WT and Sorafenib resistant HCC cell lines (Figure 29). We observed that none of the cell lines that we tested expressed a detectable amount of miR-34b-5p, whereas Ct values for RNU6B endogenous control gene were determined as expected. Based on the bioinformatics analysis, SNU-475 was determined as a cell line overexpressing miR-34b-5p; however, we did not observe any detectable miR-34b-5p in SNU-475.

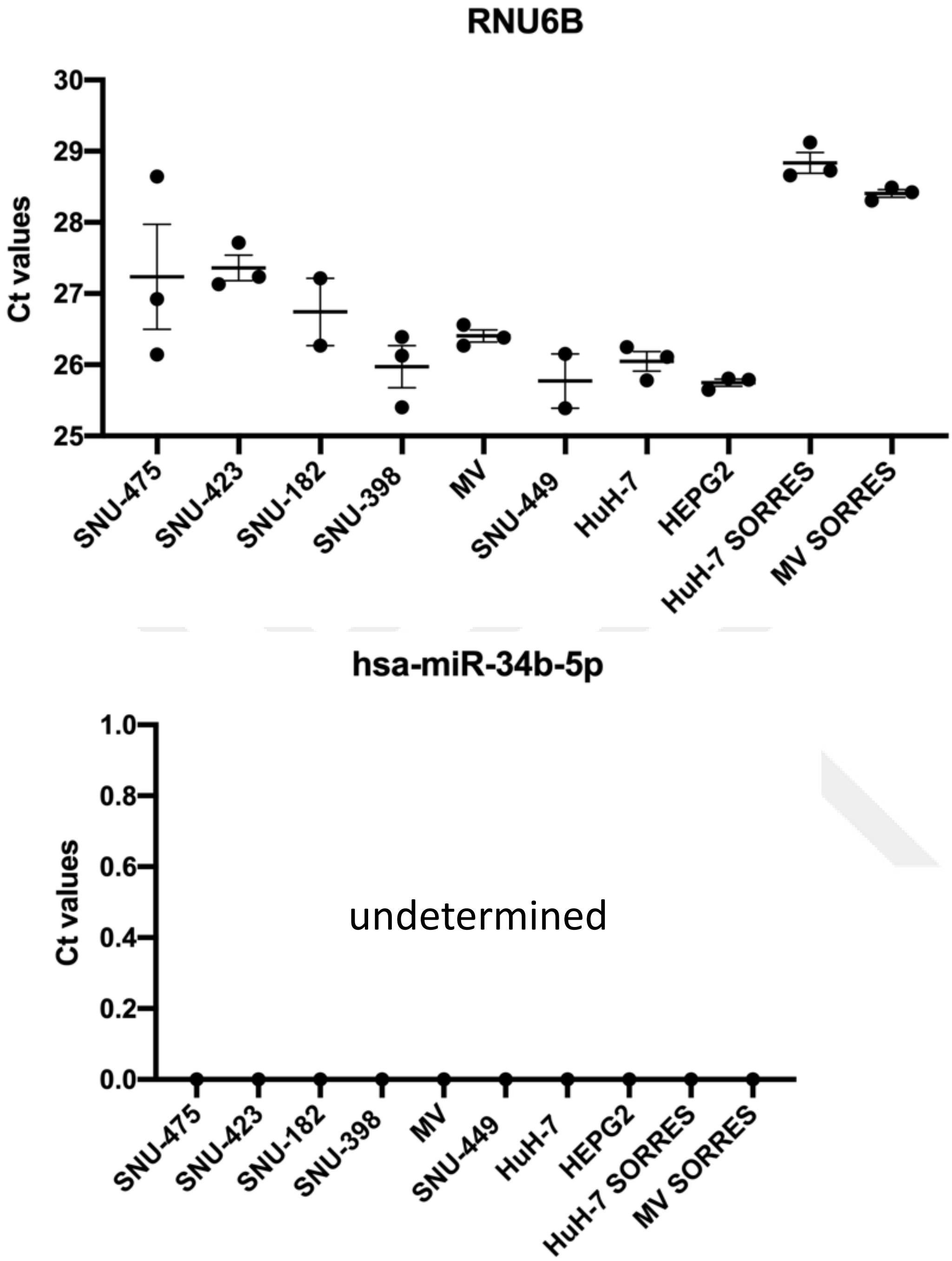

Figure 29. The result of RT-qPCR experiments performed with TaqMan probe primers for RNU6B endogenous control and the miRNA of interest, miR-34b-5p.

We then reanalyzed the bioinformatics data and literature to identify another candidate miRNA. Since our previous studies showed that miR-181a-5p directly targets c-Met, furthermore c-Met expression was increased during Sorafenib resistance, we first tested if miR-181a-5p has a role in Sorafenib resistance and whether it contributes to the resistance by regulating Cav-1 level.

The bioinformatics analysis of the HCC-SOR patient dataset showed that the MIR181A precursor gene is significantly lower in the non-responder group than in responders (Figure 30).

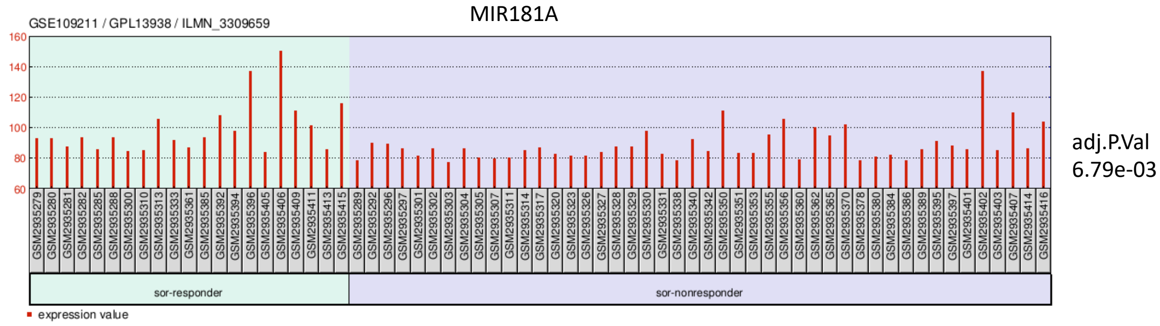

Figure 30. In the HCC patient dataset (GSE109211), MIR181A was significantly decreased in the Sorafenib non-responder group.

The miR-181a-5p expression levels analysis in seven HCC cell lines showed that almost all of them expressed miR-181a-5p with different levels, and the highest expression was determined in the SNU-182 among cell lines tested. (Figure 31).

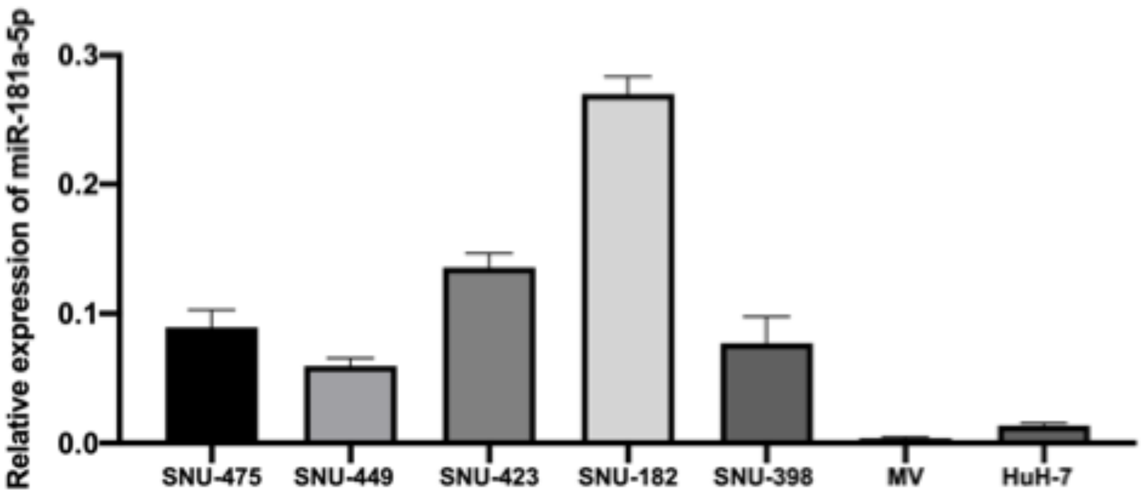

Figure 31. Expression of miR-181a-5p in HCC cells. The experiment was performed by TaqMan miRNA assay.

In Sorafenib resistant cell clones, miR-181a-5p expression levels were determined (Figure 32). In Sorafenib-resistant cells, miR-181a-5p expression was decreased except for HuH-7 SORRES cells. Since HuH-7 cells do not express Cav1 endogenously, this data supports that Sorafenib resistance mechanism of HuH-7 cells is independent from Cav-1 and mir-181a-5p.

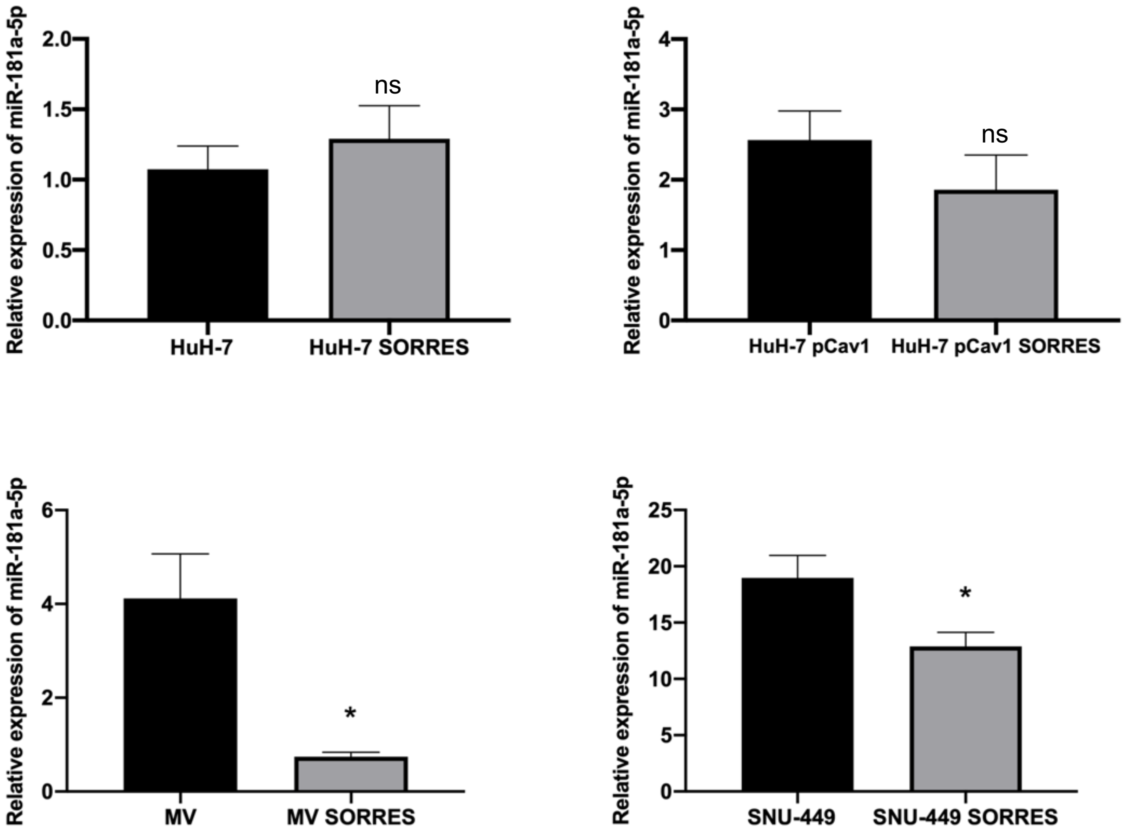

Figure 32. miR-181a-5p expressions of Sorafenib-resistant clones; the experiment was performed by TaqMan miRNA assay. Statistical analysis was done by GraphPad Prism using the Mann-Whitney test. (ns: $p>0.05$, *: $p<0.05$)

After determining that miR-181a-5p was decreased in Sorafenib-resistant cells, we selected this miRNA as a potential miRNA that might have a role in Sorafenib resistance and conducted further studies.

We have performed overexpression and silencing studies based on the basal expression level of miR-181a-5p. miRNA-mimic was used for overexpression of miR-181a-5p in MV and SNU-449 cells, and miRNA-inhibitor was used for silencing miR-181a-5p in SNU-449 cell line. By miR-181a-5p mimic transfection, miR-181a-5p expression was increased 43-fold, and by miR-181a-5p inhibitor antagomir transfection, miR-181a-5p expression was decreased 70%. (Figure 33).

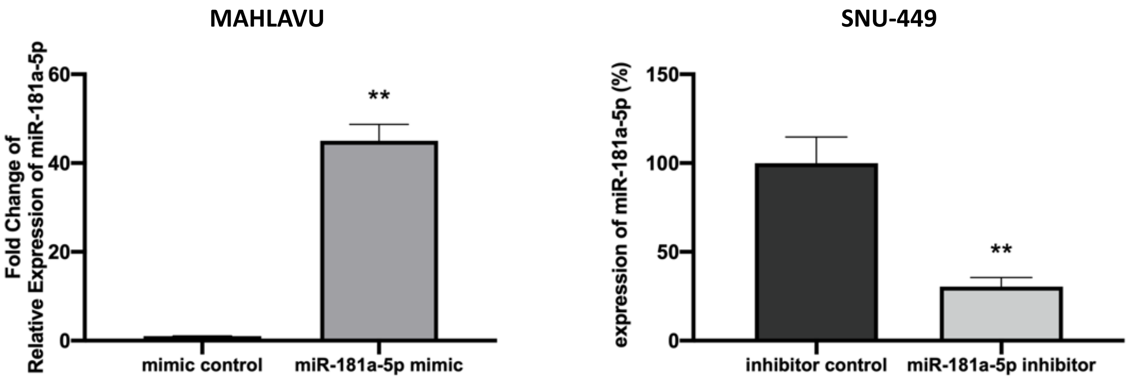

Figure 33. miR-181a-5p expressions of mimic and inhibitor transfected cells; the experiment was performed by TaqMan miRNA assay. Statistical analysis was done by GraphPad Prism using the Mann-Whitney test. (**: p<0.01)

To determine how Cav-1 expression levels change when mimic and inhibitor of miR-181a-5p was transfected into Sorafenib-resistant cells and its wild-type counterparts, RT-qPCR was performed. When miR-181a-5p expression levels were decreased with miRNA-181a-5p inhibitor, CAV1 expression levels were increased in SNU-449 cells. (Figure 34).

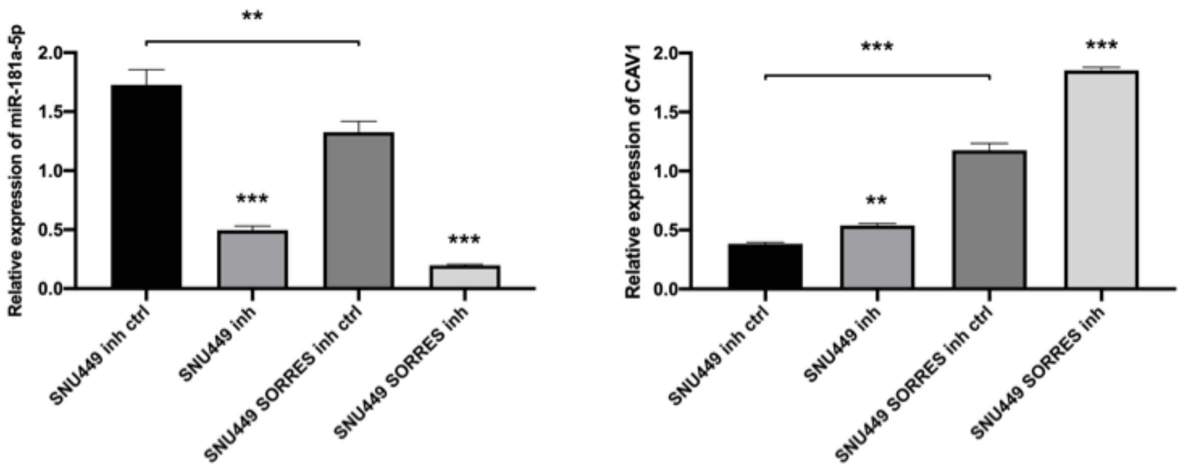

Figure 34. Expression levels of miR-181a-5p and CAV1 when inhibitor of miR-181a-5p transfected into SNU-449 SORRES and SNU-449 wild-type cells. (**: p<0.01, ***: p<0.001)

To rule out cell line type mediated differential responses we also increase miR-181a-5p expression levels with miR-181a-mimic in the same cell line, SNU 449, we observed that CAV1 expression levels were decreased (Figure 35).

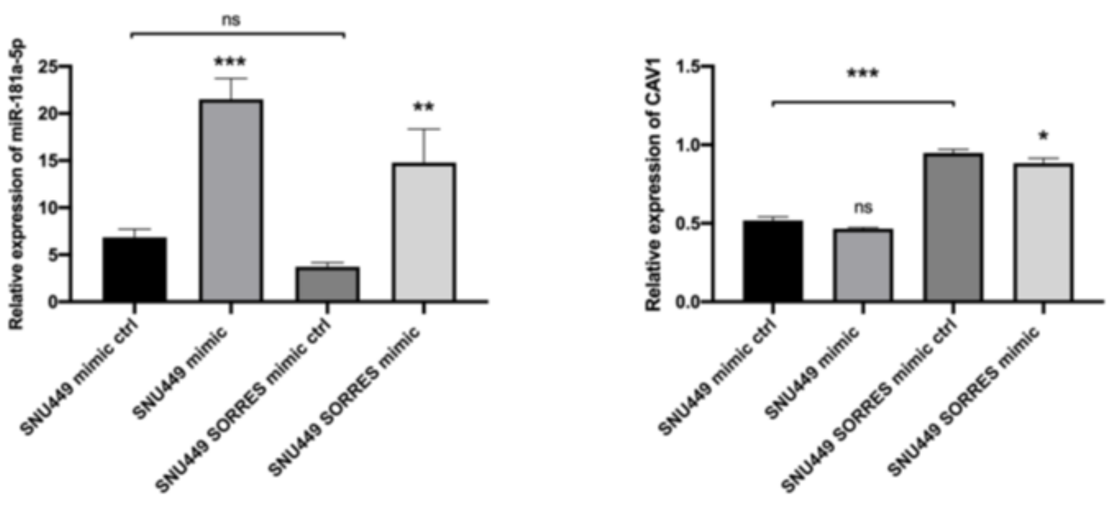

Figure 35. Expression levels of miR-181a-5p and CAV1 when mimic of miR-181a-5p transfected into SNU-449 SORRES and SNU-449 wild-type cells. (ns: $p>0.05$, *: $p<0.05$, **: $p<0.01$, ***: $p<0.001$)

Our silencing and overexpression experiments supported that miR-181a-5p is important for the regulation of Cav-1 level. Then, we performed biological assays such as proliferation and motility.

When SNU-449 SORRES cells were transfected with mimic miR-181a-5p, Sorafenib IC50 value was decreased and mimic sensitized the cells to Sorafenib (Figure 36).

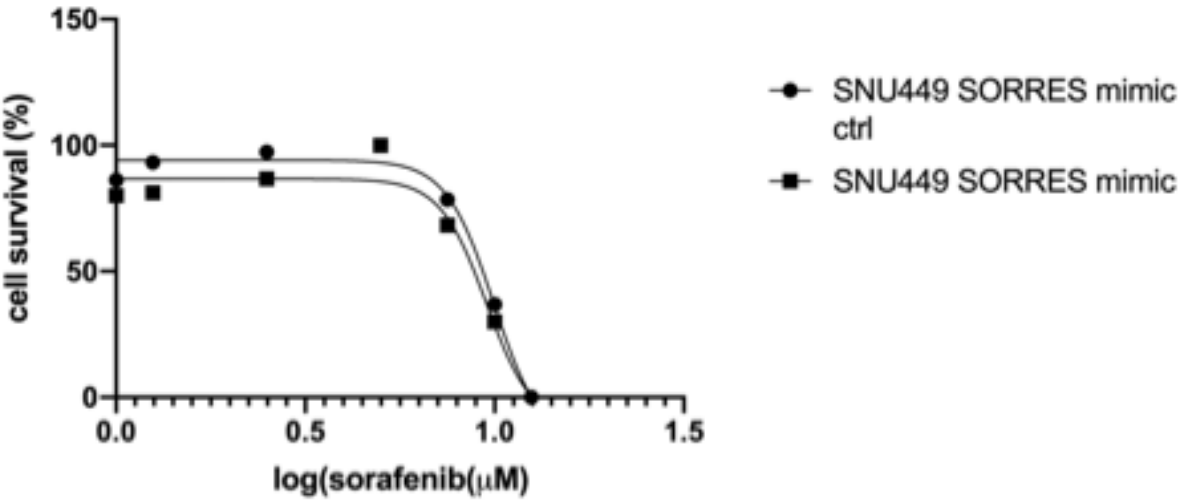

48H	SNU449 SORRES mimic ctrl	SNU449 SORRES mimic
IC50	9.941	9.510

Figure 36. SOR IC50 values of SNU-449 SORRES cells when they were transfected by miR-181a-5p mimic. The analysis was performed using the "Dose-response-Inhibition variable slope" tool in the GraphPad Prism program. IC50 value of SNU-449 SORRES mimic to control was lower.

The 2D colony formation ability of cells was determined in SNU-449 SORRES cells treated with mimic. miR-181a-5p mimic caused a slightly decrease in the area and the intensity of colonies but not significant (Figure 37).

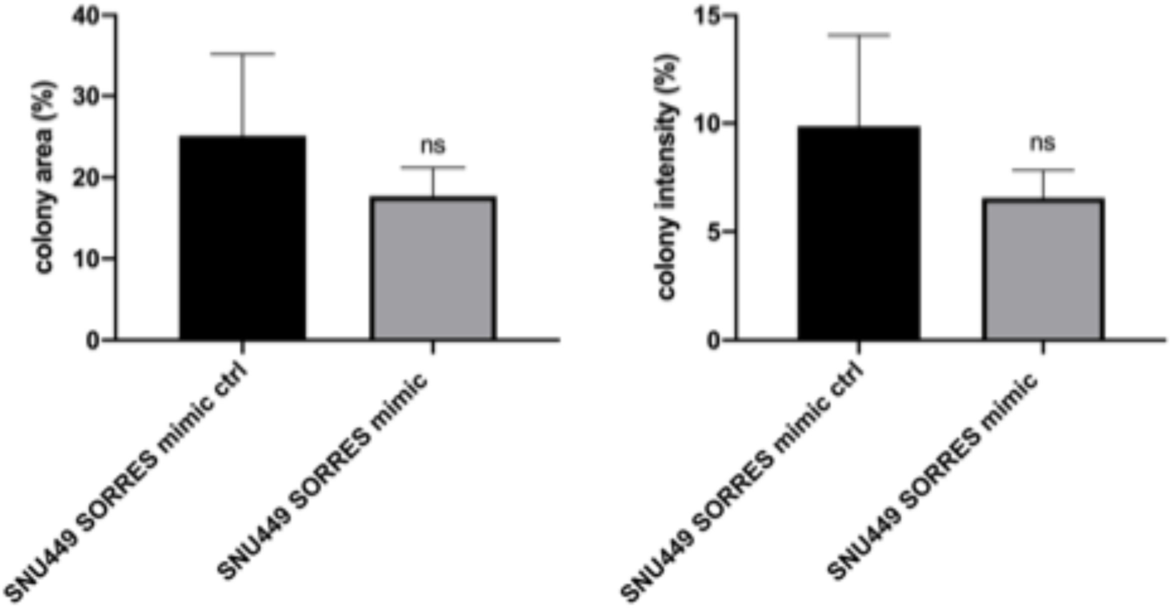

Figure 37. 2D Colony formation ability of mimic transfected SNU-449 SORRES cells was determined via 2D colony formation assay. (ns: $p>0.05$)

Motility of the HCC cells was examined via Boyden chamber motility assay. The cells that pass through the membrane were counted (Figure 38). miR-181a-5p-mimic transfection slightly decreased the motility of SNU-449 SORRES cells, but this decrase was not significant ($p>0.05$)

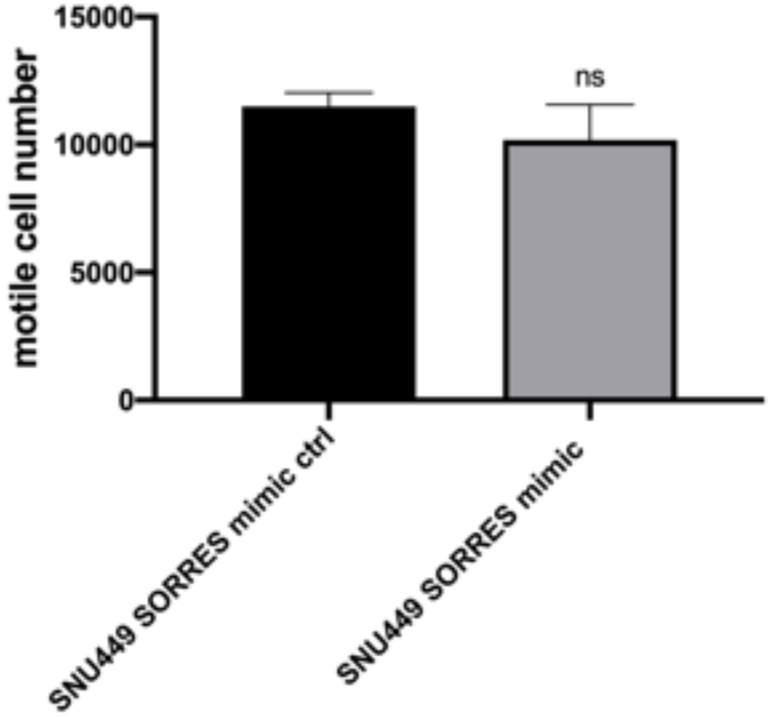

Figure 38. Motility of mimic transfected SNU-449 SORRES cells. For the assays to be performed, Boyden chambers were used. (ns: p>0.05)

When SNU-449 SORRES cells were transfected with miR-181a-5p-inhibitor, Sorafenib IC50 value was increased and inhibitor turned cells more resistant to Sorafenib (Figure 39).

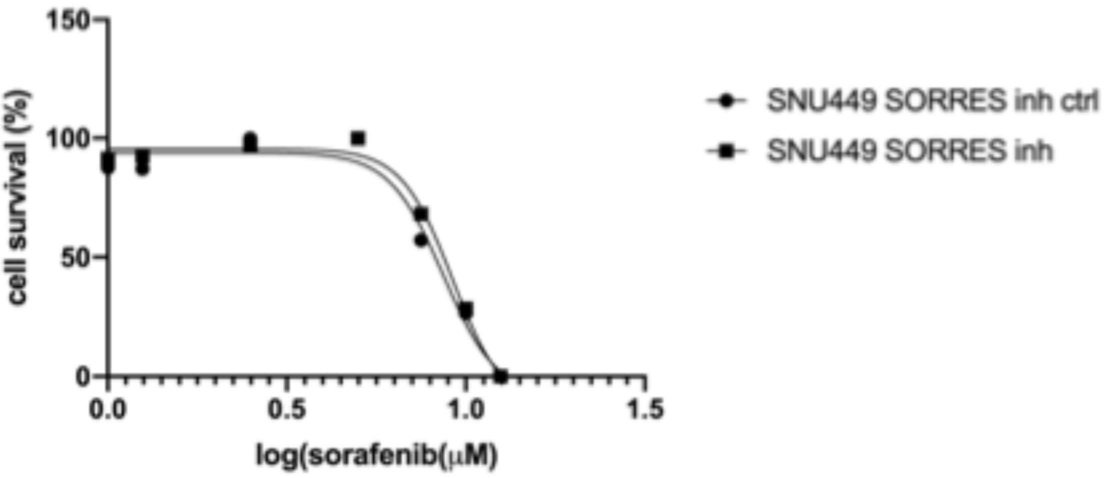

48H	SNU449 SORRES inh ctrl	SNU449 SORRES inh
IC50	8.647	9.173

Figure 39. SOR IC50 values of SNU-449 SORRES cells when they were transfected by miR-181a-5p inhibitor. The analysis was performed using the "Dose-response-Inhibition variable slope" tool in the GraphPad Prism program.

The 2D colony formation ability of cells was determined and miR-181a-5p inhibition caused a significant increase in the area and the intensity of colonies in SNU-449 SORRES cells (Figure 40).

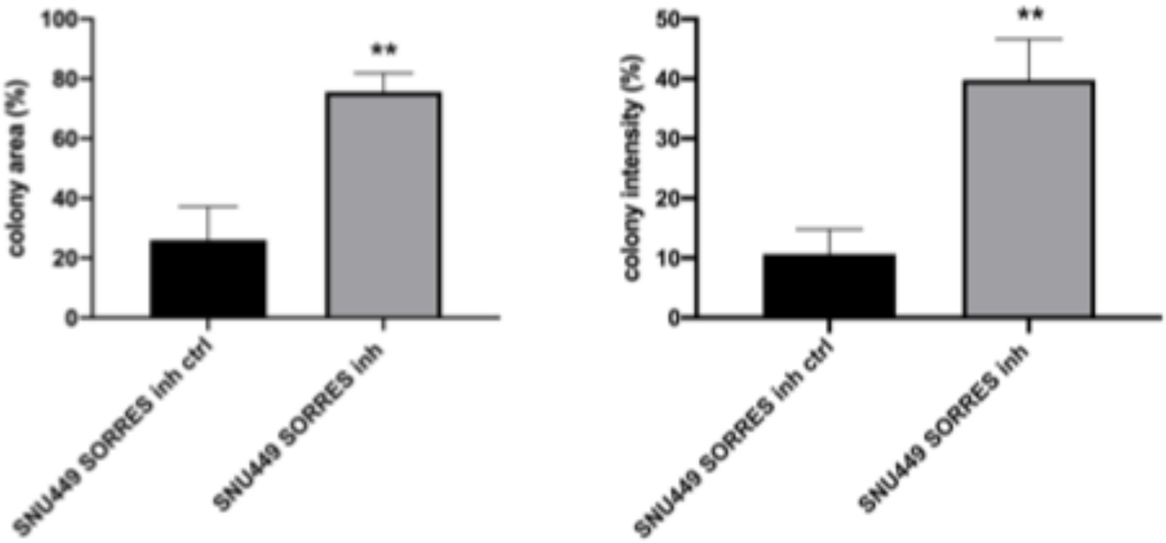

Figure 40. 2D Colony formation ability of inhibitor transfected SNU-449 SORRES cells was determined via 2D colony formation assay. (**: p<0.01)

The motility of SNU-449 SORRES cells, which were transfected by miR-181a-5p inhibitor, were examined via Boyden chamber motility assay (Figure 41). Inhibitor transfection increased the motility of SNU-449 SORRES cells.

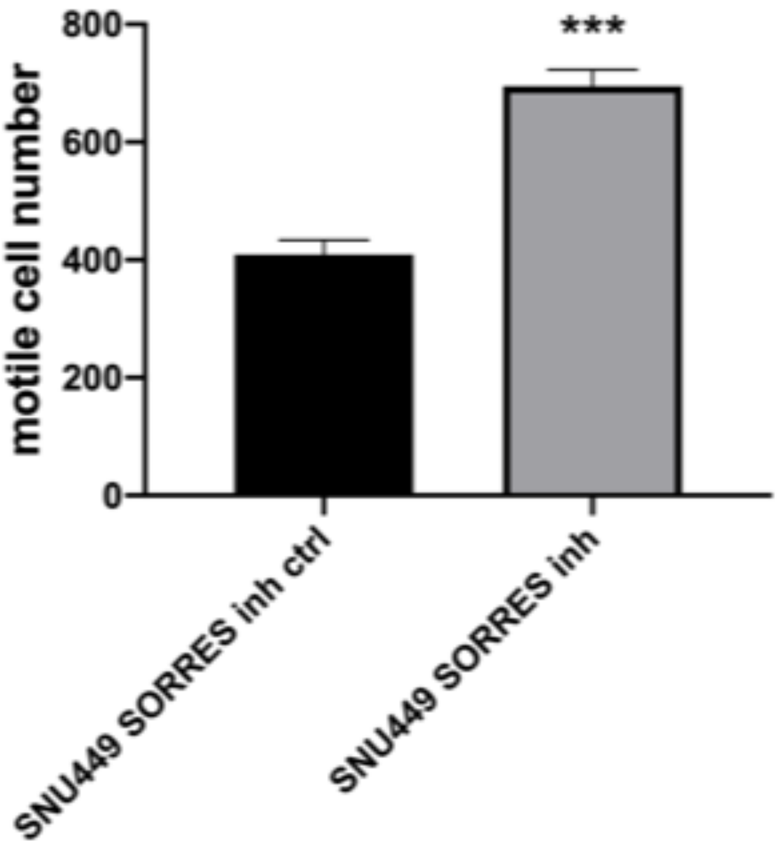

Figure 41. Motility of inhibitor transfected SNU-449 SORRES cells. Boyden chambers were used for these assays (***: p<0.001)

Expression levels of EMT marker levels were determined in miR-181a-5p-inhibitor transfected SNU-449 SORRES cells (Figure 42). Inhibitor induced hybrid E/M phenotype by increasing E-cadherin, Vimentin, and N-cadherin expressions in Sorafenib-resistant SNU 449 cells.

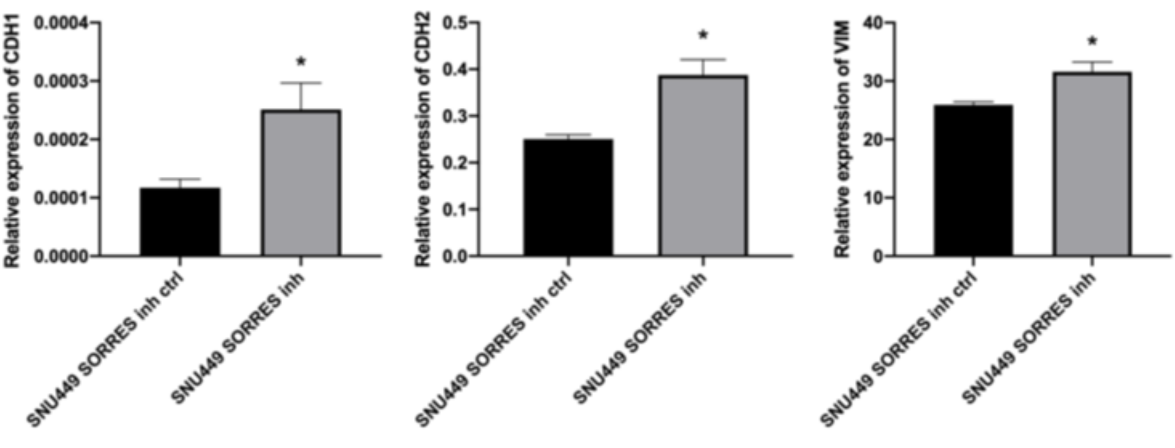

Figure 42. EMT marker expressions of miR-181a-5p inhibitor transfected SNU-449 SORRES cells performed by RT-qPCR. (*: p<0.05)

Stress fiber formation was examined via Phalloidin staining (Figure 43A). As Cav-1 expression was increased in miR-181a-5p inhibitor transfected SNU-449 SORRES cells, stress fiber formation was also increased in these cells (Figure 43B).

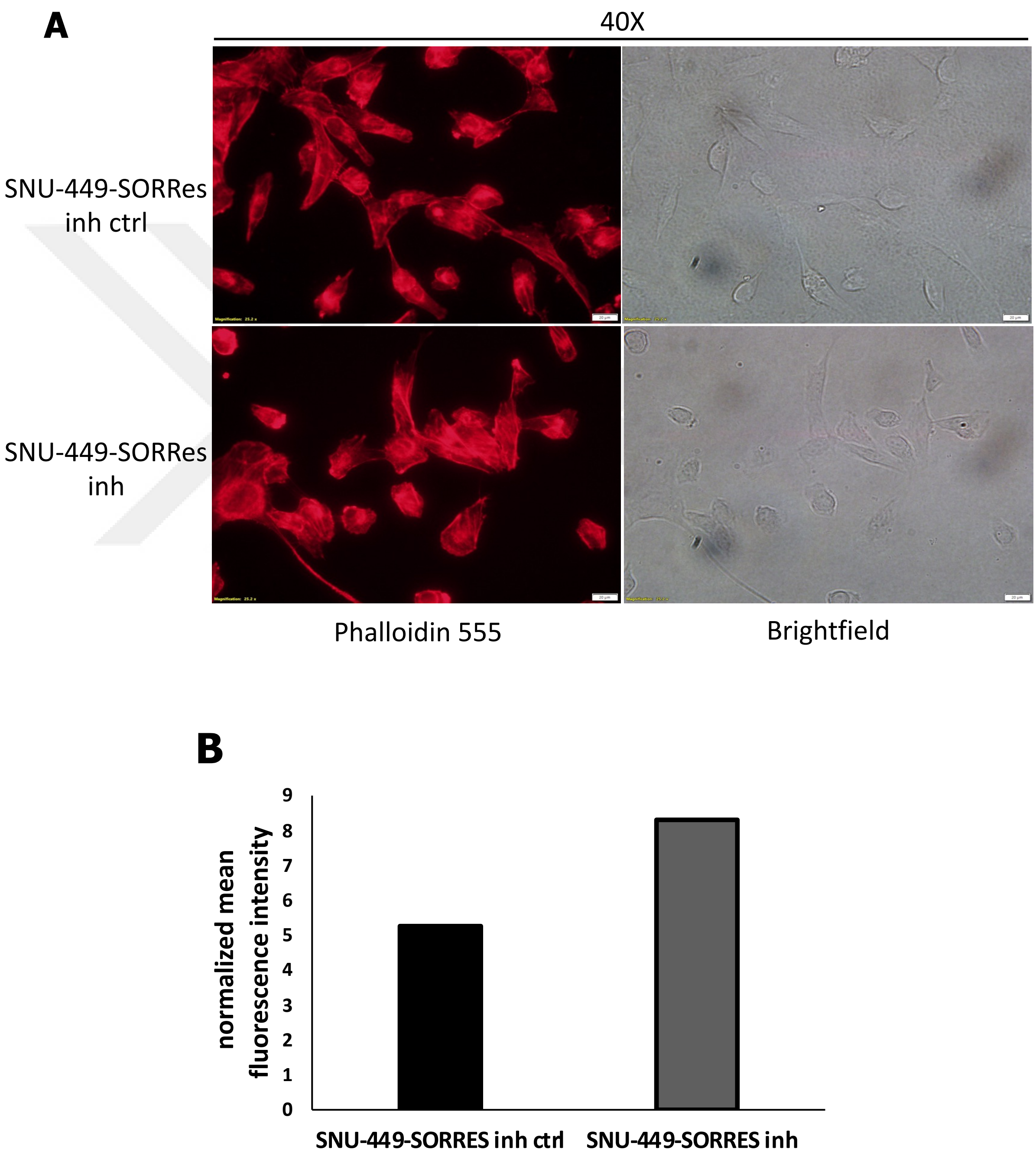

Figure 43. Determination of stress fiber formation by Phalloidin staining. Alexa 555 tagged Phalloidin was used. 40X images were taken under Olympus BX61 upright

fluorescence microscopy (A). Fluorescence intensity was measured by ImageJ and normalized to cell number in the image to compare fluorescence intensity between conditions (B).

As a result of the second chapter, we determined that miR-181a-5p has an impact on Sorafenib resistance, which might regulate Cav-1 levels. Cav-1 acts as a target of miR-181a-5p, and in miR-181a-5p inhibited conditions Cav1 level increased and HCC cells become resistant to Sorafenib treatment.

4.3. The significance of HOTAIR in Cav-1/miR-181a-5p relationship

As described above, miR-181a-5p inhibitor turns SNU-449 SORRES cells to modulate hybrid E/M phenotype. This leads us to think whether HOTAIR is a part of this relationship because our recent data showed the importance of HOTAIR overexpression in the promotion of hybrid E/M phenotype (53).

In our previous study, frequently used HCC cells do not express HOTAIR in high levels; thus, HOTAIR overexpressing stable clones were generated (Figure 44) (Figure 45).

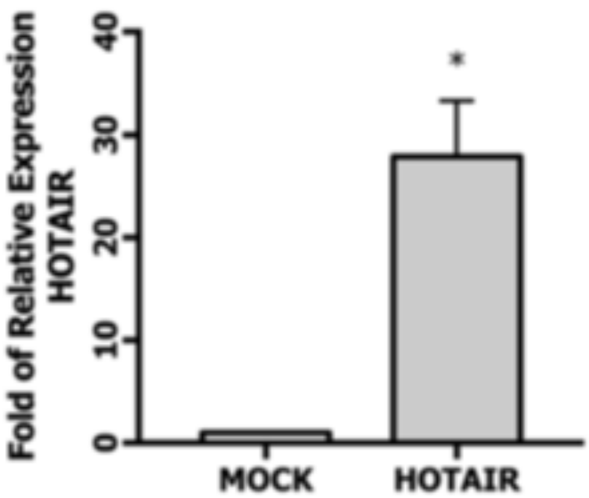

Figure 44. HOTAIR expression in HOTAIR overexpressing SNU-449 cell clone and its MOCK-transfected cells (*: p<0.05) (53).

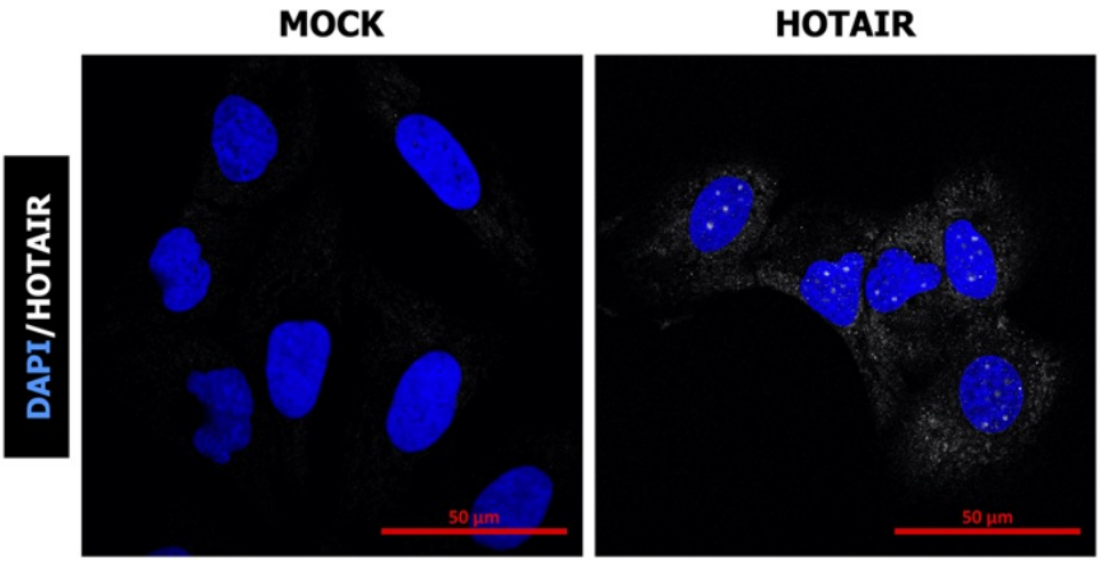

Figure 45. FISH probes specific to HOTAIR were used and detect HOTAIR in the cell where localized. Images were obtained via confocal microscopy in 63X magnification. (53).

When we tested HOTAIR expression level in SNU-449 SORRES cells, we observed that HOTAIR expression was significantly increased (*: p<0.05) (Figure 46).

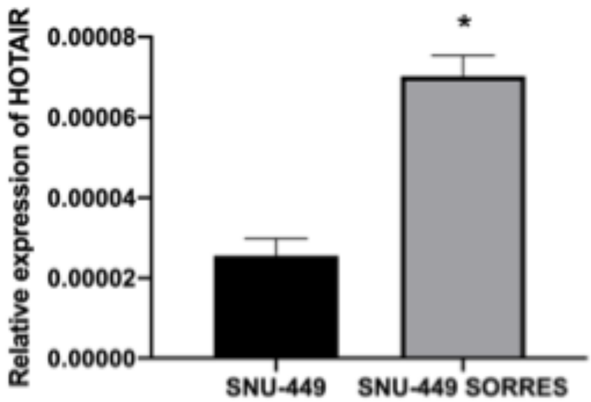

Figure 46. HOTAIR expression in SNU-449 SORRES cells and its wild-type counterparts. (*: p<0.05)

miR-181a-5p inhibition in SNU-449 SORRES cells caused a significant increase in HOTAIR expression (*: p<0.05) (Figure 47).

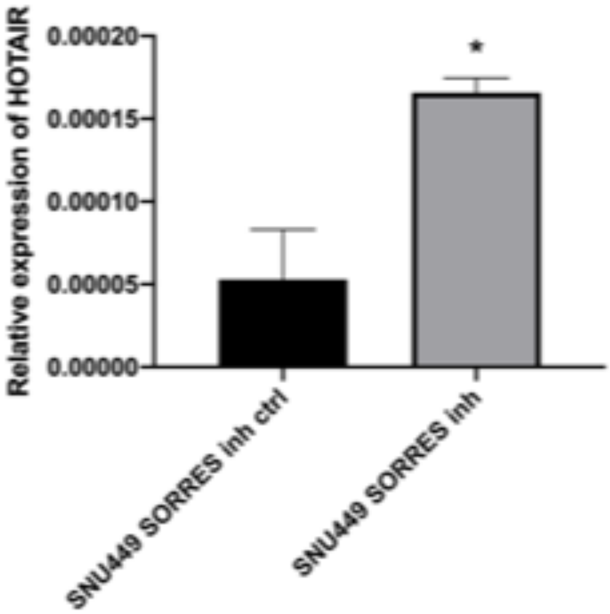

Figure 47. HOTAIR expression in miR-181a-5p inhibitor transfected SNU-449 SORRES cells (*: p<0.05)

Supportingly, miR-181a-5p expression was decreased in HOTAIR overexpressing SNU-449 cells (Figure 48).

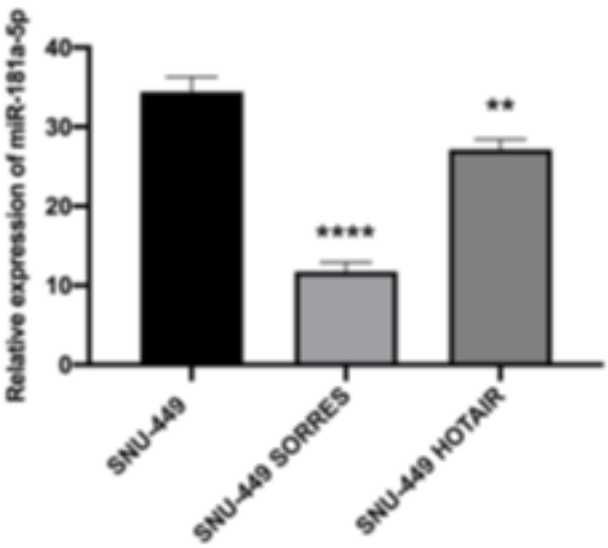

Figure 48. Expression of miR-181a-5p in SNU-449 SORRES and HOTAIR overexpressing cells. The experiment was performed by TaqMan miRNA assay. (**: $p<0.01$, ****: $p<0.0001$)

In summary, our data showed that HOTAIR expression level negatively correlated with miR-181a-5p levels. The HOTAIR-miR-181a-5p-Cav-1 axis may have contributed to Sorafenib resistance by keeping cells in the hybrid E/M phenotype. Although the individual roles of HOTAIR, miR-181a-5p, and Cav-1 in the development of aggressive phenotype are well defined in HCC, further studies are needed to determine the potential role of HOTAIR/miR-181a-5p/ CAV1 axis in Sorafenib-resistance.

5. DISCUSSION

Sorafenib resistance is one of the most important factors limiting treatment success in HCC. Although resistance and resistance mechanisms are deeply studied, the mechanism is not elucidated yet. The reason is might be the presence of several mechanisms that interact or emerge at different times or at the same time. When we deeply focus on one mechanism, the other one may emerge and make the activation of another more complicated mechanism.

In this study, we aimed to elucidate whether Cav-1 expression increase is related to Sorafenib resistance in HCC. For this study, three Sorafenib-resistant human HCC cell lines were generated. We and others have previously reported that a receptor tyrosine kinase, c-Met, overexpression and activation causes Sorafenib resistance in HCC cells (22). We have also reported that concurrent overexpression and activation of c-Met and Cav-1 increases during hepatocarcinogenesis, the reciprocal crosstalk between them promotes aggressive phenotype in HCC cells (4, 5). In light of these data, we proposed that Cav-1 might have a role in Sorafenib resistance. We showed that Cav-1 expression, stress fiber formation, mesenchymal markers, proliferation rate and adhesion-independent growth capacity were higher in Sorafenib-resistant HCC cell lines than WT cells. Furthermore, we overexpressed Cav-1 in HuH-7 cells and observed that Sorafenib IC50 values and caveolae formation were increased. When we silenced Cav-1 by using siRNA in Sorafenib-resistant cells, we observed a decrease in the aggressive phenotype of the cells. Briefly, Cav-1 siRNA-treated cells became less motile and invasive *in vitro* and less metastatic in the *in vivo* zebrafish embryo model. Thus, we can conclude that there is a relation between Cav-1 expression status and Sorafenib resistance, and Cav-1 expression increase positively contributes to Sorafenib resistance.

Then, we investigated the mechanisms that led to the Cav-1 increase during Sorafenib resistance. Among Sorafenib resistance mechanisms, we focused on non-coding RNA-based mechanisms. Several studies stated that alterations in miRNA levels in cancer may change their susceptibility to therapy (14, 47, 49, 50). Since we have observed both c-Met and Cav-1 expression increases are important in the development of Sorafenib-resistance, we first tested if there is any miRNA that simultaneously targets c-Met and Cav-1. We used miRNA target tools and found a miRNA that targets both c-Met and Cav-1, which was miR-34b-5p. However, we could not observe any detectable miR-34b-5p expression in any HCC cell line tested. Then, we focused on another miRNA, miR-181a-5p. We have previously reported that miR-181a-5p directly targets c-Met and decreases the aggressive phenotype of HCC cells (48). This led us to think that the expression of Cav-1 could be regulated by miR-181a-5p in Sorafenib resistance. We determined that miR-181a-5p expression levels in Sorafenib-resistant cells were decreased. We overexpressed or silenced the miR-181a-5p in Sorafenib-resistant cell lines by transfecting miR-181a-5p mimic and inhibitor and tested the susceptibility to Sorafenib. When we inhibited miR-181a-5p expression, HCC cells became more resistant to Sorafenib whereas when we increased miR-181a-5p expression by mimic cells sensitized to Sorafenib. Also, Cav-1 and miR-181a-5p levels were found to be negatively correlated in every condition. These findings support our hypothesis and show that, during Sorafenib resistance, cells become more motile, invasive, and metastatic by increasing Cav-1 and decreasing miR-181a-5p levels, so we can conclude that Cav-1-miR-181a-5p axis contributes to the sorafenib resistance in HCC.

In contrast to what we observed in this study, Azumi et al (57) reported that an increase in miR-181a level induces Sorafenib resistance in HCC cells through the downregulation of RASSF1. However, they did not use any Sorafenib-resistant cells for this study; they only observed a positive correlation between miR-181a level and Sorafenib IC50 values. This study supports our observations showing that the resistance mechanisms in HCC cells receiving acute Sorafenib once and in Sorafenib-resistant cell clones generated by continuous treatment with increasing concentrations of Sorafenib over a year are completely different.

When we focus more on the phenotypes of the Sorafenib-resistant HCC clones, their epithelial-mesenchymal plasticity (EMP) was noticeable. EMP has been described as a limiting factor for effective treatment in many cancer types (58). To particularly deepen into the mechanisms of which intermediate epithelial/mesenchymal (E/M) is one feature of aggressive phenotype that is directly related with metastatic capability and drug resistance. Hybrid E/M phenotype gives cells a survival advantage, anchorage-independent growth ability, and collective migration ability (54). We have previously reported that long noncoding RNA-HOTAIR induces hybrid E/M phenotype in HCC cells (53). Thus, this makes us think HOTAIR might have a role in Cav-1-miR-181a-5p mediated Sorafenib resistance. To test this, we compared HOTAIR expression levels between WT and Sorafenib-resistant cells SNU-449 and HOTAIR overexpressing SNU-449 cells. We showed that HOTAIR expression was significantly increased in SNU-449 SORRES cells. Furthermore, miR-181a-5p inhibitor treatment caused a significant increase in HOTAIR expression in SNU-449 cells. Supporting the negative correlation with miR-81a-5p and HOTAIR expression, miR-181a-5p expression was decreased in HOTAIR overexpressing SNU-449 cells. Thus, we can conclude that HOTAIR, miR-181a-5p, Cav-1, axis may contribute to Sorafenib resistance.

These three molecules, Cav-1, miR-181a-5p, and HOTAIR, individually and together induce aggressive and treatment-resistant phenotypes. Crosstalk between them might be important to maintain cells in the hybrid E/M phenotype to protect themselves from Sorafenib treatment.

Further studies are needed to clarify how they interact with each other and the detailed roles in therapy response.

6. CONCLUSIONS AND FUTURE DIRECTIONS

In this study,

- Cav-1 is overexpressed in Sorafenib-resistant cells compared to their wild-type counterparts.
- Cav-1 overexpressing cell clones have higher Sorafenib IC50 values.
- Cav-1 silenced Sorafenib-resistant cells show a decrease in the aggressive phenotype.
- In Sorafenib resistant cells, miR-181a-5p expression is decreased.
- Inhibition of miR-181a-5p expression turns cells more resistant to Sorafenib whereas an increase in miR-181a-5p expression by miRNA mimic turns cells sensitized to Sorafenib.
- Cav-1 and miR-181a-5p expressions are negatively correlated
- HOTAIR expressions were increased in SNU-449 SORRES cells
- HOTAIR expressions are negatively correlated with miR-181a-5p expressions.
- Cav-1, miR-181a-5p, and HOTAIR contribute to Sorafenib resistance via maintaining HCC cells in the hybrid E/M phenotype.

Further studies are needed (i) to define the potential interaction mechanisms of Cav-1, miR-181a-5p, and HOTAIR, (ii) to validate these interactions by in vivo studies, and (iii) in primary patient tissues.

7. REFERENCES

1. GLOBOCAN. 2022. https://gco.iarc.who.int
2. Tang W, Chen Z, Zhang W, Cheng Y, *et al*. The mechanisms of sorafenib resistance in hepatocellular carcinoma: theoretical basis and therapeutic aspects. Signal Transduct Target Ther. 2020 Jun 10;5(1):87.
3. Zhai B, Sun XY. Mechanisms of resistance to sorafenib and the corresponding strategies in hepatocellular carcinoma. World J Hepatol. 2013;5(7):345-52.
4. Cokakli M, Erdal E, Nart D, Yilmaz F, *et al*. Differential expression of Caveolin-1 in hepatocellular carcinoma: correlation with differentiation state, motility and invasion. BMC Cancer. 2009 Feb 24;9:65.
5. Korhan P, Erdal E, Kandemis E, Cokakli M, *et al*. Reciprocal activating crosstalk between c-Met and caveolin 1 promotes invasive phenotype in hepatocellular carcinoma. PLoS One. 2014;9(8):e105278.
6. Price, C., Chen, J. 2014. "MicroRNAs in cancer biology and therapy: Current status and perspectives", Genes & Diseases, 1 (1), 53-63.
7. Hanahan, D., Weinberg, R.A. 2011. "Hallmarks of cancer: the next generation", Cell, 144 (5), 646-74.
8. Si W, Shen J, Zheng H, Fan W. The role and mechanisms of action of microRNAs in cancer drug resistance. Clin Epigenetics. 2019 Feb 11;11(1):25.
9. Chakraborty E, Sarkar D. Emerging Therapies for Hepatocellular Carcinoma (HCC). Cancers (Basel). 2022 Jun 4;14(11):2798.
10. Huang A, Yang XR, Chung WY, Dennison AR, *et al*. Targeted therapy for hepatocellular carcinoma. Signal Transduct Target Ther. 2020 Aug 11;5(1):146.
11. Shannon AH, Ruff SM, Pawlik TM. Expert Insights on Current Treatments for Hepatocellular Carcinoma: Clinical and Molecular Approaches and Bottlenecks to Progress. J Hepatocell Carcinoma. 2022 Dec 7;9:1247-1261.
12. Zhang H, Zhang W, Jiang L, Chen Y. Recent advances in systemic therapy for hepatocellular carcinoma. Biomark Res. 2022 Jan 9;10(1):3.

13. Tao M, Han J, Shi J, Liao H, *et al*. Application and Resistance Mechanisms of Lenvatinib in Patients with Advanced Hepatocellular Carcinoma. J Hepatocell Carcinoma. 2023 Jul 10;10:1069-1083.
14. Callegari E, Domenicali M, Gramantieri L, Negrini M, *et al*. Emerging role of microRNAs in the treatment of hepatocellular carcinoma. Gastrointestinal Cancer: Targets and Therapy. 2015;5:89-102.
15. Dahiya M, Dureja H. Sorafenib for hepatocellular carcinoma: potential molecular targets and resistance mechanisms. J Chemother. 2022 Sep;34(5):286-301.
16. Chen J, Duda DG. Overcoming sorafenib treatment-resistance in hepatocellular carcinoma: A future perspective at a time of rapidly changing treatment paradigms. EBioMedicine. 2020 Feb;52:102644.
17. Zhu YJ, Zheng B, Wang HY, Chen L. New knowledge of the mechanisms of sorafenib resistance in liver cancer. Acta Pharmacol Sin. 2017 May;38(5):614-622.
18. Fornari F, Giovannini C, Piscaglia F, Gramantieri L. Elucidating the Molecular Basis of Sorafenib Resistance in HCC: Current Findings and Future Directions. J Hepatocell Carcinoma. 2021 Jul 2;8:741-757.
19. Lee D, Sung ES, Ahn JH, An S *et al*. Development of antibody-based c-Met inhibitors for targeted cancer therapy. Immunotargets Ther. 2015;4:35-44.
20. Comoglio PM, Giordano S, Trusolino L. Drug development of MET inhibitors: targeting oncogene addiction and expedience. Nat Rev Drug Discov. 2008 Jun;7(6):504-16.
21. Birchmeier C, Birchmeier W, Gherardi E, Vande Woude GF. Met, metastasis, motility and more. Nat Rev Mol Cell Biol. 2003;4(12):915-25.
22. Firtina Karagonlar Z, Koc D, Iscan E, Erdal E *et al*. Elevated hepatocyte growth factor expression as an autocrine c-Met activation mechanism in acquired resistance to sorafenib in hepatocellular carcinoma cells. Cancer Sci. 2016;107(4):407-16.

23. Topel H, Bağırsakçı E, Yılmaz Y, Güneş A, *et al*. High glucose induced c-Met activation promotes aggressive phenotype and regulates expression of glucose metabolism genes in HCC cells. Sci Rep. 2021 May 31;11(1):11376.
24. Gunes A, Bagirsakci E, Iscan E, Cakan-Akdogan G, *et al*. Thioredoxin interacting protein promotes invasion in hepatocellular carcinoma. Oncotarget. 2018 Dec 7;9(96):36849-36866.
25. İşcan E, Güneş A, Korhan P, Yılmaz Y, *et al*. The regulatory role of heparin on c-Met signaling in hepatocellular carcinoma cells. J Cell Commun Signal. 2017 Jun;11(2):155-166.
26. Ludwig A, Howard G, Mendoza-Topaz C, Deerinck T *et al*. Molecular composition and ultrastructure of the caveolar coat complex. PLoS Biol. 2013;11(8):e1001640.
27. Suetsugu S, Kurisu S, Takenawa T. Dynamic shaping of cellular membranes by phospholipids and membrane-deforming proteins. Physiol Rev. 2014;94(4):1219-48.
28. Frost A, Unger VM, De Camilli P. The BAR domain superfamily: membrane-molding macromolecules. Cell. 2009;137(2):191-6.
29. Henley JR, Krueger EW, Oswald BJ, McNiven MA. Dynamin-mediated internalization of caveolae. J Cell Biol. 1998;141(1):85-99.
30. Pelkmans L, Puntener D, Helenius A. Local actin polymerization and dynamin recruitment in SV40-induced internalization of caveolae. Science. 2002;296(5567):535-9.
31. Lian X, Matthaeus C, Kaßmann M, Daumke O, *et al*. Pathophysiological Role of Caveolae in Hypertension. Front Med (Lausanne). 2019 Jul 10;6:153.
32. Nethe M, Hordijk PL. A model for phospho-caveolin-1-driven turnover of focal adhesions. Cell Adh Migr. 2011;5(1):59-64.
33. Ariotti N, Rae J, Leneva N, Ferguson C *et al*. Molecular Characterization of Caveolin-induced Membrane Curvature. J Biol Chem. 2015;290(41):24875-90.
34. Diaz-Valdivia N, Bravo D, Huerta H, Henriquez S *et al*. Enhanced caveolin-1 expression increases migration, anchorage-independent growth and invasion of endometrial adenocarcinoma cells. BMC Cancer. 2015;15:463.

35. Bailey KM, Liu J. Caveolin-1 up-regulation during epithelial to mesenchymal transition is mediated by focal adhesion kinase. J Biol Chem. 2008;283(20):13714-24.
36. Liu Y, Lv JY, Shi JF, Yang M *et al*. Targeting the raft-associated Akt signaling in hepatocellular carcinoma. Biomed Res Int. 2014;2014:836025.
37. He M, Qin H, Poon TC, Sze SC *et al*. Hepatocellular carcinoma-derived exosomes promote motility of immortalized hepatocyte through transfer of oncogenic proteins and RNAs. Carcinogenesis. 2015;36(9):1008-18.
38. Li Z, Wang N, Huang C, Bao Y, *et al*. Downregulation of caveolin-1 increases the sensitivity of drug-resistant colorectal cancer HCT116 cells to 5-fluorouracil. Oncol Lett. 2017 Jan;13(1):483-487.
39. Zou W, Ma X, Hua W, Chen B, *et al*. Caveolin-1 mediates chemoresistance in cisplatin-resistant ovarian cancer cells by targeting apoptosis through the Notch-1/Akt/NF-κB pathway. Oncol Rep. 2015 Dec;34(6):3256-63.
40. Yang CP, Galbiati F, Volonte D, Horwitz SB, *et al*. Upregulation of caveolin-1 and caveolae organelles in Taxol-resistant A549 cells. FEBS Lett. 1998 Nov 20;439(3):368-72.
41. Wang X, Lu B, Dai C, Fu Y, *et al*. Caveolin-1 Promotes Chemoresistance of Gastric Cancer Cells to Cisplatin by Activating WNT/β-Catenin Pathway. Front Oncol. 2020 Feb 3;10:46.
42. Lavie Y, Fiucci G, Liscovitch M. Upregulation of caveolin in multidrug resistant cancer cells: functional implications. Adv Drug Deliv Rev. 2001 Jul 28;49(3):317-23.
43. Borel F, Konstantinova P, Jansen PL. Diagnostic and therapeutic potential of miRNA signatures in patients with hepatocellular carcinoma. J Hepatol. 2012 Jun;56(6):1371-83.
44. Misiewicz-Krzeminska I, Krzeminski P, Corchete LA, Quwaider D, *et al*. Factors Regulating microRNA Expression and Function in Multiple Myeloma. Noncoding RNA. 2019 Jan 16;5(1):9.

45. Pratama MY, Visintin A, Crocè LS, Tiribelli C, *et al*. Circulatory miRNA as a Biomarker for Therapy Response and Disease-Free Survival in Hepatocellular Carcinoma. Cancers (Basel). 2020 Sep 29;12(10):2810.
46. Yates LA, Norbury CJ, Gilbert RJ. The long and short of microRNA. Cell. 2013 Apr 25;153(3):516-9.
47. Li J, Bao H, Huang Z, Liang Z, *et al*. Little things with significant impact: miRNAs in hepatocellular carcinoma. Front Oncol. 2023 May 19;13:1191070.
48. Korhan, P., Erdal, E., Atabey, N. 2014. "MiR-181a-5p is downregulated in hepatocellular carcinoma and suppresses motility, invasion and branching-morphogenesis by directly targeting c-Met.", Biochem Biophys Res Commun., 450(4):1304-12.
49. Pratama MY, Pascut D, Massi MN, Tiribelli C. The role of microRNA in the resistance to treatment of hepatocellular carcinoma. Ann Transl Med. 2019 Oct;7(20):577.
50. Wei L, Wang X, Lv L, Liu J, *et al*. The emerging role of microRNAs and long noncoding RNAs in drug resistance of hepatocellular carcinoma. Mol Cancer. 2019 Oct 25;18(1):147.
51. Hu X, Zhu H, Shen Y, Zhang X, *et al*. The Role of Non-Coding RNAs in the Sorafenib Resistance of Hepatocellular Carcinoma. Front Oncol. 2021 Jul 22;11:696705.
52. Tang X, Zhang W, Ye Y, Li H, *et al*. LncRNA HOTAIR Contributes to Sorafenib Resistance through Suppressing miR-217 in Hepatic Carcinoma. Biomed Res Int. 2020 May 9;2020:9515071.
53. Topel H, Bagirsakci E, Comez D, Bagci G, *et al*. lncRNA HOTAIR overexpression induced downregulation of c-Met signaling promotes hybrid epithelial/mesenchymal phenotype in hepatocellular carcinoma cells. Cell Commun Signal. 2020 Jul 11;18(1):110.
54. Basu S, Cheriyamundath S, Ben-Ze'ev A. Cell-cell adhesion: linking Wnt/β-catenin signaling with partial EMT and stemness traits in tumorigenesis. F1000Res. 2018 Sep 18;7:F1000 Faculty Rev-1488.

55. McDermott M, Eustace AJ, Busschots S, Breen L, *et al*. In vitro Development of Chemotherapy and Targeted Therapy Drug-Resistant Cancer Cell Lines: A Practical Guide with Case Studies. Front Oncol. 2014 Mar 6;4:40.
56. Bagirsakci, E. Hepatoselüler Karsinoma'da Kaveolin-1'in Sorafenib Direnci Gelişimindeki Rolü, Izmir, Dokuz Eylul University, masters' thesis, 2017, 1-86.
57. Azumi J, Tsubota T, Sakabe T, Shiota G. miR-181a induces sorafenib resistance of hepatocellular carcinoma cells through downregulation of RASSF1 expression. Cancer Sci. 2016 Sep;107(9):1256-62. doi: 10.1111/cas.13006.
58. Fontana R, Mestre-Farrera A, Yang J. Update on Epithelial-Mesenchymal Plasticity in Cancer Progression. Annu Rev Pathol. 2024 Jan 24;19:133-156.

8. ADDENDA

8.1. Ethical Committee Report

İZMİR BİYOTIP VE GENOM MERKEZİ
HAYVAN DENEYLERİ YEREL ETİK KURULU (İBG-HADYEK)
KARARI

Toplantı Tarihi	: 11/11/2020	**Toplantı Günü**	: Çarşamba
Toplantı Sayısı	: 13	**Toplantı Saati**	: 15:30

Sayın Doç. Dr. Kasım DIRIL,

2020-038 Protokol No'lu; yürütücüsü olduğunuz "Hepatoselüler Karsinoma'da tedavi yanıtını düzenleyen mikroRNA'ların araştırılması" başlıklı projenin uygulanmasında etik açıdan sakınca olmadığına oy birliği ile karar verilmiştir.

Bilgilerinizi ve gereğini rica ederiz.

Doç. Dr. Güneş ÖZHAN BAYKAN **Başkan**	**Vet. Hek. Kerem ESMEN** **Başkan Yardımcısı**
Prof. Dr. H. Alper BAĞRIYANIK **Üye** (Katılmadı)	**Prof. Dr. Ensari GÜNELİ** **Üye**
(Proje Yürütücüsü) **Doç. Dr. Kasım DİRİL** **Üye**	**Dr. Öğr. Üyesi Ayşe Banu DEMİR** **Üye**
Dr. Gülçin ÇAKAN AKDOĞAN **Üye** (Katılmadı)	**Vet. Hek. Umur KELEŞ** **Üye**
H. Muammer KARAGÖZ **Üye**	

8.2. CV

EZGİ BAĞIRSAKÇI TEPE

Personal Information

Contact Information

Contact Address	Izmir Biyotıp Ve Genom Merkezi (ibg) Dokuz Eylül Üniversitesi Sağlık Yerleşkesi
Telephone	
Email	
Web Page	

Education Information

07 September 2017 - Now (6 Year 6 Month)
Doktora, Doktora, DOKUZ EYLÜL ÜNİVERSİTESİ, TÜRKİYE
İZMİR ULUSLARARASI BİYOTIP VE GENOM ENSTİTÜSÜ, MOLEKÜLER BİYOLOJİ VE GENETİK (DR) (İNGİLİZCE)
Diploma Number: -
Cumulative Grade Point Average: 3.63 / 4.0

21 January 2015 - 18 August 2017 (2 Year 7 Month)
Yüksek Lisans, Tezli Program, DOKUZ EYLÜL ÜNİVERSİTESİ, TÜRKİYE
SAĞLIK BİLİMLERİ ENSTİTÜSÜ, TIBBİ BİYOLOJİ VE GENETİK (YL) (TEZLİ)
Diploma Number: 201708131
Cumulative Grade Point Average: 3.84 / 4.0

24 August 2009 - 14 June 2014 (4 Year 10 Month)
Lisans, Anadal/Normal Öğretim, İHSAN DOĞRAMACI BİLKENT ÜNİVERSİTESİ, TÜRKİYE
FEN FAKÜLTESİ, MOLEKÜLER BİYOLOJİ VE GENETİK PR. (İNGİLİZCE) (ÜCRETLİ)
Diploma Number: 141140506
Cumulative Grade Point Average: 2.54 / 4.0

R&D Competency

Articles

G. BAGCİ, D. COMEZ, H. TOPEL, Y. YİLMAZ, E. BAGİRSAKCİ, A. GUNES, G. B. AYAZ, I. TAHMAZ, M. BİLGEN, G. SOLMAZ, D. P. OKVUR & N. ATABEY, c-Met activation promotes extravasation of hepatocellular carcinoma cells into 3D-cultured hepatocyte cells in lab-on-a-chip device, BIOCHIMICA ET BIOPHYSICA ACTA-MOLECULAR CELL RESEARCH, 2023, 0167-4889, 1870, 8, 4.

U. EKİN, H. YUZUGULLU, C. OZEN, P. KORHAN, E. BAGİRSAKCİ, F. YİLMAZ, O. G. YUZUGULLU, H. UZUNER, H. ALOTAİBİ, P. B. KİRMİZİBAYRAK, N. ATABEY, G. KARAKULAH & M. OZTURK, Evaluation of ATAD2 as a Potential Target in Hepatocellular Carcinoma, JOURNAL OF GASTROINTESTINAL CANCER, 2021, 1941-6628, 52, 4, 14.

H. TOPEL, E. BAGİRSAKCİ, Y. YİLMAZ, A. GUNES, G. BAGCİ, D. COMEZ, E. KAHRAMAN, P. KORHAN & N. ATABEY, High glucose induced c-Met activation promotes aggressive phenotype and regulates expression of glucose metabolism genes in HCC cells, SCIENTIFIC REPORTS, 2021, 2045-2322, 11, 1, 15.

H. TOPEL, E. BAGİRSAKCİ, D. COMEZ, G. BAGCİ, G. CAKAN-AKDOGAN & N. ATABEY, lncRNA HOTAIR overexpression induced downregulation of c-Met signaling promotes hybrid epithelial/mesenchymal phenotype in hepatocellular carcinoma cells, CELL COMMUNICATION AND SIGNALING, 2020, 1478-811X, 18, 1.

P. KORHAN, Y. YİLMAZ, E. BAGİRSAKCİ, A. GUNES, H. TOPEL, B. I. CARR & N. ATABEY, Pleiotropic Effects of Heparins: From Clinical Applications to Molecular Mechanisms in Hepatocellular Carcinoma, CANADIAN JOURNAL OF GASTROENTEROLOGY AND HEPATOLOGY, 2018, 2291-2789, 2018.

A. GÜNEŞ, E. BAĞIRSAKÇI TEPE, E. İŞCAN, G. ÇAKAN AKDOĞAN, U. AYKUTLU, Ş. ŞENTÜRK, H. G. ÖZHAN, Ş. E. ERDAL BAĞRIYANIK, D. NART, F. YILMAZ BARBET & S. N. ATABEY, Thioredoxin interacting protein promotes invasion in hepatocellular carcinoma, ONCOTARGET, 2018, 1949-2553, 9, 96, 36849-36866.

E. BAGİRSAKCİ, E. SAHİN, N. ATABEY, E. ERDAL, V. GUERRA & B. I. CARR, Role of Albumin in Growth Inhibition in Hepatocellular Carcinoma, ONCOLOGY, 2017, 0030-2414, 93, 2, 136-142.

Conference Papers

H. TOPEL BATARLAR, Y. YILMAZ, E. BAĞIRSAKÇI TEPE, A. GÜNEŞ, G. BAĞCI, D. ÇÖMEZ, E. KAHRAMAN & S. N. ATABEY, Yüksek Glukoz c-Met Aktivasyonunu Uyararak Hepatoselüler Karsinoma Hücrelerine Agresif Karakter Kazandırmaktadır, Sözlü Sunum, 4. Çukurova Hepatoselüler Karsinoma Kongresi, 27 February 2020, 29 February 2020.

H. TOPEL BATARLAR, D. ÇÖMEZ, Y. YILMAZ, E. BAĞIRSAKÇI TEPE, A. GÜNEŞ, G. BAĞCI & S. N. ATABEY, c-Met İnhibisyonunun Hepatoselüler Karsinoma Hücrelerinde Metabolik Genlerin Düzenlenmesine Etkisi, Sözlü Sunum, 4. Çukurova Hepatoselüler Karsinoma Kongresi, 27 February 2020, 29 February 2020.

Y. YILMAZ, B. GÜLOĞLU, E. BAĞIRSAKÇI TEPE, E. KARACA EREK, B. KAPLAN TÜRKÖZ, A. ÜREN & S. N. ATABEY, HGF Reseptörü c-Met'in Nedilasyonunun Hepatoselüler Karsinoma Progresyonunda ve Sorafenib Direncindeki Rolü, Sözlü Sunum, Onkolojide İz Bırakanlar Zirvesi, 14 November 2019, 17 November 2019, 105 - null.

E. BAĞIRSAKÇI TEPE, A. GÜNEŞ & S. N. ATABEY, Hepatoselüler Karsinomada Sorafenib Direnci Gelişiminde Kaveolin-1'in Rolü, Sözlü Sunum, Onkolojide İz Bırakanlar Zirvesi, 14 November 2019, 17 November 2019, 13 - null.

D. ÇÖMEZ, G. BAĞCI, H. TOPEL BATARLAR, E. BAĞIRSAKÇI TEPE, Y. YILMAZ, A. GÜNEŞ, G. BATI AYAZ, D. PESEN OKVUR & S. N. ATABEY, Sıvı Teğetsel Gerilme Stresinin Hepatoselüler Karsinoma Hücrelerinin Sağkalımına ve Organ Tercihine Etkisinin Mikroakışkan Lab-on-a-chip Sistemi ile İncelenmesi, Sözlü Sunum, Onkolojide İz Bırakanlar Zirvesi, 14 November 2019, 17 November 2019, 13 - null.

D. ÇÖMEZ, G. BAĞCI, H. TOPEL BATARLAR, E. BAĞIRSAKÇI TEPE, Y. YILMAZ, A. GÜNEŞ, G. BATI AYAZ, D. PESEN OKVUR & S. N. ATABEY, Fluidic Shear Stress Regulates Biological Behaviours of Hepatocellular Carcinoma Cells Through c-Met Signalling, Sözlü Sunum, 1st International Multidisciplinary Cancer Research

Congress, 18 September 2019, 22 September 2019, 70 - null.

G. BAĞCI, D. ÇÖMEZ, H. TOPEL BATARLAR, E. BAĞIRSAKÇI TEPE, Y. YILMAZ, A. GÜNEŞ, G. BATI AYAZ, D. PESEN OKVUR & S. N. ATABEY, The Role of c-Met Signaling in Organ Specific Extravasation of HCC cells, Sözlü Sunum, 1st International Multidisciplinary Cancer Research Congress, 18 September 2019, 22 September 2019, 81 - null.

G. BAĞCI, D. ÇÖMEZ, H. TOPEL BATARLAR, E. BAĞIRSAKÇI TEPE, Y. YILMAZ, A. GÜNEŞ, G. BATI AYAZ, D. PESEN OKVUR & S. N. ATABEY, HCC Hücrelerinde Organ Spesifik Metastazda c-Met Yolağı Rolünün Yonga-Üstü-Laboratuvar Cihazı Kullanılarak İncelenmesi, Poster Sunumu, 3. Çukurova Hepatoselüler Karsinoma Kongresi, 21 February 2019, 23 February 2019.

D. ÇÖMEZ, G. BAĞCI, H. TOPEL BATARLAR, E. BAĞIRSAKÇI TEPE, Y. YILMAZ, A. GÜNEŞ, G. BATI AYAZ, D. PESEN OKVUR & S. N. ATABEY, c-Met aktivasyonunun Hepatoselüler Karsinoma Hücrelerinin Sıvı Teğetsel Gerilme Stresinin Sağkalım ve Metastaza Etkisi, Sözlü Sunum, 3. Çukurova Hepatoselüler Karsinoma Kongresi, 21 February 2019, 23 February 2019.

H. TOPEL BATARLAR, Y. YILMAZ, A. GÜNEŞ, E. BAĞIRSAKÇI TEPE, G. BATI AYAZ, D. ÇÖMEZ, G. BAĞCI, E. KAHRAMAN, D. PESEN OKVUR & S. N. ATABEY, Predicting Homing Ability Of Hepatocellular Carcinoma Cells By Using A Lab-on-a-chip System, Poster Sunumu, 25th Biennial Congress Of The European Association For Cancer Research, 30 June 2018, 03 July 2018, 2059-7029, 3, 2, A91 - A92.

E. BAĞIRSAKÇI TEPE, A. GÜNEŞ & S. N. ATABEY, Kaveolin-1in Sorafenib Direnci Gelişimindeki Rolü, Sözlü Sunum, 2.çukurova Hepatoselüler Karsinoma Kongresi Hcc Biyolojisini Anlamak: Hasta Yönetimine Neler Sunacak?, 23 February 2018, 25 February 2018, 21 - null.

E. KAHRAMAN, E. BAĞIRSAKÇI TEPE, A. GÜNEŞ, Ş. E. ERDAL BAĞRIYANIK, D. NART, F. YILMAZ BARBET & S. N. ATABEY, Sestrin2 Overekspresyonunun Hcc Hücrelerini Ros Ile Uyarlan Hücre Ölümünden Koruyucu Rolü, Sözlü Sunum, 2.çukurova Hepatoselüler Karsinoma Kongresi Hcc Biyolojisini Anlamak: Hasta Yönetimine Neler Sunacak?, 23 February 2018, 25 February 2018, 16 - null.

A. GÜNEŞ, E. BAĞIRSAKÇI TEPE, E. İŞCAN, G. ÇAKAN AKDOĞAN, U. AYKUTLU, Ş. ŞENTÜRK, H. G. ÖZHAN, Ş. E. ERDAL BAĞRIYANIK, D. NART, F. YILMAZ BARBET & S. N. ATABEY, Tiyoredoksin Etkileşimli Protein Hgf/c-met Yolağnn Bir Hedefidir Ve Agresif Fenotip Ile Ilişkilidir, Sözlü Sunum, 2.çukurova Hepatoselüler Karsinoma Kongresi Hcc Biyolojisini Anlamak: Hasta Yönetimine Neler Sunacak?, 23 February 2018, 25 February 2018, 12 - null.

Y. YILMAZ, E. BAĞIRSAKÇI TEPE, A. GÜNEŞ, E. KAHRAMAN, H. TOPEL BATARLAR & S. N. ATABEY, Regulatory Roles Of C-met In Hcc Metabolism: Crosstalk Between Insulin/ir And Hgf/c-met Signaling, Sözlü Sunum, Febs Advanced Lecture Course On Oncometabolism, 18 June 2017, 24 June 2017, 44 - null.

A. GÜNEŞ, E. İŞCAN, G. ÇAKAN AKDOĞAN, E. BAĞIRSAKÇI TEPE, D. NART, F. YILMAZ BARBET, Ş. E. ERDAL BAĞRIYANIK, H. G. ÖZHAN & S. N. ATABEY, Thioredoxin Interacting Protein Promotes Aggressive Phenotype In Hepatocellular Carcinoma, Poster Sunumu, Febs Advanced Lecture Course On Oncometabolism, 18 June 2017, 24 June 2017, 59 - null.

H. TOPEL BATARLAR, E. BAĞIRSAKÇI TEPE, D. ÇÖMEZ, A. GÜNEŞ, E. KAHRAMAN, Y. YILMAZ & S. N. ATABEY, Effects Of C-met On Glucose Metabolism Of Hepatocellular Carcinoma, Poster Sunumu, Embo Workshop Metabolic Disorders And Liver Cancer, 23 April 2017, 26 April 2017, 92 - null.

A. GÜNEŞ, E. İŞCAN, E. BAĞIRSAKÇI TEPE, H. TOPEL BATARLAR, S. TERCAN AVCI, G. BAĞCI, M. GÜMÜŞTEKİN, Ş. E. ERDAL BAĞRIYANIK & S. N. ATABEY, Heparin Regulates Thioredoxin-interacting Protein Expression, A Major Regulator Of Glucose Metabolism, In Hepatocellular Carcinoma Cells, Poster Sunumu, Embo Workshop Metabolic Disorders And Liver Cancer, 23 April 2017, 26 April 2017, 51 - null.

Y. YILMAZ, E. BAĞIRSAKÇI TEPE, A. GÜNEŞ, E. KAHRAMAN, H. TOPEL BATARLAR, Ş. E. ERDAL BAĞRIYANIK & S. N. ATABEY, Regulatory Role Of Hyperglycemia And Hyperinsulinemia On C-met Insulin Receptor Interaction And Downstream Signaling In Hepatocellular Carcinoma Cells, Poster Sunumu, Embo Workshop Metabolic Disorders And Liver Cancer, 23 April 2017, 26 April 2017, 100 - null.

A. GÜNEŞ, E. İŞCAN, G. ÇAKAN AKDOĞAN, E. BAĞIRSAKÇI TEPE, H. G. ÖZHAN, Ş. E. ERDAL BAĞRIYANIK, D. NART, F. YILMAZ BARBET & S. N. ATABEY, Txnip Overexpression Promotes Aggressive Phenotype In Hcc Cell Lines, Poster Sunumu, Embo Workshop Metabolic Disorders And Liver Cancer, 23 April 2017, 26 April 2017, 65 - null.

TÜBİTAK Scholarships and Fundings

Project Info

122S547, Kolon Adenokarsinomlarında Karaciğer Metastazı Gelişiminde Olfaktör Reseptörlerin Rolünün Araştırılması, Burslu, Yürürlükte, SBAG - Sağlık Bilimleri Araştırma Destek Grubu, 1001 - Araştırma, ARDEB, Project Participation/Leave Dates: 4/5/23 - Devam ediyor, Project Start/End Dates: 11/15/22 - 11/15/25.
119S698, Karaciğer Metastazı Gelişiminde Hgf/C-Met Yolağınının Rolünün Tümör Mikroçevresini İçeren Koşullarda Incelenmesi, BİDEB Burslusu, Sonuçlandı, SBAG - Sağlık Bilimleri Araştırma Destek Grubu, 1001 - Araştırma, ARDEB, Project Participation/Leave Dates: 9/1/21 - 4/1/23, Project Start/End Dates: 2/1/20 - 4/1/23.
118Z156, Hepatoselüler Karsinoma'da Sorafenib Direnci Gelişiminde Kaveolin-1'in Rolü, BİDEB Burslusu, Sonuçlandı, KBAG - Kimya Biyoloji Araştırma Destek Grubu, 1001 - Araştırma, ARDEB, Project Participation/Leave Dates: 1/10/19 - 9/1/21, Project Start/End Dates: 12/1/18 - 9/1/21.
115E056, Metastazın Erken Tanısında Yeni Bir Yonga-Üstü-Laboratuvar (Lab-On-A-Chip, Loc) Cihazı, Burslu, Sonuçlandı, EEEAG - Elektrik, Elektronik Ve Enformatik Araştırma Destek Grubu, 1003 - Öncelikli Alanlar (2. Aşama), ARDEB, Project Participation/Leave Dates: 5/14/18 - 12/12/18, Project Start/End Dates: 10/15/15 - 4/15/19.
114S359, Yüksek Glukoz Aracılıklı Hepatosellüler Karsinoma Progresyonunun Moleküler Mekanizması: C-Met Aktivasyonu ve Yeni Adaylar Thioredoxin Interacting Protein, Sestrin2 ve IncRNA HOTAIR, Burslu, Sonuçlandı, SBAG - Sağlık Bilimleri Araştırma Destek Grubu, 1001 - Araştırma, ARDEB, Project Participation/Leave Dates: 10/16/15 - Devam ediyor, Project Start/End Dates: 10/15/14 - 6/15/17.

BIDEB Supports

EZGİ BAĞIRSAKÇI TEPE, Etkinlik Destekleri ve Eğitim Bursları Müdürlüğü, 2250-Lisansüstü Bursları Performans Programı, Destek Sona Erdi, 2022 - 1.
EZGİ BAĞIRSAKÇI TEPE, Etkinlik Destekleri ve Eğitim Bursları Müdürlüğü, 2250-Lisansüstü Bursları Performans Programı, Destek Sona Erdi, 2023 - 1.
EZGİ BAĞIRSAKÇI TEPE, Etkinlik Destekleri ve Eğitim Bursları Müdürlüğü, 2250-Lisansüstü Bursları Performans Programı, Destek Sona Erdi, 2023 - 2.
EZGİ BAĞIRSAKÇI TEPE, Araştırma Burs ve Destekleri Müdürlüğü, 2218-Yurt İçi Doktora Sonrası Araştırma Burs Programı, Burs Almaya Hak Kazandı, 2023 - 1.

EZGİ BAĞIRSAKÇI TEPE, Etkinlik Destekleri ve Eğitim Bursları Müdürlüğü, 2211-A Genel Yurt İçi Doktora Burs Programı, Başvurusu Reddedildi, 2018 - 2, 6/1/18 - 5/31/22.
EZGİ BAĞIRSAKÇI TEPE, Etkinlik Destekleri ve Eğitim Bursları Müdürlüğü, 2211-A Genel Yurt İçi Doktora Burs Programı, Başvurusu Reddedildi, 2019 - 2, 6/1/19 - 5/31/23.
EZGİ BAĞIRSAKÇI TEPE, Etkinlik Destekleri ve Eğitim Bursları Müdürlüğü, 2211-C Öncelikli Alanlara Yönelik Yurt İçi Doktora Burs Programı, Bursu Kesildi, 2020 - 2, 3/1/21 - 9/30/23.
EZGİ BAĞIRSAKÇI TEPE, Etkinlik Destekleri ve Eğitim Bursları Müdürlüğü, 2211-A Genel Yurt İçi Doktora Burs Programı, Başvurusu Reddedildi, 2019 - 3, 10/1/19 - 9/30/23.

Number of Panelist/Observer/Reporter Jobs

Refereeing/Panelist/Outer Consultant Count	ARDEB/BİDEB 0	TEYDEB 0	Total 0
Number of Observer/Consultant Jobs	ARDEB/BİDEB 0	TEYDEB 0	Total 0
Number of Reporter Jobs	ARDEB/BİDEB 0	TEYDEB 0	Total 0

8.3. Publication from the thesis

Topel *et al. Cell Communication and Signaling* (2020) 18:110
https://doi.org/10.1186/s12964-020-00602-0

Cell Communication and Signaling

RESEARCH Open Access

lncRNA HOTAIR overexpression induced downregulation of c-Met signaling promotes hybrid epithelial/mesenchymal phenotype in hepatocellular carcinoma cells

Hande Topel[1,2,3], Ezgi Bagirsakci[1,4], Dehan Comez[1,4], Gulsun Bagci[1,4], Gulcin Cakan-Akdogan[1,5] and Nese Atabey[1*]

Abstract

Background: Epithelial-to-mesenchymal transition (EMT) and mesenchymal-to-epithelial transition (MET) are both reversible processes, and regulation of phenotypical transition is very important for progression of several cancers including hepatocellular carcinoma (HCC). Recently, it is defined that cancer cells can attain a hybrid epithelial/ mesenchymal (hybrid E/M) phenotype. Cells with hybrid E/M phenotype comprise mixed epithelial and mesenchymal properties, they can be more resistant to therapeutics and also more capable of initiating metastatic lesions. However, the mechanisms regulating hybrid E/M in HCC are not well described yet. In this study, we investigated the role of the potential crosstalk between lncRNA HOTAIR and c-Met receptor tyrosine kinase, which are two essential regulators of EMT and MET, in acquiring of hybrid E/M phenotype in HCC.

Methods: Expression of c-Met and lncRNA HOTAIR were defined in HCC cell lines and patient tissues through HCC progression. lncRNA HOTAIR was overexpressed in SNU-449 cells and its effects on c-Met signaling were analyzed. c-Met was overexpressed in SNU-398 cells and its effect on HOTAIR expression was analyzed. Biological significance of HOTAIR/c-Met interplay was defined in means of adhesion, proliferation, motility behavior, invasion, spheroid formation and metastatic ability. Effect of ectopic lncRNA HOTAIR expression on phenotype was defined with investigation of molecular epithelial and mesenchymal traits.

Results: In vitro and in vivo experiments verified the pivotal role of lncRNA HOTAIR in acquisition of hybrid E/M phenotype through modulating expression and activation of c-Met and its membrane co-localizing partner Caveolin-1, and membrane organization to cope with the rate limiting steps of metastasis such as survival in adhesion independent microenvironment, escaping from anoikis and resisting to fluidic shear stress (FSS) in HCC.

Conclusions: Our work provides the first evidence suggesting a role for lncRNA HOTAIR in the modulation of c-Met to promote hybrid E/M phenotype. The balance between lncRNA HOTAIR and c-Met might be critical for cell fate decision and metastatic potential of HCC cells.

Keywords: HCC, long non-coding RNA, HOTAIR, c-Met, Caveolin-1, Hybrid E/M

* Correspondence: nese.atabey@ibg.edu.tr
[1]Izmir Biomedicine and Genome Center (IBG), Balcova, 35340 Izmir, Turkey
Full list of author information is available at the end of the article

Background

Liver cancer is ranked as 7th cancer type in the list of cancers with the highest number of cases incident between 2007 and 2017 by Global Burden of Disease (GBD) 2017 study. Hepatocellular Carcinoma (HCC) accounts more than 80% of liver cancer cases and it is estimated to be the 4th most common cause of cancer related deaths worldwide [1]. HCC is reported to have complex and heterogeneous molecular features which is previously stressed out by integrative studies combining genomic characterization, exome sequencing, transcriptome analysis and clinical trials. Molecular heterogeneity and aetiological complexity of HCC makes it unlikely for one treatment or agent to effectively target all or most HCCs [2, 3].

c-Met, a receptor tyrosine kinase, is known to be upregulated in liver diseases favoring hepatocyte proliferation. Besides potential benefits in chronic liver diseases, c-Met contributes to initiation, development and progression of HCC. c-Met activation in HCC is mostly driven by molecular networks instead of activating mutations and it is activated by non-canonical signaling mechanisms as well as canonical activation by its ligand, hepatocyte growth factor (HGF). c-Met is regarded as one of the most promising targets for HCC treatment and c-Met targeted clinical trials are being conducted, currently [4]. In addition to its contribution to HCC development and progression, c-Met is also considered to be a key player in drug resistance [5].

HOX transcript antisense intergenic RNA, HOTAIR, is a 2148-nt-long spliced and polyadenylated long non-coding RNA (lncRNA) encoded within HOXC cluster. HOTAIR is first defined to take role in epidermal tissue development by recruiting chromatin remodeling complexes to its epigenetic targets [6, 7]. Overexpression of HOTAIR has been associated with poor prognosis, invasiveness and aggressiveness of various cancer types [8–11]. Complex secondary structure and ability to form independent structural domains ensure the multi-acting nature of HOTAIR and it has been defined to contribute to various cellular mechanisms via different molecular interactions such as scaffolding protein complexes, decoying microRNAs, epigenetically targeting genes and enabling RNA-protein/DNA-protein interactions [7, 12–14].

Transcription factors, non-coding RNAs and epigenetic regulators play critical roles in cell-fate determination such as transition between epithelial and mesenchymal phenotypes. Starting from the origin of a tumor, cancer cells go through complex and dynamic phenotypical changes -epithelial to mesenchymal transition (EMT), or its reverse mesenchymal to epithelial transition (MET)- to cope with metastasis rate-limiting steps. It has been reported that, some cancer cells display both epithelial and mesenchymal markers and this phenotype is referred as hybrid, intermediate, partial, metastable or incomplete EMT phenotype [15–18]. The tumor cells simultaneously expressing both mesenchymal and epithelial markers may be more plastic and most likely to contribute to metastatic outgrowth. Cells bearing this hybrid phenotype are first defined in circulating tumor cells (CTCs) of patients with both epithelial and mesenchymal traits [19, 20]. Hybrid cells that co-express mesenchymal and epithelial markers migrate collectively, more resistant to fluidic shear stress damage in circulation, exit from anoikis and have enhanced metastatic ability than cells with complete epithelial or mesenchymal phenotypes [21]. That is why, cancer cells that attain a hybrid E/M (epithelial/mesenchymal) phenotype pose greater risk for metastasis in cancer patients [22].

c-Met is reported to play an essential and complex role in modulation of transitional states within the broad spectrum of cellular phenotypes [23]. Although HOTAIR is also reported to contribute attainment of cellular phenotypes, its role is generally defined in means of correlations with aggressiveness traits of cancer cells [10, 11, 24, 25]. As the number of the studies reporting induced expression and critical roles of these two molecules in HCC are increasing, the likelihood of their direct or indirect molecular interaction becomes non-negligible. In this study, we aimed to investigate the nature of their interaction and here, we describe the interplay between HOTAIR and c-Met in HCC context. Our data present strong evidence that HOTAIR ensures hybrid E/M phenotype and its downregulation is required for c-Met induced complete mesenchymal phenotype in HCC cells.

Materials and methods

Cell culture

All Human HCC cell lines were kindly provided by Prof. Dr. Mehmet Öztürk (Izmir Biomedicine and Genome Center, Izmir, Turkey). FOCUS, SNU-449, SK-HEP-1, SNU-475, SNU-387, SNU-423, SNU-398, MAHLAVU, HEP-3B and HuH-7 cell lines were cultured as described previously [26]. All cell lines were tested for mycoplasma infection and confirmed as negative before the experiments. SU11274 (Calbiochem, 448101) is solubilized with DMSO and used with 2500 nM concentration. c-Met kinase activity was inhibited with SU11274 (2500 nM in 2% FBS complete medium). Ligand dependent c-Met activation was induced by 10 ng/ml Hepatocyte Growth Factor (HGF) in 2% FBS complete medium (R&D system, USA). Sorafenib treatment was continuously applied with the amount of their growth inhibition 50 (GI50) values (6 µM of Sorafenib) to MAHLAVU sorafenib resistant cell clones which have been established in our previous studies [5].

Cells were sheared with 205 U/CA multichannel peristaltic pump and Marprene tube elements of 2.79 bore for tubing (Watson Marlow, UK). Adherent cells were detached with 0.25% Trypsin /EDTA (Biological Industries, #03–050-1B, Israel) and 3 million cells in 8 ml of culture media were cultured in circulation under 0.5 dyn/ cm^2 shear stress at 37 °C, in humidified incubator supplied with 5% CO_2, for 1 hour. After FSS application, cells were stained with trypan blue and counted with hemocytometer to evaluate cell viability under shear stress.

mRNA isolation, reverse transcription and RT-qPCR

NucleoSpin RNA Isolation kit (Macherey-Nagel, Germany) has been used for mRNA isolation. mRNA isolation performed according to the manufacturer's instructions. mRNA eluted with DNAse/RNAse free distilled water and its concentration is measured via NanoDrop.

SensiFast™ cDNA Synthesis Kit (Bioline Meridian Bioscience, USA) were used to transcribe cDNA from mRNA. qPCR reactions were performed with primers designed specific for cDNA sequences of gene of interests (CDS) from NCBI-Gene Bank. RT-qPCR analysis performed using SensiFast™ SYBR No-ROX kit (Bioline Meridian Bioscience, USA) with ABI 7500 Fast Real-Time PCR System (Thermo Scientific, USA) according to the manufacturer's instructions. RPL41 and/or GAPDH gene expressions were used as internal controls to normalize relative expression of the genes. Primers targeting mRNAs of interest were listed in Supplementary Document 1.

siRNA gene silencing experiments

HuH-7 cells were transfected with 10 nM non-targeting (untargeted, negative control-NC, Dharmacon, Lincode non-targeting SMARTpool, D-001320-10-50) and HOTAIR targeting siRNAs (Dharmacon, Lincode Human HOTAIR SMARTpool, R-187951-00-0050) by Roche X-tremeGENE™ HP DNA Transfection Reagent (6366244001, Roche). Cells were harvested after 48 h post-transfection and processed for further protein and mRNA investigations.

Fluorescent In-Situ Hybridization (FISH)

HOTAIR mRNA was hybridized with Stellaris® FISH Probes, Human HOTAIR with Quasar® 570 Dye (LGS Biosearch Technologies, VSMF-2178-5). HCC cells were grown on glass coverslips and fixed with 3:1 methanol-acetic acid (MeOH-AcOH) fixation solution for 10 min. Hybridization was performed according to the manufacturer's instructions with 500 nM HOTAIR targeting probes for 4 h at 37 °C. Cell nucleus was stained with DAPI.

Labeling with c-Met antibody and hybridizing HOTAIR mRNA with fluorescent-labeled probes were performed sequentially. For sequential labeling, HCC cells were firstly fixed with 3.7% (vol./vol.) formaldehyde in 1X-PBS for 10 min at room temperature. Fixed cells were incubated with primary antibody against c-Met protein (Cell Signaling, #3127) for 2 h at room temperature. After couple of washes with 1X-PBS, cells were incubated with secondary antibody (Alexa488-conjugated goat anti-mouse secondary antibody, Invitrogen, A-11001) for 1 h at RT. After immunofluorescent labeling, cells were fixed again with 3:1 methanol-acetic acid (MeOH-AcOH) fixation solution for 10 min. Following hybridization was performed according to the manufacturer's instructions with 500 nM HOTAIR targeting probes for 4 h at 37 °C. Cell nucleus was stained with DAPI and cells were analyzed with Zeiss LSM 880-Confocal Laser Scanning Microscopy with Airyscan in IBG Optic Imaging Core Facility.

Immunoblotting

The cells were lysed using RIPA lysis buffer containing 1 mM Na3VO2, 1 mM NaF, and 1% protease inhibitor cocktail (Roche Diagnostics, Indianapolis, IN, USA), and the lysates were subjected to Western blot analysis as described previously [26]. Primary antibodies are listed in Supplementary Document 1.

Producing retroviral and lentiviral virus particles and generation of stable cell lines

SNU-449 cells were infected with retroviral vector bearing viruses. Retroviral vector bearing virus particles produced by transfection of HEK-293T cells with VSV-G envelope expressing plasmid (5 μg), gag-pol expressing plasmid (5 μg) and retroviral target vectors (5 μg) together by Roche X-tremeGENE™ HP DNA Transfection Reagent (6366244001, Roche). After 24 h of transfection, cell culture media refreshed and collected 48 h post-transfection. HCC cells were infected with 1:1 titration of retrovirus containing media. After 48 h, infected SNU-449 cells were selected with 13 μg/ml and SNU-398 cells were selected with 0.5 μg/ml puromycine (Life Technologies, #A1113803, USA) for at least 3 passages.

HEK-293T cells were transfected with vectors bearing Rev (1 μg), gag-pol (6 μg) and VSV-G envelope (3 μg) genes with lentiviral target vectors (2.5 μg) by transfection reagent. After 48 h, cell culture media collected and SNU-398 cells were infected with 1:5 titration of lentivirus containing media. After 48 h of infection, infected cells were selected with 0.5 μg/ml puromycine for at least 3 passages. Lentiviral and retroviral vectors and their origins are listed in Supplementary Document 1.

Immunofluorescent analysis of the cells

HCC cells were grown on glass cover-slips and after experimental conditions set, cells were immunofluorescently labeled as described in previous study [27]. Imaging was performed with upright fluorescence microscope (Olympus - BX61) and Zeiss LSM 880-Confocal Laser Scanning Microscopy with Airyscan at IBG Optic Imaging Core Facility.

Trans-well motility and invasion assays

Trans-well inserts with 8 µm pore size (SPL Life Sciences, #37224, Korea) were used to analyze motility and invasion ability of HCC cells. The mix of 0.25 mg/ml basal membrane extract (Corning Matrigel® Growth Factor Reduced (GFR) Basement Membrane Matrix, Phenol Red-Free, #356231) was coated on invasion inserts. Trans-well motility and invasion experiments performed as described in previous study [26]. Motile and invasive cells located at the exterior surface of the inserts were counted with bright field inverted microscope and statistical analysis was performed via Prism 8.

Real-time adhesion, proliferation, motility and invasion assays

Real-time cell growth monitoring was performed with the Real-Time Cell Analyzer, xCELLigence System (Roche, Germany) as described previously [28]. 5000 cell/well was plated to analyze proliferation and adhesion to cell-culture treated wells of E-Plates. For motility and invasion assays, CIM-plates (ACEA Biosciences, # 0566581701, USA) were used with xCELLigence System. CIM-plate wells were coated with 0.25 mg/ml basal membrane extract (Corning Matrigel® Growth Factor Reduced (GFR) Basement Membrane Matrix, Phenol Red-Free, #356231) for invasion assay. For motility and invasion assays, 30.000 cells/well were plated to CIM-Plate wells and incubated for 24 h by monitoring with xCELLigence RTCA system.

Hanging drop spheroid formation assay

2500 HCC cells were incubated within 20 µl culture medium drops which were hanging from the inverted lid of 10 cm cell culture plates. The reservoir part of 10 cm of tissue culture dish was filled with 3–5 ml of 1X PBS to provide a humidified environment. The culture dish was incubated at 37 °C, 5% CO2, 95% humidified incubator for 72 h or 96 h until the spheroids formation and spheroids were imaged under Olympus SZX10 stereo microscope and SC50 camera system.

2D Colony formation assay

SNU-449 HOTAIR OE and SNU-449 MOCK cells seeded on 24-well plates as 70 cells/well. The cells were cultured until single-cell colony formation. Cell culture media was refreshed in every three days and cells were incubated for one week. The day of analysis, cell culture media was aspirated and colonies were fixed with 1:1 cold Aceton:Methanol solution at -20 °C for 10 min. Colonies stained with 20% Giemsa solution for 20 min. After washing with distilled water, plate was incubated at room temperature for air dry. Plates were imaged under BIO-RAD Gel Doc™ XR+ Gel Documentation System and the images were analyzed via ImageJ - ColonyArea plug-in [29].

Phalloidin staining

HCC cells were seeded on glass cover slips (22 × 22 cm) and incubated overnight for adhesion. Phalloidin (Abcam, abID#176756, USA)staining was performed as previously described [30]. Imaging performed at IBG Optic Imaging Core Facility with fluorescent (Olympus - BX61) and Zeiss LSM 880-Confocal Laser Scanning Microscopy with Airyscan.

MTT assay

SNU-449 HOTAIR OE and SNU-449 MOCK 1000 cells per well were seeded on 96-well plate and incubated for 24, 48 and 72 h. MTT analysis was performed as described previously [31]. Measured absorbance was analyzed by Microsoft Excel 2016 and plotted by Prism 8.

Analysis of TCGA and GEO microarray datasets

Normalized gene expression data from dataset GSE89377, GSE98091 and GSE109483 were analyzed with GEO2R and GREIN [32]. Expression and correlation analysis of HOTAIR and MET performed with LncTarD [33]. Expression values plotted and statistically analyzed with Prism 8.

Zebrafish xenograft assay

Zebrafish xenograft assay was performed with SNU-449 MOCK and SNU-449 HOTAIR cell clones. The experiment was performed as described in a previous study [30]. Briefly, 48hpf embryos were anesthetized and DiI labeled cells were injected to the yolk sack.100 cells per embryo were injected, successful injections to yolk with localized cells were selected 4 h after injection. Xenografts were analyzed with Olympus SZX16 Fluorescent stereomicroscope. Three independent experiments were performed and each group consisted average number of 50 embryos with intact tumorospheres. All experiments were performed in compliance with local ethics regulations and EU Directive 2006 and approved by IBG Animal Ethics Committee with the protocol number of 03/2019.

Statistical analysis

Statistical analysis performed using the GraphPad Prism 8 software. Statistical methods included Analysis of variance (ANOVA), Student's t-test and linear regression. Zebrafish xenograft data was statistically analyzed with chi-square with Yates correction as described in previous study [34]. Results with $p < 0.05$ were considered as statistically significant.

Results

Expression of HOTAIR is low in HCC cells with high c-Met expression and activation

To examine expression levels of HOTAIR and c-Met, we analyzed their mRNA expression in 10 HCC cell lines (FOCUS, SNU-449, SK-HEP-1, SNU-475, SNU-387, SNU-423, MAHLAVU, Hep-3B, HuH-7 and SNU-398). HOTAIR expression was only abundant in HuH-7 and SNU-398 cell lines which are also known to have low or no c-Met expression, respectively (Fig. 1a-b). To evaluate the potential relation between HOTAIR and c-Met protein expressions, we selected two cell lines with constitutive c-Met activation (SNU-449 and SK-HEP-1) and two with low c-Met expression (HuH-7 and Hep-3B). RT-qPCR analysis of HOTAIR mRNA expression levels and western blot analysis of c-Met protein expression revealed that HOTAIR expression is low in HCC cell lines with high c-Met protein expression (Fig. 1c). To understand the relationship between HOTAIR and c-Met expression in HCC, we analyzed HOTAIR and MET gene expression in a microarray dataset, GSE89377, which comprise gene expression analysis in patient tissues from normal liver, dysplasia, early and late HCC stages [35]. Expression analysis of the dataset showed that HOTAIR expression decreases through HCC progression whereas MET gene expression increases (Fig. 1d).

To evaluate the effect of ectopic HOTAIR expression on c-Met expressing HCC cells, we overexpressed HOTAIR in SNU-449 cell line which has constitutive c-Met activation. Overexpression of HOTAIR (HOTAIR OE, presented in figures as HOTAIR clone) and its effect on c-Met expression were analyzed and confirmed with confocal microscopy imaging of fluorescent in-situ hybridization (FISH) of HOTAIR, immunofluorescent labeling of c-Met (Fig. 1e), and also with RT-qPCR (Fig. 1f). HOTAIR overexpression suppressed both mRNA and protein levels of c-Met, dramatically.

To understand the possible interplay between two molecules in detail, we knocked down HOTAIR expression with siRNA transfection in HuH-7 cell line and then analyzed mRNA and protein expression of c-Met. Analysis of three independent experiments showed that average of 45% knock-down of HOTAIR (Fig. 1g) induced c-Met mRNA (Fig. 1h) and protein expression (Fig. 1i), significantly. Uncut membrane images and expression levels are presented in Supplementary Fig. 1a).

lncRNA HOTAIR overexpression suppresses c-Met downstream signaling and modulates its cellular localization via suppressing Caveolin-1 expression

To understand the effects of HOTAIR on c-Met signaling, we analyzed activation of c-Met and its downstream signaling pathways Akt, MAPK and STAT3. Western blot analysis showed that HOTAIR OE suppressed c-Met protein expression and activation (Fig. 2a). Repression of c-Met activation was a result of diminished c-Met protein expression and there was not a significant inhibition on c-Met phosphorylation (p-cMet) when normalized to total c-Met protein expression (Supplementary Fig. 1b). HOTAIR OE caused a modest decrease in Akt activation (Fig. 2b), and suppressed MAPK (Fig. 2c) and STAT3 (Fig. 2d) activations, dramatically. We confirmed these results by analyzing expression and activation of c-Met by immunofluorescent microscopy (Fig. 2e and f). Macroscopic analysis of the cells revealed that HOTAIR OE cells were smaller with roundish morphology and even the immunofluorescence staining intensities of c-Met seem to be higher in HOTAIR OE cells, analysis of immunofluorescence intensity per cells showed that is an optical illusion caused by size (smaller) and morphological (rounder) attributes of HOTAIR OE cells (Fig. 2e). Furthermore, immunofluorescent labeling revealed a differential organization and localization of c-Met in HOTAIR OE cells (Fig. 2f). In our previous studies, we reported that Caveolin-1 (CAV1), a membrane protein enriched in lipid-rafts, enhances c-Met activation and modulates its membrane localization in HCC cells [27]. To investigate the possible role of CAV1 in HOTAIR/c-Met interaction, we analyzed expression and activation of CAV1 and its activating kinase, Src, in HOTAIR OE cells. HOTAIR OE suppressed CAV1 mRNA level (Fig. 2g), protein expression and activation (Fig. 2, Supplementary Fig. 1c) as well as Src kinase expression and activation (Fig. 2i). Moreover, immunofluorescent staining revealed that membrane organization of Caveolin-1 was disrupted in HOTAIR OE cells which was compatible with disorganization of c-Met (Fig. 2j).

Overexpression and/or activation of c-Met decreases HOTAIR expression in HCC cell lines

To understand the interplay between HOTAIR and c-Met further, we applied an opposite approach by overexpressing c-Met in SNU-398 HCC cell line which lacks c-Met protein expression and activation in wild-type (Fig. 1a). Overexpression and activation phosphorylation of c-Met were confirmed by western blot (Fig. 3a), immunofluorescent labeling and RT-qPCR analysis (Fig. 3b). Analysis of

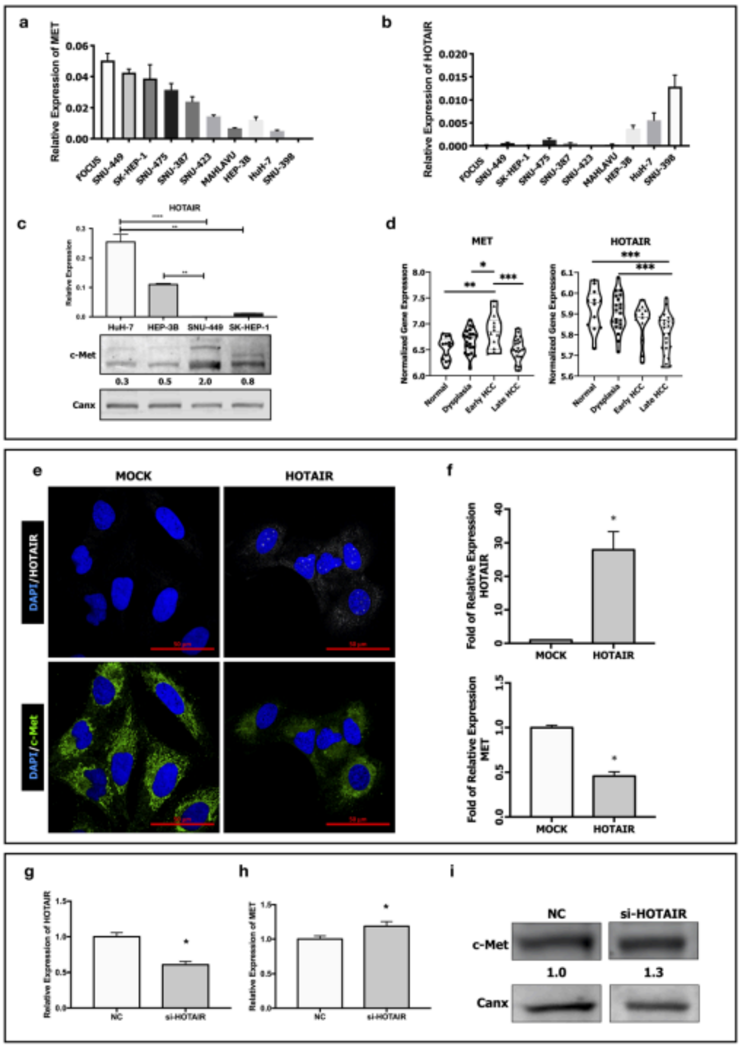

Fig. 1 Expression of HOTAIR and c-Met in HCC cell lines and patient tissues through HCC progression. RT-qPCR analysis of **(a)** MET and **(b)** HOTAIR expressions in HCC cell lines FOCUS, SNU-449, SK-HEP-1, SNU-475, SNU-387, SNU-423, MAHLAVU, Hep-3B, HuH-7 and SNU-398. **(c)** RT-qPCR analysis of HOTAIR expression and immunoblotting of c-Met protein in HuH-7, Hep-3B, SNU-449 and SK-HEP-1 cells. **(d)** Normalized expression levels of MET and HOTAIR in normal, dysplasia, early and late HCC tissues in microarray dataset GSE89377. **(e)** Confocal microscopy image of fluorescent-in-situ hybridized HOTAIR mRNA and immunofluorescent labeled c-Met protein expression in control (MOCK) and HOTAIR over-expressing (HOTAIR OE) SNU-449 cells. RT-qPCR analysis of **(f)** MET and HOTAIR mRNA expression in MOCK and HOTAIR OE clones. RT-qPCR analysis of **(g)** HOTAIR and **(h)** c-Met mRNA expression in control si-RNA (NC) and si-HOTAIR transfected HuH-7 cells. Western blot analysis of **(i)** c-Met protein expression in control (NC) and si-HOTAIR transfected HuH-7 cells. Densitometric analysis of band intensities in immunoblots were analyzed with ImageJ and normalized with internal control protein band intensities. All graphs of experiments are presented as the mean ± SEM of at least 3 independent experiments. * $p \leq 0.05$, ** $p \leq 0.01$, *** $p \leq 0.001$, **** $p \leq 0.0001$

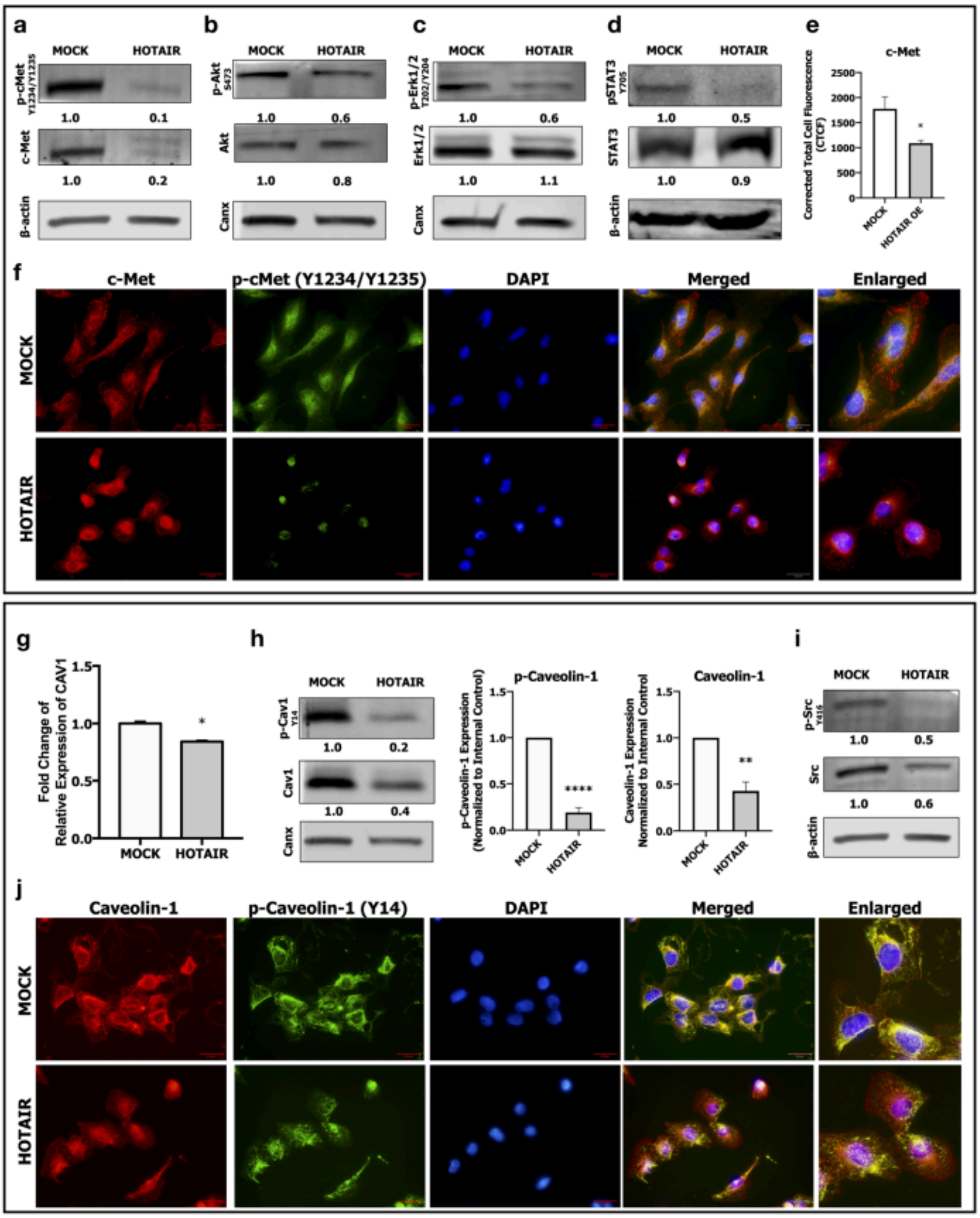

Fig. 2 (See legend on next page.)

(See figure on previous page.)
Fig. 2 Effect of HOTAIR overexpression in c-Met downstream signaling. Analysis of c-Met and downstream signaling in MOCK and HOTAIR OE cells. Immunoblot analysis of **(a)** c-Met protein expression, c-Met activation phosphorylation (Tyr-1234/Tyr-1235); **(b)** Akt1 protein expression, Akt1 activation phosphorylation (Ser-473); **(c)** Erk1/2 protein expression, Erk1/2 activation phosphorylation (Thr-202/Tyr-204); **(d)** STAT3 protein expression and activation phosphorylation (Tyr-705). Column graph of corrected total cell fluorescence of c-Met immunofluorescent staining **(e)**. Immunofluorescence imaging of **(f)** total c-Met protein (red) and its activation (green). RT- qPCR analysis of **(g)** CAV1 mRNA expression, immunoblotting of **(h)** Caveolin-1 protein and its activation phosphorylation (Tyr-14) and column graph of densitometric analysis of Caveolin-1 activation and total protein expressions. Immunoblotting of **(i)** Src kinase expression and its activation phosphorylation (Tyr-416). Immunofluorescence imaging of **(j)** total Caveolin-1 protein (red) and its activation (green). DAPI (blue) was used as a nuclear marker in immunofluorescent images. Densitometric analysis of band intensities in immunoblots were analyzed with ImageJ and normalized with internal control protein band intensities. All graphs of experiments are presented as the mean ± SEM of at least 3 independent experiments. * $p \le 0.05$, ** $p \le 0.01$, *** $p \le 0.001$, **** $p \le 0.0001$

HOTAIR expression in MET-OE-SNU 398 (presented in figures as MET-GFP) cells by FISH and RT-qPCR showed that HOTAIR mRNA expression was significantly suppressed by c-Met overexpression (Fig. 3c). To investigate HOTAIR/c-Met/Caveolin-1 axis further, we analyzed Caveolin-1 expression in c-MET OE cell lines and found that Caveolin-1 expression was significantly upregulated, consistent with HOTAIR down-regulation (Fig. 3d).

To understand the role of c-Met activation in HOTAIR expression, we analyzed the effect of HGF induced c-Met activation on HCC cell lines with different c-Met and HOTAIR expression levels such as HuH-7, HEP-3B, SNU-449, MAHLAVU and SK-HEP-1. Ligand-dependent c-Met activation by 10 ng/ml HGF for 1 h suppressed HOTAIR expression significantly in all tested cell lines (Fig. 3e). In addition to ligand-dependent activation, we examined the role of ligand-independent c-Met activation on HOTAIR transcription. In our previous studies, we showed that heparin treatment [36], acquired sorafenib resistance [5], high glucose induction [37] or fluidic shear stress treatment [38] induces ligand independent c-Met activation in HCC cell lines. Similar to HGF, heparin (Fig. 3f), sorafenib (Fig. 3g), high-glucose (Fig. 3h) and fluidic shear stress (Fig. 3i) treatments induced c-Met activation resulted in a substantial decrease in HOTAIR transcription. The maintenance of the interplay between HOTAIR and c-Met in different contexts supports the hypothesis that there is a reciprocal crosstalk between these two molecules in HCC cell lines. We further confirmed the rescue of HGF-suppressed HOTAIR expression after c-Met tyrosine kinase inhibition by SU11274 in HCC cell lines HuH-7, SNU-449, MAHLAVU and SK-HEP-1. c-Met tyrosine kinase inhibition rescued HGF-induced HOTAIR suppression in HCC cell lines (Fig. 3j).

To understand the biological significance of this interaction, we investigated the phenotypic and biological results of HOTAIR overexpression in SNU-449 HCC cell line.

HOTAIR OE induced c-Met inhibition decreases adhesion, proliferation and colony formation of SNU-449 cells

HOTAIR OE cells showed reduced adhesion capacity to cell culture-treated (Fig. 4a) and basal membrane extract coated cell culture surfaces (Fig. 4b) in xCELLigence real time cell analysis system (RTCA). To understand the cause of decreased extracellular matrix (ECM) attachment capacity, we analyzed the expression of cell surface integrins that contribute to matrix attachment. ITGA6, ITGB1, ITGA4 and ITGB4 expressions were down-regulated in HOTAIR OE cells, significantly (Fig. 4c).

Proliferation of the cells were evaluated with both xCELLigence RTCA system (Fig. 4d) and MTT analysis (Fig. 4e). HOTAIR OE cells showed significant reduction in proliferation rate in both techniques. Compatible with proliferation assays, 2D colony forming potential of HOTAIR OE cells were dramatically low. Colony counts are normalized to number of cells plated for evaluation of colonization percentage. HOTAIR OE cells showed significantly lower colonization ability in comparison to MOCK cells (Fig. 4f). Coverage area of colonies in well-plates, staining intensity of colonies and average colony sizes were also significantly lower in HOTAIR OE cells (Fig. 4g-j). These results reflect lower capacities of adhesion and proliferation.

HOTAIR OE induced c-Met inhibition decreases motility and invasion capacity of SNU-449 cells

Motility and invasion experiments were performed in parallel by both xCELLigence RTCA system and trans-well cell culture systems. Cell index of motile (Fig. 5a) and invasive (Fig. 5c) cells in HOTAIR OE clones were significantly lower in xCELLigence RTCA ($p \le 0.001$). Consistent with real-time motility and invasion analysis; the number of motile and invasive cells migrated through trans-well cell culture inserts were reduced in HOTAIR OE cells (Fig. 5b, d), significantly ($p \le 0.05$).

Since trans-well systems especially tests individual cell movement ability, we further analyzed collective migration ability of clones in scratch (wound-healing) assay. Scratch assay enables cells to move collectively, without

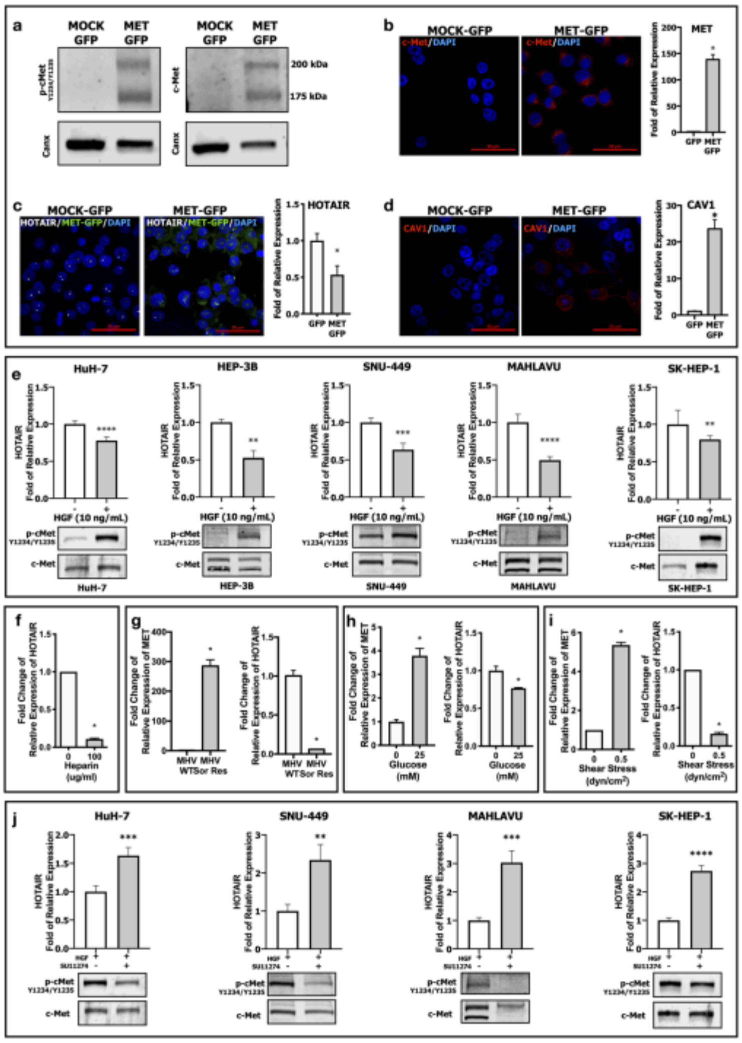

Fig. 3 Analysis of HOTAIR-c-Met interaction in MET overexpressed, activated and inhibited conditions. Immunoblotting of **(a)** c-Met activation phosphorylation (Tyr-1234/Tyr-1235), and total c-Met protein expression. Confocal microscopy imaging of **(b)** c-Met protein and RT-qPCR analysis of c-Met mRNA expression in MET OE SNU-398 clones. **(c)** Confocal imaging of FISH labeling (white dots) and RT-qPCR analysis of HOTAIR mRNA expression in MET OE clones. **(d)** Confocal imaging of Caveolin-1 protein and qPCR analysis of CAV1 mRNA expression in MET OE cells. **(e)** Immunoblot of c-Met activation and qPCR analysis of HOTAIR expression in ligand-dependent activation (HGF 10 ng/ml) of c-Met in HuH-7, HEP-3B, SNU-449, MAHLAVU and SK-HEP-1 cells. RT-qPCR analysis of HOTAIR expression **(f)**, in response to heparin (100 μg/mL) induced c-Met activation in SK-HEP-1 cells. RT-qPCR analysis of MET and HOTAIR expressions in sorafenib resistance (MAHLAVU cell line) **(g)** and high-glucose (25 mM, HuH-7 cell line) **(h)** and fluidic shear stress (0.5 dyn/cm^2, HuH-7 cell line) **(i)** induced c-Met activations. **(j)** Immunoblot of c-Met activation and qPCR analysis of HOTAIR expression in tyrosine kinase activity inhibition of c-Met by SU11274 (2500 nM) HuH-7, SNU-449, MAHLAVU and SK-HEP-1 cells. All graphs of experiments are presented as the mean ± SEM of at least 3 independent experiments. * *$p \leq 0.05$, ** $p \leq 0.01$, *** $p \leq 0.001$, **** $p \leq 0.0001$*

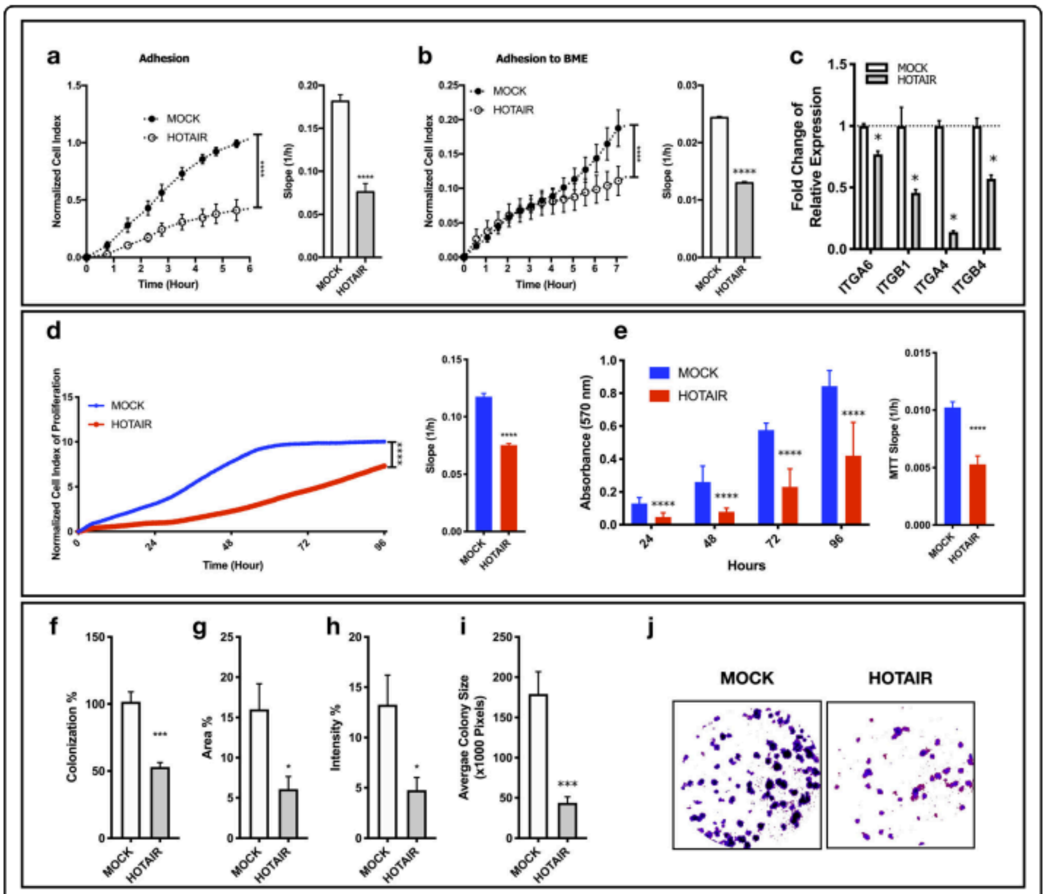

Fig. 4 HOTAIR OE induced c-Met inhibition decreases adhesion, proliferation and colony formation. Normalized cell index and slope analysis of adhesion to **(a)** cell culture treated and **(b)** basal membrane extract-coated surfaces analyzed with xCELLigence RTCA. **(c)** RT-qPCR analysis of ITGA6, ITGB1, ITGA4 and ITGB4 expressions. **(d)** Analysis of normalized cell index and rate (slope) of proliferation by xCELLigence RTCA system. Normalized **(e)** MTT absorbance (570 nm) and proliferation rate (slope) calculated by MTT absorbance. 2D colony formation analysis of MOCK and HOTAIR clones presented as **(f)** percentage of colonization, **(g)** percentage of area covered by colonies, **(h)** intensity of Giemsa-staining **(i)** average colony size in pixels and **(j)** representative images of clones generated with ImageJ plugin ColonyArea. 2D colony formation is analyzed by ImageJ plugin ColonyArea. All graphs of experiments are presented as the mean ± SEM of at least 3 independent experiments. * $p \leq 0.05$, ** $p \leq 0.01$, *** $p \leq 0.001$, **** $p \leq 0.0001$

losing cell-cell attachments. Even though HOTAIR OE cells have reduced ability to migrate individually, they were still motile. Rather than migrating individually, HOTAIR OE cells migrated without losing cell-cell contacts, collectively (Fig. 5e).

lncRNA HOTAIR inhibits c-Met induced cell scattering and promotes metastasis in zebrafish embryos

Decrease in attachment capacity to ECM led us to investigate spheroid formation capacity of HOTAIR OE cells. We analyzed spheroid formation ability of those cells with hanging-drop spheroid formation assay. SNU-449 cells have a complete mesenchymal phenotype, as a result of scattering effect of constitutive c-Met activation, and they are not inclined to form spheroids in hanging-drops. Due to their reduced ability to form cell-cell contacts maintained by constitutive c-Met activation; MOCK cells formed loose, scattered and wide clusters whereas HOTAIR OE cells formed more tight, stacked and small spheroids (Fig. 6a). Significant ability to form intact spheroids led us to investigate their survival capacity under fluidic shear stress (FSS). To test their

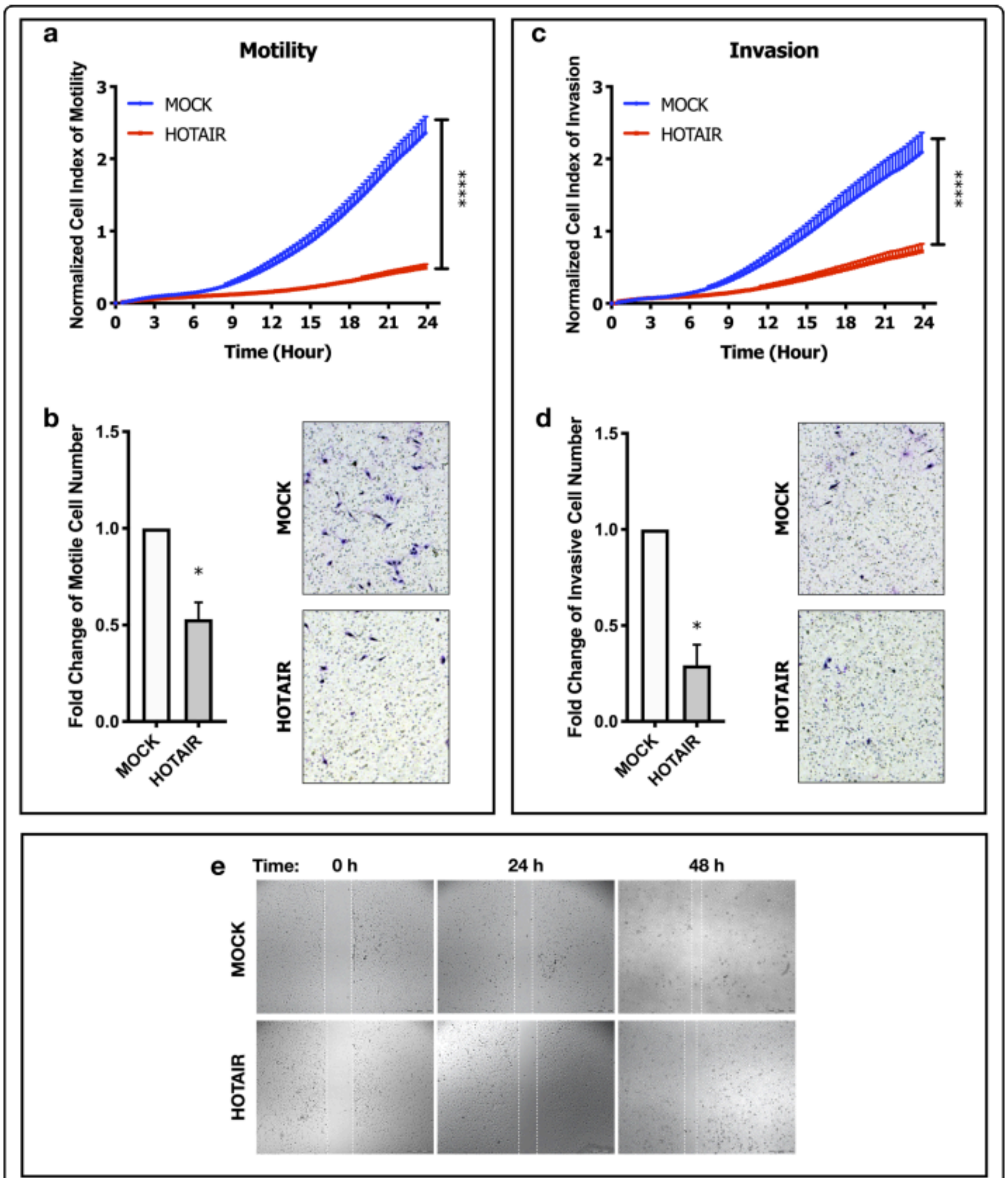

Fig. 5 HOTAIR OE induced c-Met inhibition decreases individual motility and invasion ability of SNU-449 cells. Real-time (by xCELLigence RTCA) and end-point (cell culture inserts) analysis of motility and invasion of MOCK and HOTAIR OE cell clones. Normalized cell index of (**a**) motility and (**c**) invasion analyzed by xCELLigence RTCA system. Fold change graphs and brightfield images of (**b**) motile and (**d**) invaded cells in trans-well cell culture inserts. (**e**) Brightfield microscopy images of 0-, 24- and 48-h scratch (wound-healing) assay of MOCK and HOTAIR OE clones. All graphs of experiments are presented as the mean ± SE of at least 3 independent experiments. * *p ≤ 0.05, **p ≤ 0.01, ***p ≤ 0.001*

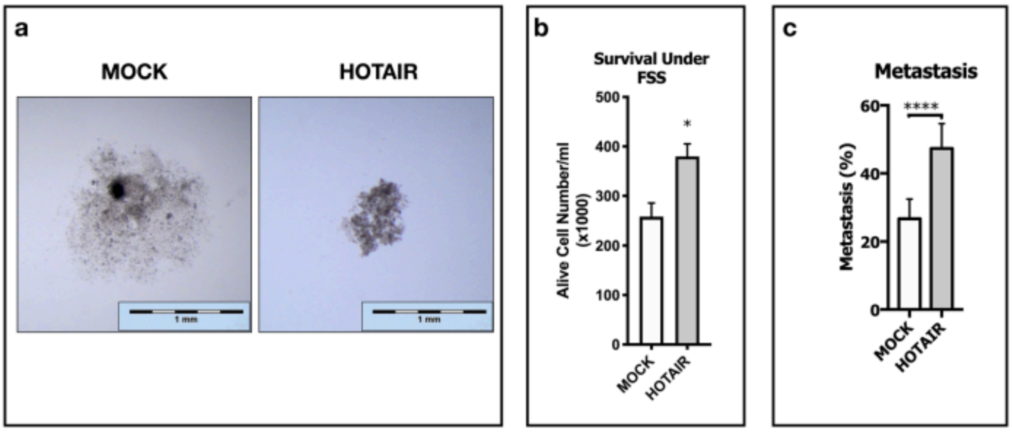

Fig. 6 lncRNA HOTAIR suppresses c-Met induced cell scattering, enhances survival under FSS and promotes metastasis in zebrafish embryos. Spheroid formation, survival under fluidic shear stress and metastatic capacity of MOCK and HOTAIR OE cells. **(a)** Spheroid images were collected with stereo-microscopy and magnified equally with scale-bars to generate more clarified presentation of data. **(b)** Graphical presentation of alive cell numbers of MOCK and HOTAIR OE clones cultured under 0.5 dyn/cm^2 fluidic shear stress for 1 h. Embryonic zebrafish xenograft experiments with MOCK and HOTAIR OE SNU-449 cell clones presented as **(c)** percentage of metastasis in groups that were analyzed in total of three biological experiments. Statistical significance was analyzed by chi-square with Yates correction. All graphs of experiments are presented as the mean ± SE of at least 3 independent experiments. * $p \leq 0.05$, ** $p \leq 0.01$, *** $p \leq 0.001$, **** $p \leq 0.0001$

survival ability, cells sheared for 1 h under FSS of 0.5 dyn/cm^2, mimicking the sinusoidal shear stress in liver [39]. HOTAIR OE improved survival ability under sinusoidal FSS. Alive cell numbers after one hour of FSS was significantly higher ($p \leq 0.05$) in HOTAIR OE clones (Fig. 6b).

Finally, embryonic zebrafish xenograft model was used to test in vivo metastatic capacity of HOTAIR OE, further. Average number of 100 HOTAIR OE and MOCK cells were injected to the yolk sac of 48 h zebrafish embryos and embryos which bear an intact tumorosphere after 4 h of injection were raised for 4 days to analyze metastatic capacity. Three independent experiments were performed and in every experiment each group consisted an average number of 50 embryos with intact tumorospheres. Metastatic capacity was calculated by number of xenograft hosts that have metastasized cells at 4 days post injection (dpi). Even though wild-type SNU-449 cells are known to be metastatic in embryonic zebrafish model [30], HOTAIR OE dramatically increased their metastatic capacity when compared to MOCK cells (Fig. 6c).

lncRNA HOTAIR maintains hybrid E/M phenotype to promote metastasis

Our experiments with HOTAIR OE cells show morphological and biological properties that are consistent with the hybrid E/M phenotype which can be defined as a fluidic state between epithelial and mesenchymal phenotypes (Fig. 7a). To test this hypothesis, we examined previously defined EMT markers in HOTAIR OE SNU-449 cells [40–42]. First, we found that in contrast to the mesenchymal and elongated phenotype, HOTAIR OE cells were round-shaped with thinner F-actin stress fibrils indicated with phalloidin staining (Fig. 7b). Then, we performed a detailed investigation of molecular biomarkers of hybrid E/M phenotype. In HOTAIR OE cells, beta-catenin was enriched in the plasma membrane (Fig. 7c), expression of epithelial biomarker E-cadherin was upregulated (Fig. 7d) whereas mesenchymal biomarker Vimentin expression was significantly down-regulated and showed polarity (Fig. 7e). Consistent with epithelial phenotype, N-Cadherin expression was down-regulated and mostly located in the plasma membrane of HOTAIR OE cells (Fig. 7f). Immunofluorescent analysis of cytoskeletal organization of F-actin and Vimentin in SNU-398 MET OE clones showed that ectopic MET expression and its suppressive effect on HOTAIR expression was also resulted in thickening of F-actin stress fibrils, and increase in Vimentin expression and polarity (Supplementary Fig. 1d).

In addition to in-vitro experiments, we performed bioinformatic analysis of available data-sets GSE98091 and GSE109483. GSE98091 dataset has an integrated RNA sequencing transcriptomic and quantitative proteomic analysis those performed to explore the regulatory role of HOTAIR in HCC [43]. Researchers inhibited HOTAIR expression by siRNA silencing in HepG2 cells and analyzed differentially expressed genes and proteins

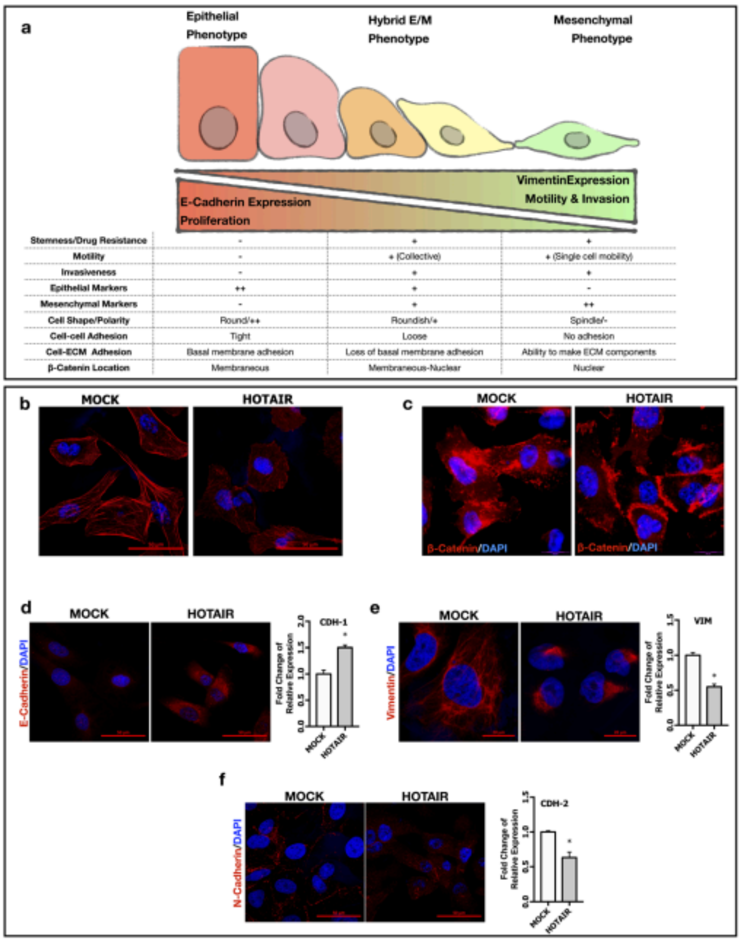

Fig. 7 lncRNA HOTAIR maintains hybrid E/M phenotype to promote metastasis. **(a)** Schematic presentation of morphological, molecular and biological biomarkers of epithelial, mesenchymal and hybrid E/M phenotypes. Confocal imaging of **(b)** Alexa-555 labeled phalloidin staining of F-actin filaments (red). Immunofluorescence imaging of **(c)** beta-Catenin protein (red) and its cellular localization. Confocal imaging and RT-qPCR analysis of **(d)** E-Cadherin **(e)** Vimentin and **(f)** N-Cadherin expressions. Alexa-594 conjugated secondary antibodies were used in all immunolabeling and confocal imaging experiments. DAPI (blue) was used as a nuclear marker in immunofluorescence and confocal images. All graphs of experiments are presented as the mean ± SEM of at least 3 independent experiments. * $p \leq 0.05$

between control-siRNA and HOTAIR-siRNA HepG2 clones. Even though transcriptional dysregulation of MET was not significant in this study, protein expression of c-Met was significantly higher in HepG2 cells transfected with HOTAIR siRNA (Fig. 8a). In GSE109483 dataset, researchers repressed HOTAIR expression in three Ewing sarcoma cell lines (ES2, A673, SK-ES) and overexpressed HOTAIR in hTERT-immortalized human mesenchymal stem cells to evaluate its effects on gene expression [44]. They performed RNA-Seq in Ewing sarcoma cell lines (control-GapmeR and HOTAIR repressing GapmeR clones), and hTERT-immortalized hMSCs with expression of control GFP and HOTAIR. MET gene expression was significantly upregulated by HOTAIR repression in ES2 and SK-ES Ewing Sarcoma cell lines and its expression was significantly repressed by HOTAIR over-expression in hTERT-immortalized human mesenchymal stem cells (Fig. 8b). The data of these datasets supports proposed interaction of HOTAIR and MET and they are very

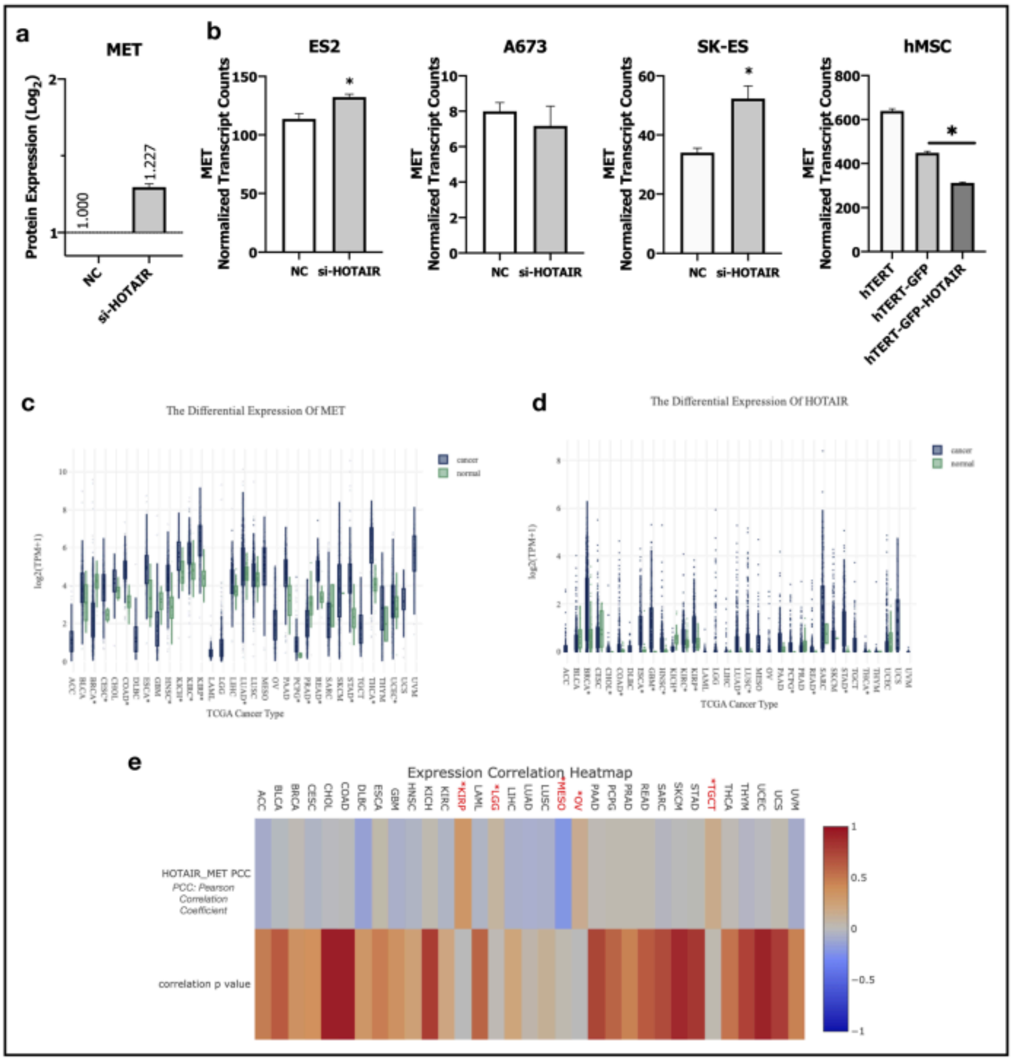

Fig. 8 Bioinformatic analyses of GEO and TCGA datasets supports HOTAIR and c-Met interplay. **(a)** Column graph of c-Met protein expression in control-siRNA and HOTAIR-siRNA transfected HepG2 cells in GEO dataset GSE98091. **(b)** MET gene expression in experimental groups of GEO dataset GSE109483. Column graphs of control-GapMeR and HOTAIR-GapmeR transfected Ewing sarcoma cell lines ES2, A673 and SK-ES (1st, 2nd and 3rd graphs). Last graph belongs to hTERT-immortalized human mesenchymal stem cells (hMSC), hMSCs transfected with GFP (hTERT-GFP) and HOTAIR-GFP (hTERT-GFP-HOTAIR) overexpression vectors. Analysis of **(c)** MET **(d)** HOTAIR gene expressions in TCGA datasets. **(e)** Heatmap of gene expression correlation analysis of HOTAIR and MET in TCGA datasets. GEO dataset analysis are performed with GREIN and TCGA gene expression and correlation analysis are performed with LncTarD. * $p \leq 0.05$

important to show similar results with HCC in different cancer and cellular contexts.

Finally, we analyzed TCGA datasets of various cancers to have a foresight about the possible relationship of two molecules [3]. HOTAIR and MET gene transcripts in TCGA datasets were analyzed by GREIN and LncTarD [32, 33]. Despite the limitations in RNAseq sample counts among TCGA datasets that comprise RNA sequencing of long non-coding RNAs, HOTAIR and c-Met were differentially expressed between normal and primary tumor tissues in various cancer types (Fig. 8c-d). While MET expression was significantly suppressed in primary tumor tissues in breast invasive carcinoma (BRCA) and upregulated in kidney chromophobe (KIHC), HOTAIR expression was significantly higher and lower, respectively (Fig. 8c-d). Analysis of the correlation of these two molecules among TCGA datasets showed that and they were reversely correlated with each other in mesothelioma (MESO) but positively correlated in kidney renal papillary cell carcinoma (KIRP), brain lower grade glioma (LGG), ovarian serous cystadenocarcinoma (OV) and testicular germ cell tumors (TGCT) with statistical significance. Even lack of significance, tendency of reverse regulation was significance in adrenocortical carcinoma (ACC), cervical squamous cell carcinoma and endocervical adenocarcinoma (CESC), lymphoid neoplasm diffuse large b-cell lymphoma (DLBC), glioblastoma multiforme (GBM), head and neck squamous cell carcinoma (HNSC), kidney renal clear cell carcinoma (KIRC), acute myeloid leukemia (LAML), liver hepatocellular carcinoma (LIHC), lung adenocarcinoma (LUAD) and ulveal melanoma (UVM), (Fig. 8e). Although lncRNA HOTAIR, one of the most studied long non-coding RNAs, is reported to be elevated in patients with metastasis and poor prognosis in many cancer types, analysis of HOTAIR in TCGA datasets revealed that HOTAIR has a context-dependent expression pattern which is not always upregulated through the progression of the disease (Fig. 8d-e).

Discussion

Our results suggest c-Met and HOTAIR axis as a modulator of epithelial/mesenchymal hybrid state in hepatocellular carcinoma cells. Mechanistically, we demonstrated that the interplay between c-Met receptor tyrosine kinase and HOTAIR is critical for maintenance of hybrid E/M state in HCC cells to cope with rate-limiting steps of tumor metastasis, such as survival in adhesion independent microenvironment, escaping from anoikis and resisting to fluidic shear stress (FSS) in HCC.

HCC cell lines with high c-Met expression and activation are defined to have mesenchymal phenotype in previous definitive studies [45, 46]. In our study, we report that HCC cells can be divided into two clusters which show differential expression tendency for HOTAIR and c-MET genes. Expression of these two molecules among 10 HCC cell lines demonstrated that most HCC cell lines show a reverse tendency in levels of c-Met and HOTAIR expression. To further confirm the possible reverse interaction between HOTAIR and c-Met, we overexpressed HOTAIR in SNU-449 cell line which has ligand-independent constitutive c-Met activation and silenced HOTAIR in HuH-7 cell line which expresses HOTAIR, abundantly. Our results show that constitutive c-Met expression is suppressed by HOTAIR overexpression and HOTAIR silencing induced c-Met expression in HCC cells. It is very important to note that inhibition of expression with siRNAs is limited mostly with cytoplasmic HOTAIR mRNA targeting and further studies should be done to address the detailed mechanism of HOTAIR action in means of molecular interactions and/or epigenetic function in HCC cells.

Analysis of microarray dataset comprised of tissues from normal liver, dysplastic liver, early and late HCC of patients (GSE89377) showed that HOTAIR was downregulated through hepatocarcinogenesis whereas c-Met expression was upregulated. This analysis supports our data showing HOTAIR downregulation is a requirement for c-Met activation and c-Met triggered complete mesenchymal phenotype in HCC cell lines. Contrary to the reports of melanoma, retinoblastoma and colon cancer studies [47–49] and expectations on the parallel expression tendencies of c-Met and HOTAIR in HCC cell lines; comparative analysis of HCC cell lines and cancer datasets shows the opposite, clearly. Indicated studies suggested HOTAIR as a competing long non-coding RNA decoying microRNAs targeting c-Met in different cancer contexts, and those microRNAs are reported to have different molecular targets in HCC rather than c-Met [50, 51].

In addition to suppression of c-Met protein expression and activation as a consequence, HOTAIR weakens downstream Akt1, MAPK and STAT3 signaling pathways not only by decreasing c-Met expression but also by modulating its membrane organization. In our previous studies, we showed that Caveolin-1 enhances c-Met signaling by co-localizing in plasma membrane [27]. Src kinase, a well-identified downstream effector of c-Met, phosphorylates Caveolin-1 from Tyr-14 residue to induce lipid-raft enrichment of c-Met with Caveolin-1 and formation of caveola structures [27, 52]. HOTAIR overexpression reduced Caveolin-1 expression and activation via suppressing activation of c-Met and its downstream effector Src kinase. In parallel to c-Met, Caveolin-1 organization in plasma membrane was also disrupted in HOTAIR OE cells. Tsai et al. defined function of HOTAIR in epigenetic regulation of its target genes and they reported Caveolin-1 as one of the most differentially expressed genes in response to HOTAIR knockdown in foreskin fibroblasts [12]. In addition to the HOTAIR OE data, we showed that HOTAIR *knockdown* elevated CAV1 expression in HuH-7 cells (Supplementary Fig. 1e). We confirmed the interaction axis of c-Met, HOTAIR and Caveolin-1 is conserved in c-Met over-expression model of SNU-398 cell line. Its wild type is lack of c-Met expression but expresses HOTAIR, abundantly. In addition to the lack of c-Met expression, SNU-398 cells also do not express Caveolin-1 [26]. As a consequence of c-Met overexpression and HOTAIR suppression, Caveolin-1 expression was induced in those cells. In addition to the over-expression studies of c-Met and HOTAIR, we showed that c-Met and HOTAIR reverse interaction is conserved in both ligand-dependent and independent c-Met activation contexts and also c-Met kinase inhibition. These results support the defined interplay between two molecules.

To understand the biological significance of HOTAIR/c-Met interaction, we analyzed the results of HOTAIR overexpression on c-Met related biological responses which are clearly defined in the literature as contributing to aggressive phenotype of HCC cells [53]. HOTAIR over-expressing cells showed delayed adhesion to surfaces and suppressed expression of adhesion-related integrins [54]. In addition to decreased attachment to surface, proliferation and colony formation ability of HOTAIR OE cells were also decreased. Suppression of individual motility and invasion of HOTAIR OE cells were consistent with suppressed scattering effect of c-Met signaling. HOTAIR OE cells were migrating collectively rather than individually which is compatible with previous studies explaining migration behavior of cells with hybrid E/M phenotype [15]. Increased expression of cell adhesion molecules such as CDH-1 and JAM-2 (Supplementary Fig. 1f) were consistent with the evidence of collective migration that requires preservation of cell-to-cell interactions [55, 56].

Surprisingly, HOTAIR over-expressing cells showed increased survival ability in adhesion independent culture and under FSS. Escaping from anoikis and overcoming damage incurred by shear forces are important necessities of survival in circulation to achieve metastasis [57]. Response to fluidic shear-stress or adhesion-independent conditions are context-dependent processes those depend on the molecular pool of the cell; HOTAIR over-expressing cells resisted those unfavorable conditions via formation of spheres [39]. Aggregation into spheroids to overcome the stress of unfavorable microenvironment, enhancing cell-cell adhesion and surviving under damage of shear forces are well-defined requirements of metastasis [39, 57]. As expected, by attainment of those abilities, HOTAIR overexpression increased metastatic ability of SNU-449 cells which was defined to be highly metastatic in our previous studies in zebrafish xenograft model [30]. Our study is the first in the literature defining the molecular basis of HOTAIR overexpression mediated increase in the metastatic ability of HCC cells.

Since the definition of EMT has been changed and broadened, transitional states between epithelial and mesenchymal phenotypes are called “partial EMT”. Existence of intermediate hybrid phenotypes have been defined in different molecular and biological processes such as fibrosis, development, wound healing and cancer [15]. In our study, we found that HOTAIR acts as a fine tuner of maintenance of hybrid E/M phenotype by modulating c-Met signaling. Compatibly with the literature, we analyzed defined morphological and molecular markers of epithelial and mesenchymal phenotypes in HOTAIR over-expressing cells [15, 16, 41, 42]. HOTAIR OE cells were round-shaped and had thinner F-actin stress fibrils. Beta-Catenin was enriched in membrane compatible with increased E-cadherin expression and hybrid E/M phenotype characteristics [18]. In comparison with MOCK cells, mesenchymal biomarkers Vimentin and N-cadherin expression was suppressed in HOTAIR OE cells (Fig. 7). Consistent with HOTAIR over-expression data in SNU-449 cells, c-Met overexpression in SNU-398 cells increased F-actin stress fibrils and Vimentin expression and, HOTAIR *knock-down* induced Vimentin expression in HuH-7 cells (Supplementary Fig. 1 g). While over-expression of c-Met in SNU-398 cells suppressed HOTAIR expression and led acquirement of mesenchymal attributes; inhibition of HOTAIR expression in HuH-7 cells enhanced mesenchymal phenotype. Changes in cytoskeletal components and dis−/re-assembling of cell-cell contacts regulates gene expression, motility and cell-cycle. Cells placed in spectrum between epithelial and mesenchymal phenotypes are reported to arrest cell cycle and decrease their proliferative activity [15, 17]. Consistent with the literature, proliferation rate of HOTAIR OE cells were decreased (Fig. 4) and cell cycle was arrested (Supplementary Fig. 1 h-i) in these cells.

Decrease in biological responses such as individual cell motility and invasion are consistent with suppressed scattering effect of c-Met signaling activity. Even individual cell motility was decreased, HOTAIR OE clones have ability to enclose the scratch via collective migration as fast as MOCK clones in wound-healing assay (Fig. 5). Collective migration is not only important for maintenance of invading front of tumors but also it is an emerging mechanism for seeding of secondary tumors [58]. Taken together, our data shows that decrease in HOTAIR expression and its effects on c-Met and Caveolin-1 activation is crucial through the completion of mesenchymal phenotype.

Concordant with our data, we report that c-Met and HOTAIR expression profiles show inverse correlation in mesothelioma but positively correlated in kidney renal papillary cell carcinoma, brain lower grade glioma, ovarian serous cystadenocarcinoma and testicular germ cell tumors with statistical significance. With the fact that all samples in TCGA cancer datasets do not compromise long non-coding gene expression data, analysis of expression correlation with HOTAIR has its limitations. HOTAIR and MET gene expression showed a remarkable tendency of reverse regulation in adrenocortical carcinoma, cervical squamous cell carcinoma and endocervical adenocarcinoma, lymphoid neoplasm diffuse large b-cell lymphoma, glioblastoma multiforme, head and neck squamous cell carcinoma, kidney renal clear cell carcinoma, acute myeloid leukemia, liver hepatocellular carcinoma, lung adenocarcinoma and uveal melanoma (Fig. 8e). The power of correlation analysis would be more enhanced by expansion of the sample sizes with non-coding gene expression data of public cancer datasets. Besides TCGA, we further analyzed available public research datasets in GEO database. Analysis of available data generated by siRNA knock-down of HOTAIR in an HCC cell line HepG2 [43], (Fig. 8a) and human sarcoma cell lines ES2, A673 and SK-ES (Fig. 8b) supported our in-vitro HOTAIR *knock-down* data in HuH-7 cells [44]. Moreover, data generated by over-expression of HOTAIR in human mesenchymal stem cells was consistent with our data in SNU-449 cells [44], (Fig. 8b, hMSC).

Our study clearly defines the fine tuning of c-Met signaling by HOTAIR to maintain hybrid E/M phenotype which ensures flexibility of commitment and enhances metastatic ability under unfavorable conditions through rate-limiting steps of metastasis. Hybrid phenotype contributes metastatic colonization and may play a crucial role in intra-and extrahepatic metastasis [59]. On the other way around, c-Met activation proceeds E/M spectrum through complete mesenchymal phenotype by suppressing HOTAIR expression. Even this study defines the interplay between two molecules, the detailed molecular interactions are still needed to be investigated. Considering the complex structure and multifunctional behavior, HOTAIR might be regulating c-Met signaling through physically interacting and epigenetic or transcriptional suppression of c-Met and/or its regulators. Further studies are needed to address the molecular cascade between HOTAIR, c-Met and Caveolin-1 in detail.

Conclusions

In conclusion, HOTAIR over-expression suppresses c-Met expression, activation and also disrupts its organization on plasma membrane by modulating Caveolin-1 expression and activation. HOTAIR over-expression provides an advantage to HCC cells via maintaining hybrid E/M phenotype thereby enhancing survival in adhesion-independent and shear-stressed conditions. HOTAIR overexpression decreases adhesion dependency and proliferation while increasing spheroid formation and improving collective migration abilities and overall improving metastatic potential of HCC cells. Further studies are needed to brighten detailed regulatory signaling cascades and mapping potential targets for therapeutic applications.

Supplementary information

Supplementary information accompanies this paper at https://doi.org/10.1186/s12964-020-00602-0.

Additional file 1: Figure S1. Includes supplementary data indicated in the text.

Additional file 2: Supplementary document 1. Includes primer sequences used in gene expression analysis and catalog numbers of antibodies used in immunoblotting and/or immunofluorescent labeling experiments.

Abbreviations

ACC: Adrenocortical carcinoma; BRCA: Breast invasive carcinoma; CESC: Cervical squamous cell carcinoma and endocervical adenocarcinoma; COAD: Colon adenocarcinoma; CTCs: Circulating tumor cells; DLBC: Lymphoid neoplasm diffuse large B-cell lymphoma; EMT: Epithelial to mesenchymal transition; FSS: Fluidic shear stress; GBD: Global Burden of Disease; GBM: Glioblastoma multiforme; HCC: Hepatocellular carcinoma; HNSC: Head and neck squamous cell carcinoma; HOTAIR: HOX Transcript Antisense Intergenic RNA; KICH: Kidney chromophobe; KIRC: Kidney renal clear cell carcinoma; KIRP: Kidney renal papillary cell carcinoma; LAML: Acute myeloid leukemia; LGG: Brain lower grade glioma; LIHC: Liver hepatocellular carcinoma; lncRNA: long non-coding RNA; LUAD: Lung adenocarcinoma; MESO: Mesothelioma; MET: Mesenchymal to epithelial transition; OE: Over-expression; OV: Ovarian serous cystadenocarcinoma; RT-qPCR: Reverse transcriptase-quantitative polymerase chain reaction; RT: Room temperature; RTCA: Real time cell analysis system; TCGA: The Cancer Genome Atlas; UVM: Uveal melanoma

Acknowledgments

We thank Prof. Dr. Mehmet Öztürk for providing HCC cells, Izmir Biomedicine and Genome Center for establishment of required technical and instrumental infrastructure for this study, IBG Vivarium Zebrafish facility for housing and providing the animals, Melek Ucuncu and Didem Cimtay from IBG Optical Imaging Core Facility for their supports for imaging processes of samples.

Materials & Correspondence:
Requests should be addressed to Nese Atabey (nese.atabey@ibg.edu.tr).

Authors' contributions

HT, EB, DC and GB performed the experiments. HT performed data analysis and curation. GCA supervised and trained HT for Zebrafish xenograft model establishment and performance. HT and NA conceived the experiments and study plan. Data was mainly interpreted by HT and NA. EB, DC and GB contributed experiment discussions. HT prepared the original draft and NA performed review edit of the manuscript. NA performed supervision, project administration and funding acquisitions. The authors critically read and approved the manuscript.

Funding

This research was funded by "Department of Scientific Research Projects of Dokuz Eylul University (BAP), grant number 2016.KB.SAG.005" and "Scientific and Technological Research Council of Turkey (TUBITAK), grant number 114S359". HT was awarded with a Short-Term Fellowship from the European Molecular Biology Organization (EMBO) between 01.06.17–01.07.17.

Availability of data and materials

Eun et al., 2016, performed expression profiling array to identify novel drivers of hepatocellular carcinoma and reveal clinical relevance as early diagnostic and prognostic biomarkers (data accessible at NCBI GEO database (Eun et al., 2016), accession GSE89377). https://www.ncbi.nlm.nih.gov/geo/query/acc.cgi?acc=GSE89377
Wu et al., 2018, performed an integrated proteomic and transcriptomic analysis to examine the overall transcriptomic changes in HepG2 cells after HOTAIR knockdown by RNA sequencing (data accessible at NCBI GEO database (Wu et al., 2018), accession GSE98091).
https://www.ncbi.nlm.nih.gov/geo/query/acc.cgi?acc=GSE98091
Shah et al., generated a next-generation RNA-sequencing data of models of Ewing sarcoma with modulated expression (repression with locked nucleic acid antisense oligonucleotides and over-expression with lentiviral

transduction) of the lncRNA HOTAIR (data accessible at NCBI GEO database (Shah et al., 2018), accession GSE109483).
https://www.ncbi.nlm.nih.gov/geo/query/acc.cgi?acc=GSE109483
The results reported here are in whole or part based upon data generated by the TCGA Research Network: https://www.cancer.gov/tcga.

Ethics approval and consent to participate
In vitro experiments of this study were approved by Non-Interventional Research Ethics Board of Dokuz Eylül University with the protocol number of 1597-GOA. Animal experiments of this study was approved by IBG Animal Ethics Committee with the protocol number of 03/2019.

Consent for publication
Not applicable.

Competing interests
The authors declare that they have no competing interests.

Author details
[1]Izmir Biomedicine and Genome Center (IBG), Balcova, 35340 Izmir, Turkey. [2]Department of Medical Biology and Genetics, Graduate School of Health Sciences, Dokuz Eylul University, 35340, Balcova, Izmir, Turkey. [3]Functional Genomics and Metabolism Unit, Department for Biochemistry and Molecular Biology, University of Southern Denmark, Campusvej 55, 5230 Odense M, Denmark. [4]Department of Molecular Biology and Genetics, Izmir International Biomedicine and Genome Institute, Dokuz Eylul University, 35340, Balcova, Izmir, Turkey. [5]Department of Medical Biology, Faculty of Medicine, Dokuz Eylul University, 35340, Balcova, Izmir, Turkey.

Received: 29 January 2020 Accepted: 25 May 2020
Published online: 11 July 2020

References
1. Global Burden of Disease Cancer C, Fitzmaurice C, Abate D, Abbasi N, Abbastabar H, Abd-Allah F, et al. Global, regional, and National Cancer Incidence, mortality, years of life lost, years lived with disability, and disability-adjusted life-years for 29 cancer groups, 1990 to 2017: a systematic analysis for the global burden of disease study. JAMA Oncol. 2019;5:1749–68.
2. Yang JD, Hainaut P, Gores GJ, Amadou A, Plymoth A, Roberts LR. A global view of hepatocellular carcinoma: trends, risk, prevention and management. Nat Rev Gastroenterol Hepatol. 2019;16(10):589–604.
3. Cancer Genome Atlas Research Network. Electronic address wbe, Cancer Genome Atlas Research N. Comprehensive and integrative genomic characterization of hepatocellular carcinoma. Cell. 2017;169(7):1327–41 e23.
4. Bouattour M, Raymond E, Qin S, Cheng AL, Stammberger U, Locatelli G, et al. Recent developments of c-met as a therapeutic target in hepatocellular carcinoma. Hepatology. 2018;67(3):1132–49.
5. Firtina Karagonlar Z, Koc D, Iscan E, Erdal E, Atabey N. Elevated hepatocyte growth factor expression as an autocrine c-met activation mechanism in acquired resistance to sorafenib in hepatocellular carcinoma cells. Cancer Sci. 2016;107(4):407–16.
6. Rinn JL, Kertesz M, Wang JK, Squazzo SL, Xu X, Brugmann SA, et al. Functional demarcation of active and silent chromatin domains in human HOX loci by noncoding RNAs. Cell. 2007;129(7):1311–23.
7. Gupta RA, Shah N, Wang KC, Kim J, Horlings HM, Wong DJ, et al. Long non-coding RNA HOTAIR reprograms chromatin state to promote cancer metastasis. Nature. 2010;464(7291):1071–6.
8. Deng J, Yang M, Jiang R, An N, Wang X, Liu B. Long non-coding RNA HOTAIR regulates the proliferation, self-renewal capacity, tumor formation and migration of the cancer stem-like cell (CSC) subpopulation enriched from breast cancer cells. PLoS One. 2017;12(1):e0170860.
9. Liu XH, Liu ZL, Sun M, Liu J, Wang ZX, De W. The long non-coding RNA HOTAIR indicates a poor prognosis and promotes metastasis in non-small cell lung cancer. BMC Cancer. 2013;13:464.
10. Tan SK, Pastori C, Penas C, Komotar RJ, Ivan ME, Wahlestedt C, et al. Serum long noncoding RNA HOTAIR as a novel diagnostic and prognostic biomarker in glioblastoma multiforme. Mol Cancer. 2018;17(1):74.
11. Wang W, He X, Zheng Z, Ma X, Hu X, Wu D, et al. Serum HOTAIR as a novel diagnostic biomarker for esophageal squamous cell carcinoma. Mol Cancer. 2017;16(1):75.
12. Tsai MC, Manor O, Wan Y, Mosammaparast N, Wang JK, Lan F, et al. Long noncoding RNA as modular scaffold of histone modification complexes. Science. 2010;329(5992):689–93.
13. Tang X, Feng D, Li M, Zhou J, Li X, Zhao D, et al. Transcriptomic analysis of mRNA-lncRNA-miRNA interactions in hepatocellular carcinoma. Sci Rep. 2019;9(1):16096.
14. Somarowthu S, Legiewicz M, Chillon I, Marcia M, Liu F, Pyle AM. HOTAIR forms an intricate and modular secondary structure. Mol Cell. 2015;58(2): 353–61.
15. Nieto MA, Huang RY, Jackson RA, Thiery JP. Emt: 2016. Cell. 2016;166(1):21–45.
16. Denisov EV, Perelmuter VM. A fixed partial epithelial-mesenchymal transition (EMT) triggers carcinogenesis, whereas asymmetrical division of hybrid EMT cells drives cancer progression. Hepatology. 2018;68(3):807–10.
17. Lovisa S, LeBleu VS, Tampe B, Sugimoto H, Vadnagara K, Carstens JL, et al. Epithelial-to-mesenchymal transition induces cell cycle arrest and parenchymal damage in renal fibrosis. Nat Med. 2015;21(9):998–1009.
18. Basu S, Cheriyamundath S, Ben-Ze'ev A. Cell-cell adhesion: linking Wnt/beta-catenin signaling with partial EMT and stemness traits in tumorigenesis. F1000Res. 2018;7:F1000 Faculty Rev-1488.
19. Lecharpentier A, Vielh P, Perez-Moreno P, Planchard D, Soria JC, Farace F. Detection of circulating tumour cells with a hybrid (epithelial/mesenchymal) phenotype in patients with metastatic non-small cell lung cancer. Br J Cancer. 2011;105(9):1338–41.
20. Armstrong AJ, Marengo MS, Oltean S, Kemeny G, Bitting RL, Turnbull JD, et al. Circulating tumor cells from patients with advanced prostate and breast cancer display both epithelial and mesenchymal markers. Mol Cancer Res. 2011;9(8):997–1007.
21. Revenu C, Gilmour D. EMT 2.0: shaping epithelia through collective migration. Curr Opin Genet Dev. 2009;19(4):338–42.
22. Grosse-Wilde A, Fouquier d'Herouel A, McIntosh E, Ertaylan G, Skupin A, Kuestner RE, et al. Stemness of the hybrid epithelial/mesenchymal state in breast cancer and its association with poor survival. PLoS One. 2015;10(5): e0126522.
23. Almale L, Garcia-Alvaro M, Martinez-Palacian A, Garcia-Bravo M, Lazcanoiturburu N, Addante A, et al. C-met signaling is essential for mouse adult liver progenitor cells expansion after transforming growth factor-beta-induced epithelial-mesenchymal transition and regulates cell phenotypic switch. Stem Cells. 2019;37(8):1108–18.
24. Yang Z, Zhou L, Wu LM, Lai MC, Xie HY, Zhang F, et al. Overexpression of long non-coding RNA HOTAIR predicts tumor recurrence in hepatocellular carcinoma patients following liver transplantation. Ann Surg Oncol. 2011; 18(5):1243–50.
25. Ishibashi M, Kogo R, Shibata K, Sawada G, Takahashi Y, Kurashige J, et al. Clinical significance of the expression of long non-coding RNA HOTAIR in primary hepatocellular carcinoma. Oncol Rep. 2013;29(3):946–50.
26. Cokakli M, Erdal E, Nart D, Yilmaz F, Sagol O, Kilic M, et al. Differential expression of Caveolin-1 in hepatocellular carcinoma: correlation with differentiation state, motility and invasion. BMC Cancer. 2009;9:65.
27. Korhan P, Erdal E, Kandemis E, Cokakli M, Nart D, Yilmaz F, et al. Reciprocal activating crosstalk between c-met and caveolin 1 promotes invasive phenotype in hepatocellular carcinoma. PLoS One. 2014;9(8):e105278.
28. Gunes A, Iscan E, Topel H, Avci ST, Gumustekin M, Erdal E, et al. Heparin treatment increases thioredoxin interacting protein expression in hepatocellular carcinoma cells. Int J Biochem Cell Biol. 2015;65:169–81.
29. Guzman C, Bagga M, Kaur A, Westermarck J, Abankwa D. ColonyArea: an ImageJ plugin to automatically quantify colony formation in clonogenic assays. PLoS One. 2014;9(3):e92444.
30. Gunes A, Bagirsakci E, Iscan E, Cakan-Akdogan G, Aykutlu U, Senturk S, et al. Thioredoxin interacting protein promotes invasion in hepatocellular carcinoma. Oncotarget. 2018;9(96):36849–66.
31. Bagirsakci E, Sahin E, Atabey N, Erdal E, Guerra V, Carr BI. Role of albumin in growth inhibition in hepatocellular carcinoma. Oncology. 2017;93(2):136–42.
32. Mahi NA, Najafabadi MF, Pilarczyk M, Kouril M, Medvedovic M. GREIN: An interactive web platform for re-analyzing GEO RNA-seq data. Sci Rep. 2019; 9(1):7580.
33. Zhao H, Shi J, Zhang Y, Xie A, Yu L, Zhang C, et al. LncTarD: a manually-curated database of experimentally-supported functional lncRNA-target regulations in human diseases. Nucleic Acids Res. 2020;48(D1):D118–D26.
34. Avci ME, Keskus AG, Targen S, Isilak ME, Ozturk M, Atalay RC, et al. Development of a novel zebrafish xenograft model in ache mutants using liver cancer cell lines. Sci Rep. 2018;8(1):1570.

35. Eun J, Nam S. Identifying novel drivers of human hepatocellular carcinoma and revealing clinical relevance as early diagnostic and prognostic biomarkerKorea TCUo, editor. South KoreaDec 31; 2017.
36. Iscan E, Gunes A, Korhan P, Yilmaz Y, Erdal E, Atabey N. The regulatory role of heparin on c-met signaling in hepatocellular carcinoma cells. J Cell Commun Signal. 2017;11(2):155–66.
37. Yilmaz Y, Topel H, Atabey N. Identification of C-met and insulin receptor heterodimer as a mediator for hepatocellular carcinoma. In: 25th biennial congress of the European Association for Cancer Research; 2018/7/1. Amsterdam: ESMO Open: BMJ Publishing Group Limited; 2018. p. A297-A.
38. Topel H, Comez D, Atabey N. HGF/c-met signalling pathway downregulates lncRNA HOTAIR to induce adhesion independent growth in HCC by increasing caveolin-1 expression. In: 25th biennial congress of the European Association for Cancer Research; 2018/7/1. Amsterdam: BMJ Publishing Group Limited; 2018. p. A282–A3.
39. Huang Q, Hu X, He W, Zhao Y, Hao S, Wu Q, et al. Fluid shear stress and tumor metastasis. Am J Cancer Res. 2018;8(5):763–77.
40. Jolly MK, Somarelli JA, Sheth M, Biddle A, Tripathi SC, Armstrong AJ, et al. Hybrid epithelial/mesenchymal phenotypes promote metastasis and therapy resistance across carcinomas. Pharmacol Ther. 2019;194:161–84.
41. Kroger C, Afeyan A, Mraz J, Eaton EN, Reinhardt F, Khodor YL, et al. Acquisition of a hybrid E/M state is essential for tumorigenicity of basal breast cancer cells. Proc Natl Acad Sci U S A. 2019;116(15):7353–62.
42. Jolly MK, Boareto M, Huang B, Jia D, Lu M, Ben-Jacob E, et al. Implications of the hybrid epithelial/mesenchymal phenotype in metastasis. Front Oncol. 2015;5:155.
43. Wu Y, Xiong Q, Li S, Yang X, Ge F. Integrated proteomic and transcriptomic analysis reveals long noncoding RNA HOX transcript antisense intergenic RNA (HOTAIR) promotes hepatocellular carcinoma cell proliferation by regulating opioid growth factor receptor (OGFr). Mol Cell Proteomics. 2018; 17(1):146–59.
44. Shah N. In: Geo N, editor. USA Next-generation RNA-sequencing data of models of Ewing sarcoma with modulated expression of the lncRNA HOTAIR; 2018.
45. Hirschfield H, Bian CB, Higashi T, Nakagawa S, Zeleke TZ, Nair VD, et al. In vitro modeling of hepatocellular carcinoma molecular subtypes for anti-cancer drug assessment. Exp Mol Med. 2018;50(1):e419.
46. Yuzugullu H, Benhaj K, Ozturk N, Senturk S, Celik E, Toylu A, et al. Canonical Wnt signaling is antagonized by noncanonical Wnt5a in hepatocellular carcinoma cells. Mol Cancer. 2009;8:90.
47. Luan W, Li R, Liu L, Ni X, Shi Y, Xia Y, et al. Long non-coding RNA HOTAIR acts as a competing endogenous RNA to promote malignant melanoma progression by sponging miR-152-3p. Oncotarget. 2017;8(49):85401–14.
48. Yang G, Fu Y, Lu X, Wang M, Dong H, Li Q. LncRNA HOTAIR/miR-613/c-met axis modulated epithelial-mesenchymal transition of retinoblastoma cells. J Cell Mol Med. 2018;22(10):5083–96.
49. Liu B, Liu Q, Pan S, Huang Y, Qi Y, Li S, et al. The HOTAIR/miR-214/ST6GAL1 crosstalk modulates colorectal cancer procession through mediating sialylated c-met via JAK2/STAT3 cascade. J Exp Clin Cancer Res. 2019;38(1):455.
50. Jiang X, Wu J, Zhang Y, Wang S, Yu X, Li R, et al. MiR-613 functions as tumor suppressor in hepatocellular carcinoma by targeting YWHAZ. Gene. 2018;659:168–74.
51. Wang W, Zhang H, Wang L, Zhang S, Tang M. miR-613 inhibits the growth and invasiveness of human hepatocellular carcinoma via targeting DCLK1. Biochem Biophys Res Commun. 2016;473(4):987–92.
52. Gottlieb-Abraham E, Shvartsman DE, Donaldson JC, Ehrlich M, Gutman O, Martin GS, et al. Src-mediated caveolin-1 phosphorylation affects the targeting of active Src to specific membrane sites. Mol Biol Cell. 2013;24(24): 3881–95.
53. Garcia-Vilas JA, Medina MA. Updates on the hepatocyte growth factor/c-met axis in hepatocellular carcinoma and its therapeutic implications. World J Gastroenterol. 2018;24(33):3695–708.
54. Sokeland G, Schumacher U. The functional role of integrins during intra- and extravasation within the metastatic cascade. Mol Cancer. 2019;18(1):12.
55. Aurrand-Lions M, Johnson-Leger C, Wong C, Du Pasquier L, Imhof BA. Heterogeneity of endothelial junctions is reflected by differential expression and specific subcellular localization of the three JAM family members. Blood. 2001;98(13):3699–707.
56. Zhao H, Yu H, Martin TA, Zhang Y, Chen G, Jiang WG. Effect of junctional adhesion molecule-2 expression on cell growth, invasion and migration in human colorectal cancer. Int J Oncol. 2016;48(3):929–36.
57. Valastyan S, Weinberg RA. Tumor metastasis: molecular insights and evolving paradigms. Cell. 2011;147(2):275–92.
58. Campbell K, Casanova J. A common framework for EMT and collective cell migration. Development. 2016;143(23):4291–300.
59. Giannelli G, Koudelkova P, Dituri F, Mikulits W. Role of epithelial to mesenchymal transition in hepatocellular carcinoma. J Hepatol. 2016;65(4): 798–808.

Publisher's Note

Springer Nature remains neutral with regard to jurisdictional claims in published maps and institutional affiliations.